Mode Matching Technique for Calculating the Dispersion Curve of One-Dimensional Periodic Structures

by

Hamid Reza Mohebbi

A thesis

Presented to Concordia University

in fulfillment of the

thesis requirement for the degree of

Master of Applied Science

in

Electrical and Computer Engineering

Montreal, Quebec, Canada, 2006

Your file Votre référence
ISBN: 0-494-14273-1
Our file Notre référence
ISBN: 0-494-14273-1

Abstract

MODE MATCHING TECHNIQUE FOR CALCULATING THE DISPERSION CURVE OF ONE-DIMENSIONAL PERIODIC STRUCTURES

Hamid Reza Mohebbi

In this thesis, the rigorous Mode Matching (MM) technique is utilized to find the dispersion curve of the traveling wave in one-dimensional planar periodic structures. The structure consists of a homogenous dielectric substrate backed by a ground plane and infinite number of periodic perfect strip conductors on the top. The thickness of the strips is infinitely small. Such a structure is also known as Strip Grating in frequency selective surface (FSS) applications. The technique is first applied to a shielded microstrip line, and then to the 1-D printed periodic structure.

A general formulation for rigorous modeling of shielded microstrip line as well as strip grating structures is introduced. The modeling is based on hybrid transverse electric (TE) and transverse magnetic (TM) mode analysis. After matching the fields at the junction of the air-dielectric, a set of equations on the area of interface is driven. Unlike the conventional MM technique, a simple sub-domain orthogonal set is used to convert the algebraic equations obtained from the boundary conditions into a matrix format. This technique is similar to the well-known Point Matching (PM) technique which is frequently used in Method of Moment (MoM). This homogenous matrix equation has all information required for the calculation of dispersion curve.

To find the singularities of the matrix, this research focuses on the use of the numerically stable technique of the Singular Value Decomposition (SVD). Since the dimension of the matrix depends on both the amount of truncation and the number of matching points, this matrix is subject to ill-conditional behavior and convergence issue. Thus, we pay a special attention and care to the convergence and conditional behavior of the matrix.

Based on the hybrid technique investigated in this thesis, numerical results are generated and presented. Both dispersion curves of shielded microstrip line and strip grating are depicted. The computed results are shown to be in excellent agreement with results obtained from Singular Integral Equation (SIE) method and MoM in the spectral domain. The advantage of this method is the simple derivation of the equations and the high speed of the dispersion diagram's calculation.

Acknowledgment

I would like to acknowledge the support and guidance of my supervisor, Professor Abdel Razik Sebak, during the course of this research. His kindly trust and wonderful personality made my master program at Concordia University more enjoyable. I would like to express my deepest gratitude to him for providing me with such a great opportunity for doing research in this area.

I would like to express my deepest gratitude to Dr. Jafar Shaker from Communication Research Centre (CRC) in Canada for introducing this topic as my master thesis subject. His great vision and invaluable comments helped me to successfully carry out this research project.

I am deeply indebted to Dr. Mohammad Reza Chaharmir from CRC for his invaluable guidance, great patience, enthusiastic support and constant encouragement during this project. I never forget once he introduced the topic of EBG materials as a project topic for my Antenna course which drew me into the Computational EM.

I am deeply grateful to my kind friend, Mr. Aref Bakhtazad who is studying in University of McGill toward his Ph.D degree for his vast knowledge in EM and his crucial advice during writing my code in MATLAB. I also appreciate Dr. Amir Borji at University of Waterloo for carefully responding to my questions.

To my family

for their encouragement, support and patience.

Contents

List of Figures

List of Tables

List of Symbols

ε_0	Free Space Permittivity
μ_0	Free Space Permeability
$\varepsilon_{r(i)}$	Relative Permittivity in the region i
f	Frequency
ω	Angular frequency
$A_{z(i)}$	z-component of the vector potential A in the region i
$A_{zn(i)}$	nth Floquet harmonic associated to the z-component of the vector potential A in the region i
$F_{z(i)}$	z-component of the vector potential F in the region i
$F_{zn(i)}$	nth Floquet harmonic associated to the z-component of the vector potential F in the region i
$\psi_i^{(e)}$	Scalar wave function for the TM mode in the region i
$\psi_{n(i)}^{(e)}$	nth Floquet harmonic associated to the scalar wave function for the TM mode in the region i
$\psi_i^{(h)}$	Scalar wave function for the TE mode in the region i
$\psi_{n(i)}^{(h)}$	nth Floquet harmonic associated to the scalar wave function for the TE mode in the region i
k_0	Free space wavenumber
k_i	Wavenumber in the region i

β_z	Phase constant of the wave in the z direction
$\overline{\beta}_z$	Normalized β_z
β_n	Phase constant of the nth Floquet harmonic wave in the direction of periodicity (i.e. x direction)
$\beta_{x(i)}^{(e)}$	Phase constant for the TM mode in the region i in the x direction
$\beta_{x(i)}^{(h)}$	Phase constant for the TE mode in the region i in the x direction
$E_{x(i)}^{(e)}$	Electric field for the TM mode in the region i in the x direction
$E_{x(i)}^{(h)}$	Electric field for the TE mode in the region i in the x direction
$E_{xn(i)}^{(e)}$	nth Floquet harmonic associated to the electric field for the TM mode in the region i in the x direction
$E_{xn(i)}^{(h)}$	nth Floquet harmonic associated to the electric field for the TE mode in the region i in the x direction
$E_{x(i)}$	Total Electric field in the region i in the x direction
E_n	nth Floquet harmonic electric field
$H_{x(i)}^{(e)}$	Magnetic field for the TM mode in the region i in the x direction
$H_{x(i)}^{(h)}$	Magnetic field for the TE mode in the region i in the x direction
$H_{xn(i)}^{(e)}$	nth Floquet harmonic associated to the magnetic field for the TM mode in the region i in the x direction
$H_{xn(i)}^{(h)}$	nth Floquet harmonic associated to the magnetic field for the TE mode in the region i in the x direction

$H_{x(i)}$	Total magnetic field in the region i in the x direction
$\alpha_n^{(i)}$	Attenuation constant corresponding to the nth Floquet harmonic [or nth mode] in the region i in the y direction
k_n	Phase constant (nth eigenvalue) in the *x*-direction corresponding to the nth mode
$A_{n(i)}^{(e)}, B_{n(i)}^{(e)}$	Unknown coefficient involved in the solution for the nth scalar function of $\psi_{n(i)}^{(e)}$
$A_{n(i)}^{(h)}, B_{n(i)}^{(h)}$	Unknown coefficient involved in the solution for the nth scalar function of $\psi_{n(i)}^{(h)}$
$A_n^{(e)}$	Unknown coefficient associated to the nth Floquet harmonic [or nth mode] for the TM mode in the region 1 (dielectric)
$A_n^{(h)}$	Unknown coefficient associated to the nth Floquet harmonic [or nth mode] for the TE mode in the region 1 (dielectric)
$B_n^{(e)}$	Unknown coefficient associated to the nth Floquet harmonic [or nth mode] for the TM mode in the region 2 (air)
$B_n^{(h)}$	Unknown coefficient associated to the nth Floquet harmonic [or nth mode] for the TE mode in the region 2 (air)

Abbreviation

EM	Electromagnetic
MM	Mode Matching
PM	Point Matching
MoM	Method of Moment
TEM	Transverse Electric Magnetic mode
TE	Transverse Electric mode
TM	Transverse Magnetic mode
FDTD	Finite Difference Time Domain
FEM	Finite Element Method
PEC	Perfect Electric Conductor
PMC	Perfect Magnetic Conductor
HFSS	High-Frequency Structure Simulator
FSS	Frequency Selective Surface
BC	Boundary Condition
PBG	Photonic Band Gap
EBG	Electromagnetic Band Gap
SVD	Singular Value Decomposition
SIE	Singular Integral Equation Method
SD	Spectral Domain
BV	Boundary Value

Chapter 1

Introduction

For decades, planar periodic structures have been used in many microwave devices. Continuous development in this area finally led to the remarkable finding of the band gap in the1990's. This simply shows that periodic structures have the possibility to create a range of forbidden frequencies for electromagnetic waves called "Photonic Band Gap" (PBG). The discovery of this fact caused rapid development in the technology of periodic structures; consequently; tremendous efforts were carried out to find efficient, fast and accurate simulation techniques on the characterization of dispersion curve of periodic structures.

The focus of this thesis is to calculate the dispersion diagram of the traveling wave in two planar structures: Shielded microstrip line and one-dimensional printed periodic structure consisting of a homogenous dielectric substrate backed by a ground plane and infinite number of periodic perfect strip conductors on the top. The thickness of the strips is infinitely small. This periodic structure is sometimes called Grating Strip.

Mode Matching (MM) technique is used for full-wave analysis of these structures leading to a set of algebraic equation. To convert this equation into the matrix format, the

conventional Point Matching (PM) technique is applied. To find the singularity of the matrix, the numerically stable method of Singular Value Decomposition (SVD) is also used.

1.1 Motivation

In 1960's, periodic structures were encountered in a variety of applications in Electromagnetic discipline such as traveling-wave slot, dipole arrays, log periodic antennas, phased arrays and so on. They are also used in Frequency Selective Surface (FSS) due to their good reflection properties. However, after developing the Photonic Band Gap (PBG) in dielectric materials in 1990's, periodic media are well acknowledged for their capability to control the propagation and emission of EM waves and have gained a substantial attention as photonic crystals or photonic band gap (PBG) structures.

PBG materials are characterized by three parameters: the lattice topology, the spatial period, and the dielectric constants of the constituent materials. By suitable selection of these parameters, a gap in the EM dispersion relation can be created, within which the linear propagation of EM waves is forbidden. This forbidden frequency range is called photonic band gap. It is said that a photonic band gap is complete, if a forbidden band gap exists for all polarizations and all propagation directions.

In the microwave and millimeter domain, photonic band gap materials usually are called "Electromagnetic Band Gap" (EBG) or electromagnetic crystals. They usually consist of some metallic components. Electromagnetic crystals are mainly used as antenna substrates which have a number of applications [1]. For example, conventional integrated circuit antennas on a semiconductor substrate with the ε dielectric constant have the

drawback that the power radiated into the substrate is a factor $\varepsilon^{3/2}$ larger than the power radiated in free-space. Thus, antenna on the typical substrate radiates only about 2% of its power. By fabrication the antenna on an EBG structures with a driving frequency within the band gap, no power should be transmitted into the substrate, if there are no evanescent surface mode. Several successful antenna designs with improved directivity and efficiency up to 70% have been reported [2]. To suppress the surface modes of an antenna substrate an EBG material can be used as a high-impedance surface. Microwave and millimeter wave filters, couplers, resonators, reflectors and guiding structures can also be designed on the basis of EBG materials. Therefore, the dispersion relation for one and two dimensional periodic structures with metallic elements has become of particular interest which leads a number of research papers

1.2 Objectives

The goal of this research is to develop a new technique, which is called MM-PM, to find the dispersion curves of millimeter planar structures particularly periodic structures. For this purpose, this new technique which is a combination of two matching methods is applied on shielded microstrip line and 1-D printed periodic structure in order to find their dispersion curves. Derivation of MM is a simple and straightforward task, and also numerical implementation of PM is an easy job. The results for microstrip line and 1-D periodic structure should be verified by comparing with reported results of Singular Integral Equation (SIE) and MoM in spectral domain, respectively.

1.3 Brief Review of this Thesis

As mentioned, the subject of this thesis is to develop a fast and simple electromagnetic technique specialized for calculation and characterization of dispersion curves of various planar periodic structures. In this thesis, in order to utilize the inherent flexibility, accuracy, and efficiency of the Mode Matching (MM) technique for structures with infinitely thin strips, a new approach for rapid implementation of MM is introduced which is very similar to the well-known Point Matching (PM) technique in MoM.

In chapter two, some introductory materials which are needed to better understand the MM-PM technique in analyzing periodic structures are discussed. The concept of the mode and the technique of normalization are explained in this chapter. Also, a classical example of MM technique is introduced. The Floquet theory which is the infrastructure of the analysis of any periodic structure is presented. A brief but comprehensive review about Field Analysis and the Boundary Conditions (BC) in EM is given. At the end of this chapter, there is a useful subject about the ways to find the value of the parameters which makes a matrix singular such as the Single Value Decomposition (SVD).

In chapter three, the formulation of full-wave analysis of a shielded microstrip line is given. Then, it is extended to a one-dimensional periodic structure which is called "Strip Grating". This structure consists of a periodic array of infinitely long but infinitely thin perfect conductor of strips on the interface of the substrate that is backed by a ground plane. The goal of this formulation is to prepare the needed mathematical model to calculate the dispersion curve for traveling wave in this structure.

After mathematical modeling of the structures in chapter three, a simple Matlab code is written to generate numerical results in chapter four for either microstrip line or Strip

Grating. The results containing dispersion curves are compared with those from published papers to verify the validity of this computational method.

In chapter five, after a brief summary of the thesis, some ideas for future stages of this research are explored and new directions for future research are briefly discussed.

Chapter 2

Theoretical Framework

The goal of this chapter is to introduce the main mathematical tools and underlying physics behind the theory of propagation of electromagnetic waves in planar structures such as microstrip line and one-dimensional printed periodic structure. The chapter consists of eight sections. In section 2.1, a general review of periodic structures, the literature review and the EM techniques to calculate the dispersion curve of periodic structures are presented. Also, the advantage and disadvantage of MM technique are presented in this section. In section 2.2, and soon, the concept of mode which is widely used in this thesis is explained. The general properties of EM wave are presented in section 2.3. The influence of the periodicity on the solution of Helmholtz equations is given in section 2.4 in terms of Floquet theorem. The advantage of normalization and the brief review of all necessary boundary conditions in planar structures are discussed in sections 2.5 and 2.6. In section 2.7, a classical example of using MM technique in waveguide discontinuities is given to get familiar with essential steps to implement MM method. A useful discussion of finding singularities in the matrix extracted from MM is discussed in section 2.8.

2.1 Literature Review

2.1.1 Periodic Structures

Historically, the concept of periodic structure first arose in the Solid State Physics under the subject of crystals and electrons in crystals. When a crystal grows in a constant environment, the form develops as if identical building blocks were added continuously. Many concepts which is used today in periodic structure topic such as lattice, basis, translation vector, reciprocal lattice, irreducible Brillouin zone, k-space, primitive lattice cell, band gap, band structure and so on had been developed well in this field [3]. In 1990's, the same approach was applied in periodic structures constructed of some repeated dielectric materials in a dielectric background [4]. It was seen that such a structure produces a very good band gap in its dispersion diagram [3], [4]. After that, the same concept was extended into periodic arrays of metallic strips or patches in various research [1],[2],[5]-[15]. Hence, recently a great interest has been shown to find the dispersion curve of infinite arrays of strips or patches to see if they produce a good forbidden frequency band or not [2],[9]-[13].

A periodic structure is an assembly of identical elements arranged in one, two or three dimensional infinite arrays. Periodic structures were conceived to control the propagation of electromagnetic waves, so periodic structures have found many applications. They are used in photonic or electromagnetic band gap (PBG, EBG) materials, reflectarray antennas, leaky wave antenna, frequency selective surfaces (FSS), microwave filters, polarizers, artificial dielectric, radomes, harmonic tuning in power amplifier, active girds in RF devices, metamaterials and TEM waveguides [4]-[16].

A good example of periodic structures is a photonic crystal which has a dielectric material containing a periodicity in dielectric constant. A periodic structure can be regarded as one, two or three periodic structure, as shown in Fig. 1.1, provided it has periodicity in one, two or three direction respectively.

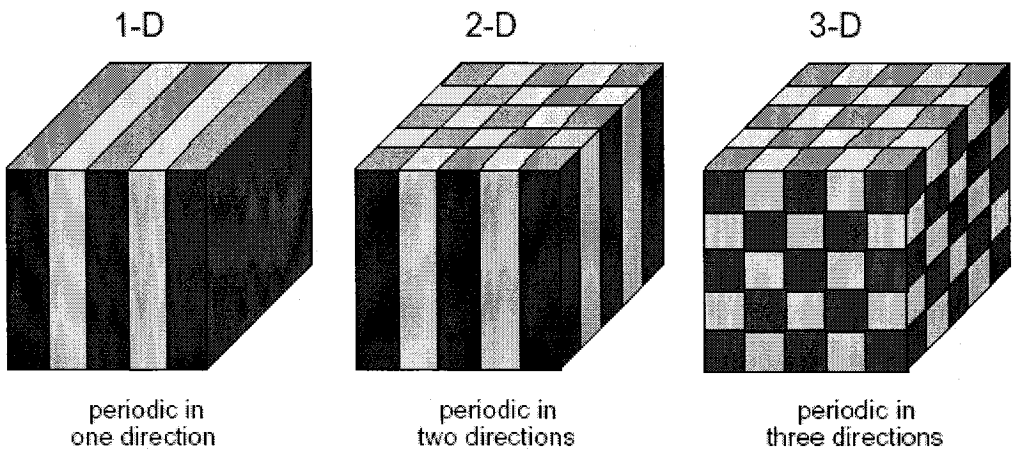

Fig. 2.1: Schematic depiction of a periodic structure in one, two, and three directions [4].

The periodicity in photonic crystals is proportional to the wavelength of light. The periodic dielectric constant can create a range of forbidden frequencies for electromagnetic waves called a photonic band gap. Sometimes metallic-dielectric photonic band gap materials, which are for instance reserved to the centimeter and millimeter wavelengths, are called electromagnetic band gap (EBG) materials. However, some of these structures may be used at higher frequencies, in the infrared or sub-millimetric domain, for example. Also purely dielectric structures may be used at lower frequencies. Therefore, the distinction between PBG and EBG materials is not evident [17].

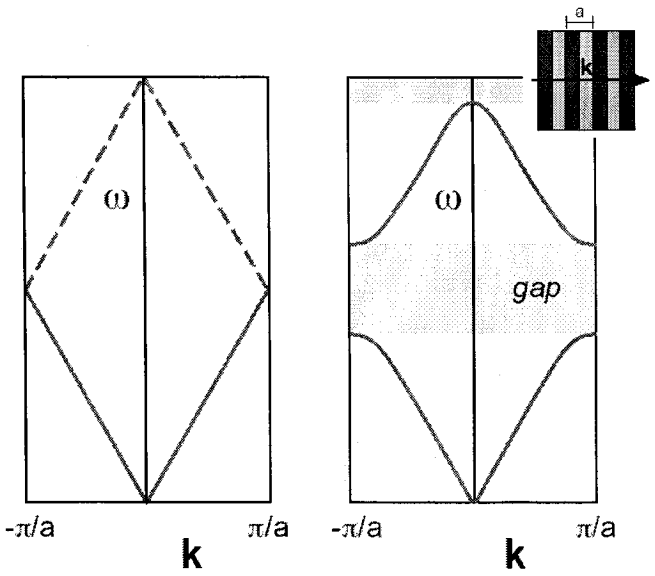

Fig. 2.2: Dispersion Curve (band diagram), frequency versus wavenumber *k*, of a uniform structure (left) and one-dimensional periodic structure (right) [4].

In recent years, there has been a great interest in determining the electromagnetic band gap structures, also known as dispersion curves, for electromagnetic waves propagating in various planar periodic structures [7]-[15]. EBG structures are widely used for improving the electromagnetic performance in microwave circuits and antennas [11]-[13]. Structures operating in the microwave range commonly consist of periodic arrays of metal patches patterned on a grounded dielectric substrate, and possibly connected to the ground plane through metal pins or vias [2].

Although most of the PBG (dielectric periodic structure in dielectric background) produce a good band gap as a wave suppression, only two types of the EBG (metallic patch on a dielectric substrate) structures are reported to have a good EM wave suppression and in-phase reflection: the mushroom-like EBG [2], and uniplanar compact EBG (UC-EBG) [2],[10]-[13]. Both of them have periodicity in two dimensions, so they are considered as 2-D periodic structure and they are shown in Fig.2.3. The mushroom-

like EBG consists of a ground plane, a dielectric substrate, metallic patches, and connecting vias as displayed in Fig.2.3 (a). A unit cell of the UC-EBG consists of metallic patches with narrow inset lines on a dielectric ground as shown in Fig.2.3 (b).

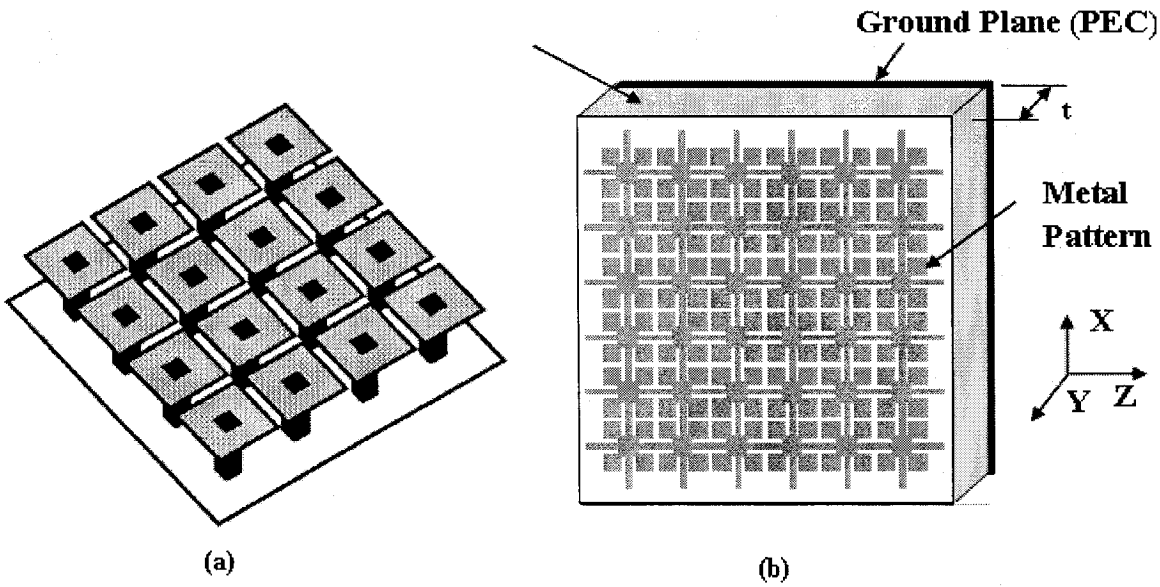

Fig. 2.3: (a) Mushroom-Like EBG [2] (b) Uniplanar Compact EBG [11].

When their geometrical properties are chosen properly, these structures exhibit two different kinds of performance. On the other hand, they can be used to prevent the propagation of substrate waves in a frequency band (EBG behavior). Thus, they reduce the leakage in guided-wave circuits and improve the efficiency of patch antennas [16]. On the other hand, they can behave as an artificial perfect magnetic conductor (PMC), reflecting an incident plane wave without phase reversal because of their in-phase reflection features [18]. This permits the design of transverse electromagnetic TEM waveguides and low-profile patch antennas [12].

Therefore, the analysis of electromagnetic band-gap structures should ideally provide two kinds of information: the dispersion curve of the modes supported by the periodic

structure, and the phase of the reflection coefficient of the structure under a plane-wave illumination. However, in many practical cases, the most useful information is the frequency range where the propagation of electromagnetic waves is forbidden (bandgap). This information can be retrieved by considering only the boundary of the irreducible Brillouin zone [3].

2.1.2 Electromagnetic Methods in Dispersion Curve Calculation

In 1960's and 1970's, when microstrip lines were used in microwave integrated circuits as essential elements, a large amount of research and interest were made to analyze and model these transmission lines. Thus a large number of publications exist in this topic [19]. Among them, dispersion analysis of either shielded or open microstrip line devoted significant effort which leads a number of research papers. The dispersion curve of a microstrip line was of interest, because it was an easy task to find the effective permittivity of the microstrip line from the study of dispersion characteristic of the structure according to the following equation:

$$\varepsilon_{eff} = \left(\frac{\lambda_0}{\lambda_g} \right)^2 \tag{2.1}$$

Various methods to this goal are listed [20]:

(1) Integral equation (with MoM)

(2) Method of lines

(3) Spectral domain method (with MoM such as Galerkin's method)

(4) Singular integral equation

(5) Fourier analysis method

(6) Finite difference method

(7) Mode matching method (for finitely thick strip)

Also, there are a number of methods to numerically calculate the dispersion curve of a periodic structure:

(1) Plane Wave Expansion Method [4],

(2) Finite Difference Time Domain, particularly Spectral FDTD [11], [21],

(3) Finite Element Method [2], [22]

(4) Method of Moment and Green's function, either in space or spectral domain [9], [10].

All of these methods are very efficient and reveal highly accurate results when compared to experimental results. However, depending on the problem tackled, they are not equivalent. Plane Wave Expansion method is limited to dielectric period structures, because it is based on expanding the periodic permittivity in an equation which is so-called the master equation of photonic crystals.

$$\nabla\times\frac{1}{\varepsilon(\mathbf{r})}\nabla\times\mathbf{H}(r)=\left(\frac{\omega}{c}\right)^2\mathbf{H}(\mathbf{r}) \tag{2.2}$$

FDTD and FEM methods have a high flexibility in the geometry of components. In other words, they can simulate any periodic structure, but due to the volume-by-volume analysis they require large computer time and memory in addition to the lack of required accuracy. Among them, MoM is very efficient and accurate but many factors such as Green's function, basis functions, integrations, singularities, and so on should be taken into account [9], [14], [23]. Therefore, it is reasonable to use former computational techniques such as those which had been used for microstrip line.

2.1.3 Mode Matching Technique

The Mode-matching technique is a computational method in EM which is commonly used to solve electromagnetic problems. Indeed, this method is one of the most frequently used methods to formulate boundary-value problems. This method has been applied to solve the scattering problem due to various discontinuities in waveguides [23]-[25] and microstrip lines [26], [27]. It has also been extended to analyze composite structures such as E-plane filters, direct-coupled cavity filters, waveguide impedance transformers, power dividers, and microstrip filters [23].

In addition to scattering problems, the mode-matching method is useful in solving eigenvalue problems. It can be formulated to obtain the resonant frequency of a cavity, the cutoff frequency of a waveguide, or the propagation constant of a transmission lines, such as microstrip lines with final metal thickness. This method has already been used to find dispersion curve of microstrip lines with finite metal thickness [24], but has never been used to find dispersion curve of periodic structures. In this research an effort is made to utilize this method in order to find the dispersion curve of a planar periodic structure, because this method looks to be fast and simple in comparison with other methods.

Generally speaking, this technique is useful when the geometry of the structure can be identified as an interface of two or more regions, each belonging to a separable coordinate system. In other words, in each region there exists a set of well-defined solutions of Maxwell's equations that satisfy all the boundary conditions except at the interface. The electromagnetic fields traveling along an axially periodic structure as guided waves are described by the Floquet theory.

The first step in mode-matching procedure entails the expansion of unknown fields in the individual regions in terms of their respective normal modes. Since the functional form of the normal modes is known, the problem is reduced to that of determining the set of modal coefficients associated with the field expansions in various regions. This procedure in conjunction with orthogonality property of the normal modes, eventually leads to an infinite set of linear simultaneous equations for the unknown modal coefficients.

After formulation, a simple programming code, for example by Matlab, should be written to solve the problem numerically. In general, it is not possible to extract an exact solution of this infinite system of equations, and one is forced to resort to approximation techniques, such as truncation or iteration. The accuracy of the approximated results should be verified carefully because of the relative convergence [28] problem found in the evaluation of the mode-matching equations. Therefore, the results obtained from this method must be verified with some other results that have already been published or other commercial simulation software such as HFSS or ADS as a benchmark.

2.2 Modes

"Mode" is a term widely used in electromagnetic texts, particularly in dispersion curve terminology, so in this section a brief review of the concept of mode has been performed. Generally, a mode is a particular field configuration. For a given electromagnetic boundary-value problem, many field configurations that satisfy both Maxwell's equations and the boundary conditions usually exist. All these different field configurations (solutions) are usually referred to as modes [25].

Moreover, a mode is a nontrivial solution of a homogenous differential equation with homogenous boundary condition such as Sturm-Liouvelle problem. In such cases, a mode has been recognized as an eigenfunction corresponding to an eigenvalue which is often recognized as propagation constant. Thus, they are sometimes described as "eigenmodes" [29]. This set of existing modes constitutes an orthogonal set, so sometimes they are called as "normal modes".

Sometimes, modes are physically interpreted as an electromagnetic wave; it is usually the case when there are just peripheral boundary conditions, e.g. in waveguides. Such a mode is capable of propagating through the medium surrounded by boundary conditions. The source excitation of the problem can determine that each mode can propagate. Moreover, the source excitation can specify the amplitude of that mode as well. However, if there is another extra boundary condition, the superposition principle is invoked to meet the extra boundary conditions, because each mode alone is not able to satisfy the BC, so we must consider the summation of the modes as a solution of the differential equation to meet the BCs at a junction. It is the reason that the solution of boundary value problem is shown as a summation of modes with unknown amplitude coefficients. In this case, each mode has no physical interpretation like electromagnetic wave; instead; it has just a mathematical meaning [29].

Sometimes the term of mode is referred to those solutions which are found by setting the determinant of a matrix into zero instead of a BV problem. This mostly happens in moment method (MoM) and mode matching (MM) technique. In such a case, the calculated modes might not be orthogonal to each other. Furthermore, they have a physical interpretation as propagating electromagnetic wave with particular propagation

constant which is mostly the root of the determinant. Although they are not normal they are also known as modes.

Moreover, in some problems spurious modes exist. When we are dealing with these modes that often come from the roots of a determinant, it should be noted that due to the nonlinearity of the functions available among the entries of the matrix, some spurious modes may be found probably. They can be spurious propagation constant at particular frequency. Spurious modes are not real, and they do not exist as an EM wave. Thus, we should eliminate them from our results. One way that sometimes works is to draw the dispersion curve, and consequently the spurious eigenvalues will be removed. The other powerful test is to check if the tangential components of the fields corresponding to this eigenvalue satisfy the boundary conditions or not. If they do, they are real modes; otherwise; they are spurious modes.

The most widely known modes are those referred to as Transverse ElectroMagnetic (TEM), Transverse Electric (TE) and Transverse Magnetic (TM) [30], [31].

2.3 Field Analysis in Mode Matching

An arbitrary field in a homogenous source-free region can be expressed as the sum of the TM and TE field [31]. The total fields can be decomposed into TE and TM modes; then we will analyze each of them separately, and finally we will end up with the total field according to the superposition. Thus for such a problem we may decompose the fields into TE (H-wave) and TM (E-wave) modes.

There is a variety of ways to calculate the fields of TE and TM wave inside of an electromagnetic structure which has been described in different text books [24], [30],

[31], and [32]. All are completely matched with each other. The difference is just in notations and some calculations. As a brief, some of them take benefit from auxiliary wave scalar function; some others used vector potentials and others express the fields in terms of axial (longitudinal) E and H field. The first approach is a normalized version of other methods which is widely used in IEEE papers such as [31], [32], [33]. The second approach is mostly used in Antenna problems [30]. Both TE and TM modes can be expressed with respect to the vector potentials and the vector potentials can be found by forcing the Helmholtz equation. The third method id based on the simplification of Maxwell's equation by decomposing all fields into transverse and axial components [24]. Mostly, the direction of traveling wave, or the direction which medium has axial symmetry around it is assumed as an axial direction.

2.4 Normalization

In field analysis of a structure, it is helpful to apply the idea of normalization. There are two kinds of normalization: Amplitude normalization and frequency normalization. Since the fields must satisfy the BCs, it doesn't matter if they are multiplied by an expression in order to be simplified. Hence, as long as this multiplier is constant for all fields in all regions, we can multiply all fields by this factor. In other words, this multiplier must be independent of region factor, but it can be expressed in terms of frequency, propagation constants, phase constant, attenuation constant, free-space wavenumber, ε_0, μ_0 and any other constant. If it is the case, the exact value of the amplitudes can be found by excitation.

The other kind of normalization is called frequency normalization. In this process, all propagation constants are divided by free-space wavenumber, k_0 and all length variables such as x, y and z are multiplied by k_0 in order to be converted into electrical length. Hence, the affect of frequency just appears one time in k_0, and there is no need to consider the frequency in our implementation.

2.5 Floquet Theorem

2.5.1 Floquet Theorem Statement

The form of guided waves traveling along an axially periodic structure is significantly described with the help of a representation commonly referred to as Floquet's theorem. This theorem actually constitutes a generalization to linear partial differential equations of a theorem in ordinary, linear differential equations with periodic coefficients established by Floquet. Actually Floquet's work dealt with differential equation with periodic coefficients. The case of periodic boundary conditions is an extension of that work. Such a generalization has been carried out by Bloch, for the case of Schrödinger's equation, in connection with propagation of electron waves in large, but finite, crystals. However, this theorem has a lot of applications in electromagnetic waves.

For the sake of simplicity, we discuss the Floquet theorem in periodic structures having the periodicity just in one direction. It means that the structure consists of infinite assembly of unit cell – a single period – in one specific direction. With the axial direction denoted by z and the period by d, the unit cell will be expressed

by $(n-1)d \le z \le nd$. Actually, Floquet's theorem may be stated in three equivalent forms [32]:

I. *A time-harmonic electromagnetic field* $E(x,y,z)$ *or* $H(x,y,z)$ *along an axially periodic structure is described by the solution of the form of*

$$E(x,y,z) = e^{-\gamma z} E_p(x,y,z) \tag{2.3a}$$

$$H(x,y,z) = e^{-\gamma z} H_p(x,y,z) \tag{2.3b}$$

where E_p *and* H_p *are periodic function of z with period d:*

$$E_p(x,y,z+nd) = E_p(x,y,z) \tag{2.4a}$$

$$H_p(x,y,z+nd) = H_p(x,y,z). \tag{2.4b}$$

The above relation may be rephrased as follows, which is useful when dealing with periodical boundary conditions.

II. *A time-harmonic electromagnetic field* $E(x,y,z)$ *or* $H(x,y,z)$ *along an axially periodic structure at any point in a unit cell will take on exactly the same value at a similar point in any other unit cell except for a propagation factor* $e^{-\gamma d}$ *from one cell to the next. Thus, if the field in the unit cell between* $0 \le z \le d$ *is* $E(x,y,z)$ *and* $H(x,y,z)$*, the field in the unit cell located in the region* $d \le z \le 2d$ *possess the property*

$$E(x,y,z+d) = e^{-\gamma d} E\ (x,y,z) \tag{2.5a}$$

$$H(x,y,z+d) = e^{-\gamma d} H(x,y,z). \tag{2.5b}$$

III. *The field in periodic a periodic structure can be presented as (The Spatial Harmonic Expansion)*

$$E(x,y,z) = \sum_{n=-\infty}^{\infty} E_{pn}(x,y)e^{-j\beta_n z} \tag{2.6}$$

where $$\beta_n = \beta + \frac{2n\pi}{d}. \tag{2.7}$$

Each term in this expansion is called a spatial harmonic (or a Hartree harmonic) and has a propagation phase constant β_n.

2.5.2 Partial Sums in Floquet Harmonic Expansion

Since Floquet theorem should be stated in Fourier series expansion, it would be a good idea to investigate how they can be truncated. Generally, in complex Fourier series expansion, the number of complex terms should be infinite. However, for computational purpose they must be truncated. Therefore, this question may arise that how many numbers is enough to have a good approximation. In follow, there is an investigation to find out which partial sum has a good approximation for the exponential function

$$y = e^{-x} \qquad -\pi < x < \pi. \tag{2.8}$$

This function can be expressed in Fourier series

$$y = \frac{\sinh \pi}{\pi} \sum_{n=-\infty}^{\infty} (-1)^n \frac{1-jn}{n^2+1} e^{jnx}. \tag{2.9}$$

The corresponding truncated sum (partial sum) is

$$y_n = \frac{\sinh \pi}{\pi} \sum_{n=-N}^{N} (-1)^n \frac{1-jn}{n^2+1} e^{jnx} \tag{2.10}$$

and we sketched the related graphs for different values of N in Fig. 1.2 and Fig.2.2.

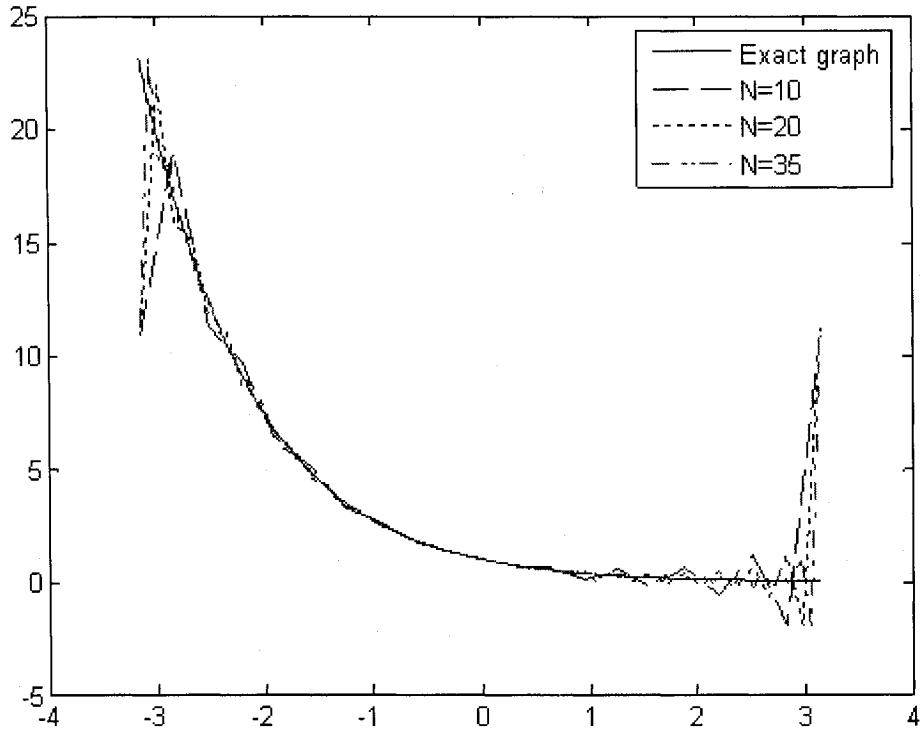

Fig 2.4: Graphs of periodic $y=e^{-x}$ in $-\pi<x<\pi$ in terms of partial summation in Fourier Expansion

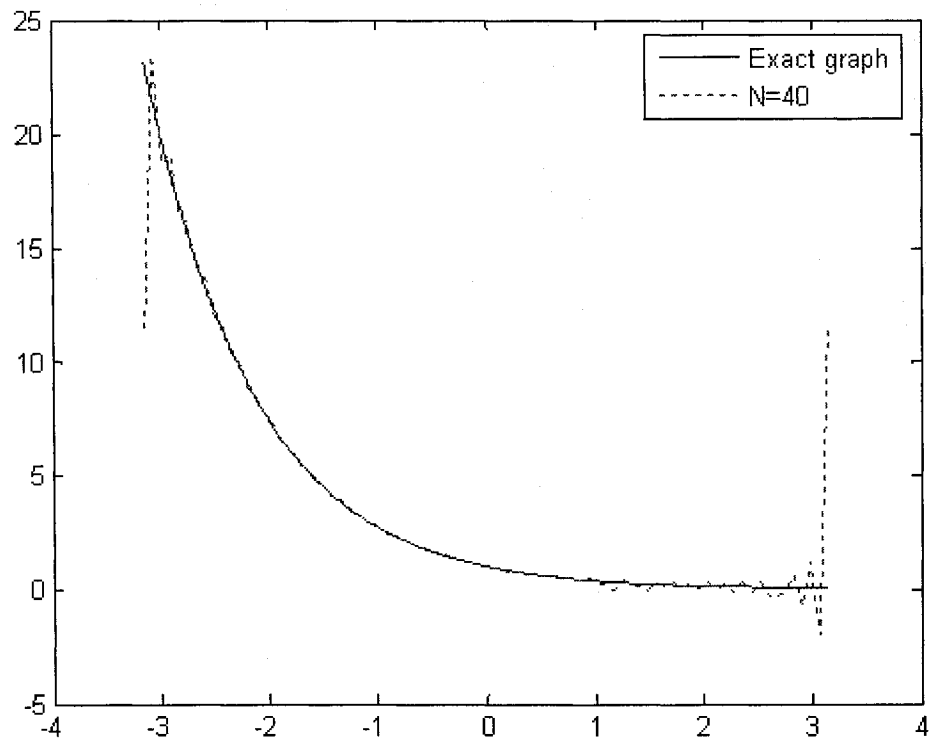

Fig 2.5: The graph of periodic $y=e^{-x}$ in $-\pi<x<\pi$ when there are N=40 terms contributed in partial summation.

These graphs show this fact that by increasing the number of Fourier terms, we will reach a good representation of the function. Roughly, the number of 35 or 40 term is accurate enough. However, they has pronounced spikes near the discontinuities at $x = -\pi$ and $x = \pi$. This overshooting by the partial sums from the functional values near a point of discontinuity is known as **Gibbs phenomenon**. This phenomenon remains fairly constant, if not worse, even when the value N is taken to be large. However, when there is no discontinuity in the boundary of physical problem such as periodic structures in EM, the Gibbs effect never happens.

2.6 Boundary Conditions for Planar Structures

A complete set of boundary conditions at the interface for planar structures such as microstrip line, fin-lines, strip grating, FSS surfaces and array of patches consists of following equations.

(1) $E_{x1} = E_{x2}$ on the interface

(2) $E_{z1} = E_{z2}$ on the interface

(3) $E_{x1} = \begin{cases} 0 & \text{on the strip} \\ f(x) & \text{on the aperture} \end{cases}$

(4) $E_{z1} = \begin{cases} 0 & \text{on the strip} \\ g(x) & \text{on the aperture} \end{cases}$

(5) $H_{x1} - H_{x2} = \begin{cases} J_z(x) & \text{on the strip} \\ 0 & \text{on th eaperture} \end{cases}$

(6) $H_{z1} - H_{z2} = \begin{cases} J_x(x) & \text{on the strip} \\ 0 & \text{on the aperture} \end{cases}$

(7) *Edge Condition*

(8) *Radiation Condition*

(9) *Periodical Boundary Condition*

Edge Condition: Another situation, where the solution of Maxwell's equations may not be unique, arises when the configuration of the problem contains geometrical singularities, such as sharp edge. The additional physical condition needed here, known as an edge condition, is supplied by the requirement that the electric and magnetic energies stored in any finite neighborhood of the edge must be finite [25]. It can be simply stated that the component of surface J (the current on the strip or patch) which is parallel to the edge should be infinity, and the component of surface J which is perpendicular to the edge should be zero. Also, the component of tangential E (the electric field on the aperture or slot) which is parallel to the edge should be zero, and the component of tangential E which is perpendicular to the edge should be infinity.

Radiation Condition: In an unbounded space with all sources contained in a finite region, the additional constraint that governs the behavior of the fields at infinity is stated in terms of the radiation condition, which may be applied in one of two ways. If the medium in the space is lossy, we require that the fields vanish at infinity. If the medium is lossless and isotropic, the behavior of the fields at infinity is governed by the Sommerfield radiation condition [25], [34]. When the fields in open direction are expressed in terms of exponential or hyperbolic functions, most of the time this condition has been met. In some structures, a shield of PEC is put on the top of the structure to

meet this condition. In some situation, radiation condition can be involved as a proper sign in square root that we will be explained in section 2.6.

Periodical Boundary Condition: When there is a periodicity in the structure, the boundaries that are perpendicular to the direction of periodicity should be regarded as periodical boundaries. It means that they must comply with Floquet theorem in that there is a phase shift between electric or magnetic fields at such walls. If, in full wave formulations, the fields have been written in terms of Floquet harmonics, this condition has already been considered.

As a general rule, more BC's we involve to match two fields in two media, more accuracy we obtain in results. Since more BC's get involved in MoM than those in MM, the results of MoM are more accurate than those from MM.

2.7 Classical Example of Mode Matching Technique

Generally, the mode matching technique consists of three important steps: First the electric and magnetic fields should be written as an expansion of normal modes in each region, second the electric and magnetic fields should be matched through proper boundary conditions which leads to some equations, and third the equations which are resulted from boundary conditions should be transformed into an infinite set of homogeneous simultaneous equations for unknown variables via the conventional technique of taking a scalar product with a complete set of functions appropriate for the various regions. The solution for phase constant may then be determined by seeking the zeros of the determinant associated with the above matrix equation. However, the relative

convergence should be taken care of by choosing appropriate truncation for the number of modes.

The purpose of this section is to get familiar with classic modal analysis (or mode matching technique). Modal analysis is a rigorous and versatile technique that can be applied to many coax, waveguide, and planar transmission line discontinuity problems, and lends itself well to computer implementation. The instructive version of mode matching method is typically applied to the problem of scattering into wave guiding structures on both sides discontinuity. We will present the technique of modal analysis by applying it to the problem containing an H-plane step (change in width) in rectangular waveguide.

The geometry of the H-plane step is shown in the Fig.2.6. It is assumed that only the dominant TE_{10} mode is propagating in the guide 1 ($z < 0$), and that such a mode is incident on the junction from $z < 0$. Because there is no y variation introduced by this discontinuity, TE_{nm} modes for $m > 0$ are not excited, nor are any TM modes. A more general discontinuity, however, may excite such modes.

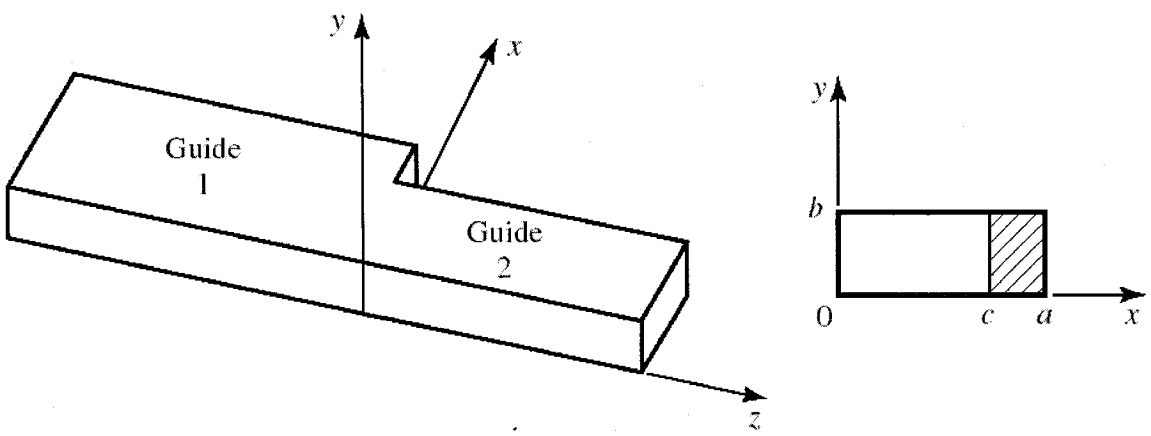

Fig 2.6: H-plane discontinuty in a rectangular waveguide [24].

The transverse fields in each region can be written; however; a care should be taken in writing the fields in the guide region (1), because they consist of the incident TE_{10} field in addition to reflected fields:

$$E_y^{(1)} = \sin\frac{\pi x}{a} e^{j\beta_1^{(1)} z} + \sum_{n=1}^{\infty} A_n \sin\frac{n\pi x}{a} e^{j\beta_n^{(1)} z} \tag{2.11a}$$

$$E_y^{(2)} = \sum_{n=1}^{\infty} B_n \sin\frac{n\pi x}{c} e^{j\beta_n^{(2)} z} \tag{2.11b}$$

$$H_x^{(1)} = \frac{-1}{Z_1^{(1)}} \sin\frac{\pi x}{a} e^{j\beta_1^{(1)} z} + \sum_{n=1}^{\infty} \frac{A_n}{Z_n^{(1)}} \sin\frac{n\pi x}{a} e^{j\beta_n^{(1)} z} \tag{2.11c}$$

$$H_x^{(2)} = \sum_{n=1}^{\infty} \frac{B_n}{Z_n^{(2)}} \sin\frac{n\pi x}{c} e^{j\beta_n^{(2)} z} \tag{2.11d}$$

$$\beta_n^{(1)} = \sqrt{k_0^2 - \left(\frac{n\pi}{a}\right)^2} \tag{2.12a}$$

$$\beta_n^{(2)} = \sqrt{k_0^2 - \left(\frac{n\pi}{c}\right)^2} \tag{2.12b}$$

$$Z_n^{(1)} = \frac{k_0 \eta_0}{\beta_n^{(1)}} \tag{2.12c}$$

$$Z_n^{(2)} = \frac{k_0 \eta_0}{\beta_n^{(2)}} \tag{2.12d}$$

where A_n and B_n are the unknown amplitude coefficient of the reflected and transmitted TE_{n0} mode in guide (1) and (2) respectively.

Now at z = 0, due to the boundary condition, the transverse fields E_y and H_x must be continuous for $0 < x < c$; in addition, E_y must be zero for $c < x < a$ because of the step. Enforcing these boundary conditions leads to the following equations:

$$E_y = \sin\frac{\pi x}{a} + \sum_{n=1}^{\infty} A_n \sin\frac{n\pi x}{a} = \begin{cases} \sum_{n=1}^{\infty} B_n \sin\frac{n\pi x}{c} & 0 < x < c \\ 0 & c < x < a \end{cases} \tag{2.13}$$

$$H_x = \frac{-1}{Z_1^{(1)}}\sin\frac{\pi x}{a} + \sum_{n=1}^{\infty}\frac{A_n}{Z_n^{(1)}}\sin\frac{n\pi x}{a} = \sum_{n=1}^{\infty}\frac{B_n}{Z_n^{(2)}}\sin\frac{n\pi x}{c} \qquad 0 < x < c \tag{2.14}$$

Equations (2.11) and (2.12) represent a doubly infinite set of linear equations for the modal coefficients A_n and B_n. The next step is to eliminate the x dependence in above equations. To do this, we use the orthogonality of sine functions. Here, we have two orthogonal sets, the first is $\left\{\sin\frac{m\pi x}{a}\right\}$ which is called the wide set and the second is $\left\{\sin\frac{m\pi x}{c}\right\}$ which is called the narrow set. As a general rule, we multiply the B.Cs for E field with the orthogonal functions of the wider set and we multiply the B.Cs for H field with the modes of the narrower set. Then, we can take integral from each equations over the proper intervals at which they are orthogonal. Now, we have to truncate the number of modes and equations to form a linear system of equations, so we choose N modes and N equations for each equation. Finally, we will end up with 2N unknowns A_n and B_n and 2N equations, and they can be solved by computer implementation [24].

2.8 Roots of Determinants

2.8.1 Matrix Equation

Many applications of existing numerical methods for analyzing electromagnetic problems, particularly Method of Moment or Mode Matching technique, lead to a linear homogenous system of equations which is denoted by a matrix notation as follows

$$\mathbf{A}(f,\beta)\mathbf{X} = \mathbf{0} \tag{2.15}$$

where **X** is the vector of the unknown coefficients (amplitudes in mode matching or coefficients of the basis functions in moment method) and the entries of **A** can be real or complex.

The electromagnetic problem is satisfied only if (2.15) presents a nontrivial solution, i.e., if the determinant of **A** vanishes. Therefore, the calculation of the dispersion curve is based on the solution of equation $\det(A(f,\beta)) = 0$.

The most common strategy to solve this problem is based on the calculation of the frequency points where the determinant of the matrix **A** vanishes. By considering a given propagation constant (even in complex plane), the frequency range is scanned with a given frequency step in order to find the zeros of determinant. However, if the propagation constant β is real (traveling wave), it doesn't matter we start from given f or β and then seeking the roots of determinant in terms of other one. The nature of the mode matching technique is based on giving the frequency and then finding the β such that the pair (f, β) sets the determinant zero. There are three ways to find the solution of singularity; we can set the determinant, the smallest eigenvalue or the smallest singular value to zero.

2.8.2 Logarithm of the Absolute Value of Determinant

This approach is the first one that looks straightforward to be done. It is common practice to vary the unknown parameters until $\det(A(f,\beta)) = 0$. However, this approach doesn't work well when we deal with a large matrix which it is the case in mode matching technique. The case will be worse when we have a sparse matrix, i.e. only a relatively small number of matrix's elements are nonzero. If the dimension of a matrix increase or the matrix has so many small value entries, it becomes more ill-conditional. When the matrix of the numerical method is so badly conditioned such that its determinant is so small, i.e. 10^{-100}, then we would never trust any results that we get from that method. The meaning of "ill-condition" will be discussed in section 2.8.4. Another disadvantage of this approach is that the determinant is a rapidly changing function of the parameter such that sometimes we are unable to find the notch in the determinant.

2.8.3 Smallest Eigenvalue in Magnitude

Since the product of eigenvalues of a matrix is equal to its determinant, when the determinant is zero it means that at least one of the eigenvalues is definitely zero. As it is zero, this eigenvalue is the smallest one in magnitude. Thus, instead of looking for when the determinant becomes zero, we can look for when the smallest eigenvalue is zero. This approach is more reliable because we get rid of so many eigenvalues which makes the matrix more ill-conditioned.

2.8.4 Smallest Singular Value

This method is based on singular value decomposition which is a powerful algorithm for dealing with the ill-conditional matrix. Formally, the *condition number* of a matrix is defined as the ratio of the largest singular value (in magnitude) to the smallest singular value. A matrix is singular if its condition number is infinite, and it is *ill-conditioned* if its condition number is too large.

It is demonstrated that by detecting the minima of the minimum singular value, instead of the zeros of the system determinant, the accuracy of the calculation increases [35]. This procedure provides numerical stability than others and we will discuss it in the next section.

SVD methods are based on the following theorem of linear algebra, whose proof is beyond this work:

*Any $M \times N$ matrix **A** with real or complex elements whose number of rows M is greater than or equal to its number of columns N ($M \geq N$), can be written as the product of an $M \times N$ column-orthogonal matrix **W**, and $N \times N$ diagonal matrix **S** with positive or zero elements in decreasing order (the singular values), and the transpose conjugate of an $N \times N$ orthogonal matrix **V**:*

$$[\mathbf{A}]_{M\times N} = [\mathbf{W}]_{M\times N}[\mathbf{S}]_{N\times N}[\mathbf{V}]_{N\times N}^{T} \tag{2.16}$$

As a matter of fact, the square of the singular values of the matrix **A** are eigenvalues of the matrix $\mathbf{AA}^{\mathrm{T}}$ where **A** is an arbitrary $M \times N$ matrix. Since $\mathbf{AA}^{\mathrm{T}}$ is a symmetric and positive definite matrix, its eigenvlues are real and nonnegative. Thus, the singular values of any square matrix are real and nonnegative [36].

For a square matrix **A** which is the case for most numerical problems related to microwave and electromagnetic, the singular values σ_1 to σ_N are real. The algorithm now searches for the minima of the last element σ_N of the diagonal matrix **S** according to the following theorem:

$$\sigma_N = 0 \Leftrightarrow \det(\mathbf{A}) = 0 . \tag{2.17}$$

Detecting the minima of σ_N is extremely simple and far more reliable than the search for zeros of $\det(\mathbf{A})$ [35]. Moreover, if these equations $\sigma_N = 0$ or $\det(\mathbf{A}) = 0$ satisfy, the last column of **[V]** automatically contains the corresponding solution vector **X** in homogenous equation of **A.X=0**. The comparison of these three methods will come later in chapter 4.

Chapter 3

Formulation of the Problem

This chapter contains three sections. The necessary assumptions to model the problem are presented in section 3.1. In section 3.2, we explain the essential steps to derive formulations pertaining to the simple shielded microstrip line, in addition to the computational technique to obtain the final matrix by MM-PM technique in this structure. Then, in section 3.3, the same procedure is extended for 1-D planar periodic structure (strip grating).

3.1 Assumption

For both structures, it is assumed that the fields are time-harmonic with a $e^{j\omega t}$ dependence, and the wave is traveling along the +z direction with the objective to find the dispersion curve along this direction. Furthermore, both structures are assumed to be uniform and infinitely long in the z direction. By saying axial uniformity we mean that cross-sectional shape and electrical properties do not vary along the z axis. Also, the regions are homogenous and source-free. The strips are perfect conductors with ignorable thickness. Moreover, the substrate is a lossless dielectric. The geometry is well-expressed in rectangular coordinate, so we use rectangular coordinate for this problem.

3.2 Microstrip Line

The open microstrip line can be analyzed as a boundary-value problem using modal solutions of the form used for the partially filled waveguide or dielectric covered ground plane. In fact, the open microstrip line can be represented as a partially filled waveguide with the addition of a center conductor placed along the air-dielectric interface, as shown in Fig.3.1. This shielded configuration is considered a good model for the open microstrip provided that the dimensions of h and L of the waveguide are equal to or greater than about 10 to 20 times the center conductor strip width. As the waveguide width and height are chosen to be even greater, the results of the open and shielded microstrip lines agree even better [30].

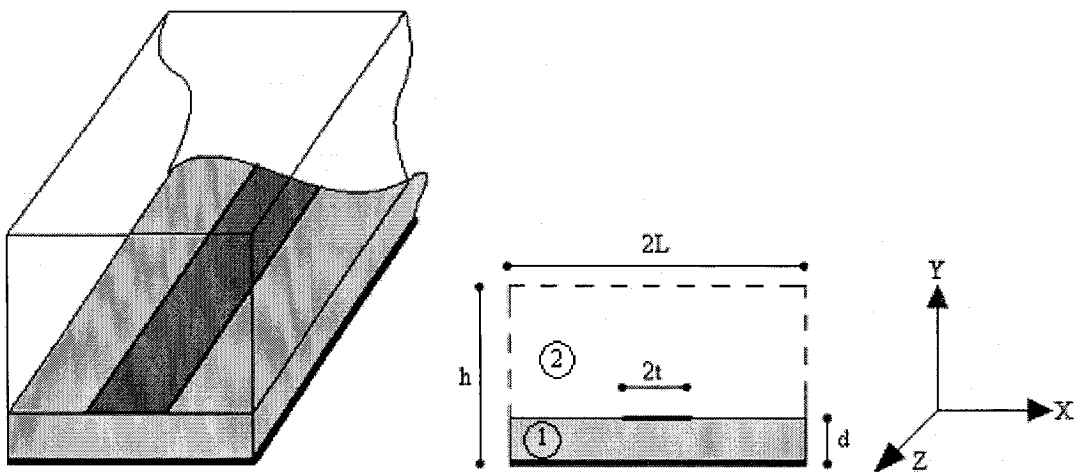

Fig.3.1: Shielded Microstrip Line

3.2.1 Electromagnetic Fields in Microstrip Line

The field configurations of this structure that satisfy all the boundary conditions are hybrid modes that are a superposition of TE^z and TM^z modes. Since the structure on the study is homogeneous and source-free in each region, the waves can be decomposed into TE^z and TM^z modes. It has been assumed that waves are traveling along z-direction. Initially the auxiliary vector potentials which are mentioned in chapter 2 are used to derive the EM fields. Because of the separation of variables and traveling wave in the z direction, we can write,

$$TM^z: \qquad \overline{\mathbf{A}}_i = \hat{a}_z A_{z(i)}(x,y,z) = \hat{a}_z \psi_i^{(e)}(x,y) e^{-j\beta_z z} \tag{3.1}$$

$$TE^z: \qquad \overline{\mathbf{F}}_i = \hat{a}_z F_{z(i)}(x,y,z) = \hat{a}_z \psi_i^{(h)}(x,y) e^{-j\beta_z z} \tag{3.2}$$

where i refers to the two media; $i=1$ is for dielectric region and $i=2$ is for air region in Fig. 3.1.

The scalar function of $\psi(x,z)$ must satisfy the transverse wave equation. This equation has been obtained by letting the potential vectors of **A** and **F** in Helmholtz equations:

$$TM^z: \left(\frac{\partial^2 \psi_i^{(e)}}{\partial x^2} + \frac{\partial^2 \psi_i^{(e)}}{\partial y^2}\right) + \left(k_i^2 - \beta_z^2\right)\psi_i^{(e)} = 0, \quad i=1, 2 \tag{3.3}$$

$$TE^z: \left(\frac{\partial^2 \psi_i^{(h)}}{\partial x^2} + \frac{\partial^2 \psi_i^{(h)}}{\partial y^2}\right) + \left(k_i^2 - \beta_z^2\right)\psi_i^{(h)} = 0, \quad i=1, 2 \tag{3.4}$$

where

$$k_1 = \sqrt{\varepsilon_r} k_0 = \omega\sqrt{\varepsilon_r \varepsilon_0 \mu_0} \tag{3.5 a}$$

$$k_2 = k_0 = \omega\sqrt{\varepsilon_0 \mu_0} \tag{3.5 b}$$

are wavenumbers in region 1 and 2, and k_0 is the free space wavenumber. The superscripts of (e) and (h) above ψ functions indicate the TM mode (E-wave) and TE mode (H-wave) respectively.

Invoking separation of variables technique and some manipulations, $\psi(x,y)$ functions can be written as follows for region i=1 (dielectric) and region i=2 (air).

$$\psi_{1n}^{(e)} = \left[A_1^{(e)}\cos(\beta_{x(1)}^{(e)}x) + B_1^{(e)}\sin(\beta_{x(1)}^{(e)}x)\right]\left[C_1^{(e)}\cos(\beta_{y(1)}^{(e)}y) + D_1^{(e)}\sin(\beta_{y(1)}^{(e)}y)\right] \quad (3.6)$$

$$\psi_{1n}^{(h)} = \left[A_1^{(h)}\cos(\beta_{x(1)}^{(h)}x) + B_1^{(h)}\sin(\beta_{x(1)}^{(h)}x)\right]\left[C_1^{(h)}\cos(\beta_{y(1)}^{(h)}y) + D_1^{(h)}\sin(\beta_{y(1)}^{(h)}y)\right] \quad (3.7)$$

$$\psi_{2n}^{(e)} = \left[A_2^{(e)}\cos(\beta_{x(2)}^{(e)}x) + B_2^{(e)}\sin(\beta_{x(2)}^{(e)}x)\right]\left[C_2^{(e)}\cos(\beta_{y(2)}^{(e)}(h-y)) + D_2^{(e)}\sin(\beta_{y(2)}^{(e)}(h-y))\right] \quad (3.8)$$

$$\psi_{2n}^{(h)} = \left[A_2^{(h)}\cos(\beta_{x(2)}^{(h)}x) + B_2^{(h)}\sin(\beta_{x(2)}^{(h)}x)\right]\left[C_2^{(h)}\cos(\beta_{y(2)}^{(h)}(h-y)) + D_2^{(h)}\sin(\beta_{y(2)}^{(h)}(h-y))\right] \quad (3.9)$$

The unknown eigenvalues of $\beta_{x(i)}$, $\beta_{y(i)}$ and β_z must satisfy the below constraint equation.

$$\beta_{x(i)}^2 + \beta_{y(i)}^2 + \beta_z^2 = k_i^2, \text{ i=}1, 2 \quad (3.10)$$

The fields can be written in terms of $\psi_i(x,y)$ [30], and after normalizing by the factor of $\frac{-\beta_z}{\omega\mu_0\varepsilon_0}$, they reduce to the expressions given in table 3.1:

TM^z	TE^z
$E_{x(i)}^{(e)} = \frac{1}{\varepsilon_{r(i)}} \frac{\partial \psi_i^{(e)}}{\partial x} e^{-j\beta_z z}$	$E_{x(i)}^{(h)} = \frac{\omega \mu_0}{\beta_z \varepsilon_{r(i)}} \frac{\partial \psi_i^{(h)}}{\partial y} e^{-j\beta_z z}$
$E_{y(i)}^{(e)} = \frac{1}{\varepsilon_{r(i)}} \frac{\partial \psi_i^{(e)}}{\partial y} e^{-j\beta_z z}$	$E_{y(i)}^{(h)} = \frac{-\omega \mu_0}{\beta_z \varepsilon_{r(i)}} \frac{\partial \psi_i^{(h)}}{\partial x} e^{-j\beta_z z}$
$E_{z(i)}^{(e)} = \frac{j}{\varepsilon_{r(i)}} \frac{k_i^2 - \beta_z^2}{\beta_z} \psi_i^{(e)} e^{-j\beta_z z}$	$E_{z(i)}^{(h)} = 0$
$H_{x(i)}^{(e)} = \frac{-\omega \varepsilon_0}{\beta_z} \frac{\partial \psi_i^{(e)}}{\partial y} e^{-j\beta_z z}$	$H_{x(i)}^{(h)} = \frac{1}{\varepsilon_{r(i)}} \frac{\partial \psi_i^{(h)}}{\partial x} e^{-j\beta_z z}$
$H_{y(i)}^{(e)} = \frac{\omega \varepsilon_0}{\beta_z} \frac{\partial \psi_i^{(e)}}{\partial x} e^{-j\beta_z z}$	$H_{y(i)}^{(h)} = \frac{1}{\varepsilon_{r(i)}} \frac{\partial \psi_i^{(h)}}{\partial y} e^{-j\beta_z z}$
$H_{z(i)}^{(e)} = 0$	$H_{z(i)}^{(h)} = \frac{j}{\varepsilon_{r(i)}} \frac{k_i^2 - \beta_z^2}{\beta_z} \psi_i^{(h)} e^{-j\beta_z z}$

Table 3.1: The Fields' formulation in shielded microstrip line, i=1, 2 for dielectric and air region respectively.

Now, we should force metallic periphery boundary conditions on E-fields for each TM and TE configuration separately to simplify the equations (3.6)-(3.9). Thus, the tangential components of electric fields for each *TM* and *TE* modes should vanish over metallic walls.

- ***TE* mode in region 1 ($\psi_1^{(h)}$):**

$$E_{x(1)}^{(h)}(y=0) = 0 \rightarrow \left.\frac{\partial \psi_1^{(h)}}{\partial y}\right|_{y=0} = 0 \rightarrow D_1^{(h)} = 0$$

$$E_{y(1)}^{(h)}(x=\pm L) = 0 \rightarrow \left.\frac{\partial \psi_1^{(h)}}{\partial x}\right|_{y=\pm L} = 0 \rightarrow \begin{cases} A_1^{(h)} \sin(\beta_{x(1)}^{(h)} L) + B_1^{(h)} \cos(\beta_{x(1)}^{(h)} L) = 0 \\ -A_1^{(h)} \sin(\beta_{x(1)}^{(h)} L) + B_1^{(h)} \cos(\beta_{x(1)}^{(h)} L) = 0 \end{cases}$$

Adding and subtracting above equations, two solutions can be found:

$$A_1^{(h)} = 0, \cos(\beta_{x(1)}^{(h)} L) = 0 \rightarrow A_1^{(h)} = 0, \beta_{x(1)n}^{(h)} L = (2n-1)\frac{\pi}{2} \rightarrow A_1^{(h)} = 0,\ \beta_{x(1)n}^{(h)} = (2n-1)\frac{\pi}{2L}$$

$$B_1^{(h)} = 0, \sin(\beta_{x(1)}^{(h)} L) = 0 \rightarrow B_1^{(h)} = 0, \beta_{x(1)n}^{(h)} L = n\pi \rightarrow B_1^{(h)} = 0,\ \beta_{x(1)n}^{(h)} = n\frac{\pi}{L}$$

The parameter n is an integer which can be $n = 1, 2, 3....$

From the symmetry of the structure, it is clear that two orthogonal sets of modes exist, one of which has a symmetric E_z and an antisymmetric H_z components (E_z-even, H_z-odd), while the other is characterized by E_z-odd, H_z-even. The dominant mode is the lowest order E_z-even, H_z-odd which approaches the quasi-TEM solution for low frequencies. Moreover, to reduce the complexity of the problem, in what follows we consider only E_z-even, H_z-odd modes. This is the first solution mentioned above which require the tangential magnetic field components to vanish along the symmetry plane of this partially waveguide. However, the methods presented here are equally applicable to the other types of modes as well.

$E_{z(1)}^{(h)}(y = 0) = 0 \rightarrow$ *Already satisfied*

- ***TE* mode in region 2 ($\psi_2^{(h)}$):**

$$E_{x(2)}^{(h)}(y = h) = 0 \rightarrow \left.\frac{\partial \psi_2^{(h)}}{\partial y}\right|_{y=h} = 0 \rightarrow D_2^{(h)} = 0$$

$$E_{y(2)}^{(h)}(x = \pm L) = 0 \rightarrow \left.\frac{\partial \psi_2^{(h)}}{\partial x}\right|_{y=\pm L} = 0 \xrightarrow{Like\,(2)} A_2^{(h)} = 0,\ \beta_{x(2)n}^{(h)} = (2n-1)\frac{\pi}{2L}$$

$E_{z(2)}^{(h)}(y = h) = 0 \rightarrow$ *Already satisfied*

- ***TM* mode in region 1($\psi_1^{(e)}$):**

$$E_{x(1)}^{(e)}(y=0)=0 \rightarrow \left.\frac{\partial \psi_1^{(e)}}{\partial x}\right|_{y=0}=0 \rightarrow C_1^{(e)}=0$$

$$E_{y(1)}^{(e)}(x=\pm L)=0 \rightarrow \left.\frac{\partial \psi_1^{(e)}}{\partial y}\right|_{x=\pm L}=0 \xrightarrow{Like\,(2)} B_1^{(e)}=0,\ \beta_{x(1)n}^{(e)}=(2n-1)\frac{\pi}{2L}$$

$$E_{z(1)}^{(e)}(y=0)=0 \rightarrow \psi_1^{(e)}(y=0)=0 \rightarrow \textit{Automatically will be satisfied}$$

- ***TM* mode in region 2 ($\psi_2^{(e)}$):**

$$E_{x(2)}^{(e)}(y=h)=0 \rightarrow \left.\frac{\partial \psi_2^{(e)}}{\partial x}\right|_{y=h}=0 \rightarrow C_2^{(e)}=0$$

$$E_{y(2)}^{(e)}(x=\pm L)=0 \rightarrow \left.\frac{\partial \psi_2^{(e)}}{\partial y}\right|_{x=\pm L}=0 \xrightarrow{Like\,(2)} B_2^{(e)}=0,\ \beta_{x(2)n}^{(e)}=(2n-1)\frac{\pi}{2L}$$

$$E_{z(2)}^{(e)}(y=h)=0 \rightarrow \psi_2^{(e)}(y=h)=0 \rightarrow \textit{Automatically will be satisfied}$$

By substitution the above results in equations (3.6)-(3.9), the ψ function reduces to:

$$\psi_{1n}^{(h)}=\left[B_1^{(h)}\sin(\beta_{x(1)n}^{(h)}x)\right]\left[C_1^{(h)}\cos(\beta_{y(1)}^{(h)}y)\right] \tag{3.11}$$

$$\psi_{2n}^{(h)}=\left[B_2^{(h)}\sin(\beta_{x(2)n}^{(h)}x)\right]\left[C_2^{(h)}\cos(\beta_{y(2)}^{(h)}(h-y))\right] \tag{3.12}$$

$$\psi_{1n}^{(e)}=\left[A_1^{(e)}\cos(\beta_{x(1)n}^{(e)}x)\right]\left[D_1^{(e)}\sin(\beta_{y(1)}^{(e)}y)\right] \tag{3.13}$$

$$\psi_{2n}^{(e)}=\left[A_2^{(e)}\cos(\beta_{x(2)n}^{(e)}x)\right]\left[D_2^{(e)}\sin(\beta_{y(2)}^{(e)}(h-y))\right] \tag{3.14}$$

The phase constants in x-direction are denoted by k_n:

$$k_n=\beta_{x(1)n}^{(e)}=\beta_{x(2)n}^{(e)}=\beta_{x(1)n}^{(h)}=\beta_{x(2)n}^{(h)}=(2n-1)\frac{\pi}{2L},\quad n=1, 2, 3 \ldots \tag{3.15}$$

Phase constants in y-direction are denoted by $\alpha_n^{(1)}$ and $\alpha_n^{(2)}$, and according to the equation (10.3) they can be presented as follows:

$$\beta_{x(i)}^2+\beta_{y(i)}^2+\beta_z^2=k_i^2 \rightarrow \begin{cases} \text{i}=1: k_n^2+\beta_{y(1)n}^2+\beta_z^2=k_1^2=\varepsilon_r k_0^2 \\ \text{i}=2: k_n^2+\beta_{y(2)n}^2+\beta_z^2=k_2^2=k_0^2 \end{cases} \rightarrow$$

$$\begin{cases} \beta_{y(1)n}^2=k_1^2-(k_n^2+\beta_z^2) \\ \beta_{y(1)n}^2=k_2^2-(k_n^2+\beta_z^2) \end{cases} \rightarrow \begin{cases} \beta_{y(1)n}^{(e)}=\beta_{y(1)n}^{(h)}=\sqrt{k_1^2-(k_n^2+\beta_z^2)}=j\sqrt{(k_n^2+\beta_z^2)-k_1^2} \\ \beta_{y(2)n}^{(e)}=\beta_{y(2)n}^{(h)}=\sqrt{k_2^2-(k_n^2+\beta_z^2)}=j\sqrt{(k_n^2+\beta_z^2)-k_2^2} \end{cases}$$

$$\alpha_n^{(1)}=-j\beta_{y(1)n}^{(e)}=-j\beta_{y(1)n}^{(h)}=\sqrt{(k_n^2+\beta_z^2)-\varepsilon_r k_0^2} \tag{3.16a}$$

$$\alpha_n^{(2)}=-j\beta_{y(2)n}^{(e)}=-j\beta_{y(2)n}^{(h)}=\sqrt{(k_n^2+\beta_z^2)-k_0^2} \tag{3.16b}$$

Why the negative sign was chosen for square root will come at the end of section 3.3.2.

Now, the total ψ functions are the summations on ψ_n in equations (3.11)-(3.14), so after some rearrangements ultimately they can be written as:

$$\psi_1^{(h)}=\sum_{n=1}^{\infty}A_n^{(h)}\sin(k_n x)\cosh(\alpha_n^{(1)}y) \tag{3.17}$$

$$\psi_2^{(h)}=\sum_{n=1}^{\infty}B_n^{(h)}\sin(k_n x)\cosh(\alpha_n^{(2)}(h-y)) \tag{3.18}$$

$$\psi_1^{(e)}=\sum_{n=1}^{\infty}A_n^{(e)}\cos(k_n x)\sinh(\alpha_n^{(1)}y) \tag{3.18}$$

$$\psi_2^{(e)}=\sum_{n=1}^{\infty}B_n^{(e)}\cos(k_n x)\sinh(\alpha_n^{(2)}(h-y)) \tag{3.19}$$

Consequently, the total fields for each *TE* and *TM* modes in each region are given by equations (3.20a)-(3.21*l*). For the sake of simplicity, we can consider the new variables of $\frac{A_n^{(h)}}{\varepsilon_r}\rightarrow A_n^{(h)}$ and $\frac{A_n^{(e)}}{\varepsilon_r}\rightarrow A_n^{(e)}$ instead of the previous $A_n^{(h)}$ and $A_n^{(e)}$.

- **TE fields**

$$E_{x(1)}^{(h)} = \frac{\omega\mu_0}{\beta_z}\left(\sum_{n=1}^{\infty} A_n^{(h)}\alpha_n^{(1)}\sin(k_n x)\sinh(\alpha_n^{(1)} y)\right)e^{-j\beta_z z} \tag{3.20a}$$

$$E_{x(2)}^{(h)} = \frac{-\omega\mu_0}{\beta_z}\left(\sum_{n=1}^{\infty} B_n^{(h)}\alpha_n^{(2)}\sin(k_n x)\sinh(\alpha_n^{(2)}(h-y))\right)e^{-j\beta_z z} \tag{3.20b}$$

$$E_{y(1)}^{(h)} = \frac{-\omega\mu_0}{\beta_z}\left(\sum_{n=1}^{\infty} A_n^{(h)}k_n\cos(k_n x)\cosh(\alpha_n^{(1)} y)\right)e^{-j\beta_z z} \tag{3.20c}$$

$$E_{y(2)}^{(h)} = \frac{-\omega\mu_0}{\beta_z}\left(\sum_{n=1}^{\infty} B_n^{(h)}k_n\cos(k_n x)\cosh(\alpha_n^{(2)}(h-y))\right)e^{-j\beta_z z} \tag{3.20d}$$

$$E_{z(1)}^{(h)} = 0 \tag{3.20e}$$

$$E_{z(2)}^{(h)} = 0 \tag{3.20f}$$

$$H_{x(1)}^{(h)} = \left(\sum_{n=1}^{\infty} A_n^{(h)}k_n\cos(k_n x)\cosh(\alpha_n^{(1)} y)\right)e^{-j\beta_z z} \tag{3.20g}$$

$$H_{x(2)}^{(h)} = \left(\sum_{n=1}^{\infty} B_n^{(h)}k_n\cos(k_n x)\cosh(\alpha_n^{(2)}(h-y))\right)e^{-j\beta_z z} \tag{3.20h}$$

$$H_{y(1)}^{(h)} = \left(\sum_{n=1}^{\infty} A_n^{(h)}\alpha_n^{(1)}\sin(k_n x)\sinh(\alpha_n^{(1)} y)\right)e^{-j\beta_z z} \tag{3.20i}$$

$$H_{y(2)}^{(h)} = -\left(\sum_{n=1}^{\infty} B_n^{(h)}\alpha_n^{(2)}\sin(k_n x)\sinh(\alpha_n^{(2)}(h-y))\right)e^{-j\beta_z z} \tag{3.20j}$$

$$H_{z(1)}^{(h)} = j\frac{k_1^2-\beta_z^2}{\beta_z}\left(\sum_{n=1}^{\infty} A_n^{(h)}\sin(k_n x)\cosh(\alpha_n^{(1)} y)\right)e^{-j\beta_z z} \tag{3.20k}$$

$$H_{z(2)}^{(h)} = j\frac{k_2^2-\beta_z^2}{\beta_z}\left(\sum_{n=1}^{\infty} B_n^{(h)}\sin(k_n x)\cosh(\alpha_n^{(2)}(h-y))\right)e^{-j\beta_z z} \tag{3.20l}$$

- **TM fields**

$$E_{x(1)}^{(e)} = -\left(\sum_{n=1}^{\infty} A_n^{(e)} k_n \sin(k_n x)\sinh(\alpha_n^{(1)} y)\right) e^{-j\beta_z z} \tag{3.21a}$$

$$E_{x(2)}^{(e)} = -\left(\sum_{n=1}^{\infty} B_n^{(e)} k_n \sin(k_n x)\sinh(\alpha_n^{(2)} (h-y))\right) e^{-j\beta_z z} \tag{3.21b}$$

$$E_{y(1)}^{(e)} = \left(\sum_{n=1}^{\infty} A_n^{(e)} \alpha_n^{(1)} \cos(k_n x)\cosh(\alpha_n^{(1)} y)\right) e^{-j\beta_z z} \tag{3.21c}$$

$$E_{y(2)}^{(e)} = -\left(\sum_{n=1}^{\infty} B_n^{(e)} \alpha_n^{(2)} \cos(k_n x)\cosh(\alpha_n^{(2)} (h-y))\right) e^{-j\beta_z z} \tag{3.21d}$$

$$E_{z(1)}^{(e)} = j\frac{k_1^2 - \beta_z^2}{\beta_z}\left(\sum_{n=1}^{\infty} A_n^{(e)} \cos(k_n x)\sinh(\alpha_n^{(1)} y)\right) e^{-j\beta_z z} \tag{3.21e}$$

$$E_{z(2)}^{(e)} = j\frac{k_2^2 - \beta_z^2}{\beta_z}\left(\sum_{n=1}^{\infty} B_n^{(e)} \cos(k_n x)\sinh(\alpha_n^{(2)} (h-y))\right) e^{-j\beta_z z} \tag{3.21f}$$

$$H_{x(1)}^{(e)} = \frac{-\omega\varepsilon_1}{\beta_z}\left(\sum_{n=1}^{\infty} A_n^{(e)} \alpha_n^{(1)} \cos(k_n x)\cosh(\alpha_n^{(1)} y)\right) e^{-j\beta_z z} \tag{3.21g}$$

$$H_{x(2)}^{(e)} = \frac{\omega\varepsilon_0}{\beta_z}\left(\sum_{n=1}^{\infty} B_n^{(e)} \alpha_n^{(2)} \cos(k_n x)\cosh(\alpha_n^{(2)} (h-y))\right) e^{-j\beta_z z} \tag{3.21h}$$

$$H_{y(1)}^{(e)} = \frac{-\omega\varepsilon_1}{\beta_z}\left(\sum_{n=1}^{\infty} A_n^{(e)} k_n \sin(k_n x)\sinh(\alpha_n^{(1)} y)\right) e^{-j\beta_z z} \tag{3.21i}$$

$$H_{y(2)}^{(e)} = \frac{-\omega\varepsilon_0}{\beta_z}\left(\sum_{n=1}^{\infty} B_n^{(e)} k_n \sin(k_n x)\sinh(\alpha_n^{(2)} (h-y))\right) e^{-j\beta_z z} \tag{3.21j}$$

$$H_{z(1)}^{(e)} = 0 \tag{3.21k}$$

$$H_{z(2)}^{(e)} = 0 \tag{3.21l}$$

As mentioned before [31], the final fields are the superposition of TE and TM fields:

$$E_{x(1)} = \left(\sum_{n=1}^{\infty} \left(-A_n^{(e)} k_n + \frac{\omega\mu_0}{\beta_z} A_n^{(h)} \alpha_n^{(1)} \right) \sin(k_n x) \sinh(\alpha_n^{(1)} y) \right) e^{-j\beta_z z} \tag{3.22a}$$

$$E_{x(2)} = \left(\sum_{n=1}^{\infty} \left(-B_n^{(e)} k_n - \frac{\omega\mu_0}{\beta_z} B_n^{(h)} \alpha_n^{(2)} \right) \sin(k_n x) \sinh(\alpha_n^{(2)} (h-y)) \right) e^{-j\beta_z z} \tag{3.22b}$$

$$E_{y(1)} = \left(\sum_{n=1}^{\infty} \left(A_n^{(e)} \alpha_n^{(1)} - \frac{\omega\mu_0}{\beta_z} A_n^{(h)} k_n \right) \cos(k_n x) \cosh(\alpha_n^{(1)} y) \right) e^{-j\beta_z z} \tag{3.22c}$$

$$E_{y(2)} = \left(\sum_{n=1}^{\infty} \left(-B_n^{(e)} \alpha_n^{(2)} - \frac{\omega\mu_0}{\beta_z} B_n^{(h)} k_n \right) \cos(k_n x) \cosh(\alpha_n^{(2)} (h-y)) \right) e^{-j\beta_z z} \tag{3.22d}$$

$$E_{z(1)} = j \frac{k_1^2 - \beta_z^2}{\beta_z} \left(\sum_{n=1}^{\infty} A_n^{(e)} \cos(k_n x) \sinh(\alpha_n^{(1)} y) \right) e^{-j\beta_z z} \tag{3.22e}$$

$$E_{z(2)} = j \frac{k_2^2 - \beta_z^2}{\beta_z} \left(\sum_{n=1}^{\infty} B_n^{(e)} \cos(k_n x) \sinh(\alpha_n^{(2)} (h-y)) \right) e^{-j\beta_z z} \tag{3.22f}$$

$$H_{x(1)} = \left(\sum_{n=1}^{\infty} \left(\frac{-\omega\varepsilon_1}{\beta_z} A_n^{(e)} \alpha_n^{(1)} + A_n^{(h)} k_n \right) \cos(k_n x) \cosh(\alpha_n^{(1)} y) \right) e^{-j\beta_z z} \tag{3.22g}$$

$$H_{x(2)} = \left(\sum_{n=1}^{\infty} \left(\frac{\omega\varepsilon_0}{\beta_z} B_n^{(e)} \alpha_n^{(2)} + B_n^{(h)} k_n \right) \cos(k_n x) \cosh(\alpha_n^{(2)} (h-y)) \right) e^{-j\beta_z z} \tag{3.22h}$$

$$H_{y(1)} = \left(\sum_{n=1}^{\infty} \left(\frac{-\omega\varepsilon_1}{\beta_z} A_n^{(e)} k_n + A_n^{(h)} \alpha_n^{(1)} \right) \sin(k_n x) \sinh(\alpha_n^{(1)} y) \right) e^{-j\beta_z z} \tag{3.22i}$$

$$H_{y(2)} = \left(\sum_{n=1}^{\infty} \left(\frac{-\omega\varepsilon_0}{\beta_z} B_n^{(e)} k_n - B_n^{(h)} \alpha_n^{(2)} \right) \sin(k_n x) \sinh(\alpha_n^{(2)} (h-y)) \right) e^{-j\beta_z z} \tag{3.22j}$$

$$H_{z(1)} = j \frac{k_1^2 - \beta_z^2}{\beta_z} \left(\sum_{n=1}^{\infty} A_n^{(h)} \sin(k_n x) \cosh(\alpha_n^{(1)} y) \right) e^{-j\beta_z z} \tag{3.22k}$$

$$H_{z(2)} = j \frac{k_2^2 - \beta_z^2}{\beta_z} \left(\sum_{n=1}^{\infty} B_n^{(h)} \sin(k_n x) \cosh(\alpha_n^{(2)} (h-y)) \right) e^{-j\beta_z z} \tag{3.22l}$$

The coefficients $A_n^{(e)}$, $A_n^{(h)}$ (for region 1 which is dielectric), $B_n^{(e)}$ and $B_n^{(h)}$ (for region 2 which is air) are yet unknowns, and their relations will be found by applying boundary conditions along the air-dielectric interface.

3.2.2 Boundary Conditions in Microstrip Line

The next step is to apply the appropriate boundary conditions along the air-dielectric interface including the center conductor. It should be stated again that the superposition of the *TE* and *TM* modes must satisfy the BCs along this interface. Considering the symmetry with respect to the y axis, the appropriate boundary conditions along the interface for $x>0$ that must be enforced are following four equations which are mutually independent (the same apply for $x<0$):

(1) $E_{z1} = E_{z2}$ $(x,z) \in$ Whole area $0 < x < L$ (3.23)

(2) $E_{x1} = E_{x2}$ $(x,z) \in$ Whole area $0 < x < L$ (3.24)

(3) $\begin{cases} (a)\ E_{z1} = 0 & (x,z) \in \text{Patch} & 0 < x < t \\ (b)\ H_{x1} = H_{x2} & (x,z) \in \textit{Aperture} & t < x < L \end{cases}$ (3.25 a,b)

(4) $\begin{cases} (a)\ E_{x1} = 0 & (x,z) \in \text{Patch} & 0 < x < t \\ (b)\ H_{z1} = H_{z2} & (x,z) \in \textit{Aperture} & t < x < L \end{cases}$ (3.26 a,b)

Applying these equations leads to the following algebraic equations. The details of proof are given in Appendix I.

$$\begin{cases} \sum_{n=1}^{\infty} \overline{A}_n^{(e)} \cos(k_n x) = 0 & 0 < x < t \\ \sum_{n=1}^{\infty} \overline{A}_n^{(e)} k_n P_n(\beta_z) \cos(k_n x) - \sum_{n=1}^{\infty} \overline{A}_n^{(h)} k_n T_n(\beta_z) \cos(k_n x) = 0 & t < x < L \end{cases} \quad (3.27a,b)$$

$$\begin{cases} \sum_{n=1}^{\infty} \overline{A}_n^{(e)} k_n \sin(k_n x) - \sum_{n=1}^{\infty} \overline{A}_n^{(h)} k_n \sin(k_n x) = 0 & 0 < x < t \\ \sum_{n=1}^{\infty} \overline{A}_n^{(e)} Q_n(\beta_z) \sin(k_n x) - \sum_{n=1}^{\infty} \overline{A}_n^{(h)} W_n(\beta_z) \sin(k_n x) = 0 & t < x < L \end{cases} \quad (3.28\ a,b)$$

where

$$\overline{A}_n^{(e)} = A_n^{(e)} \sinh(\alpha_n^{(1)} d) \quad (3.29)$$

$$\overline{A}_n^{(h)} = \frac{\omega\mu_0}{\beta_z} \frac{\alpha_n^{(1)}}{k_n} A_n^{(h)} \sinh(\alpha_n^{(1)} d) \quad (3.30)$$

$$\overline{\beta}_z = \beta_z / k_0 \quad (3.31)$$

$$P_n(\beta_z) = \varepsilon_r \frac{\alpha_n^{(1)}}{k_n} \coth(\alpha_n^{(1)} d) + \frac{\varepsilon_r - \overline{\beta}^2}{1 - \overline{\beta}^2} \frac{\alpha_n^{(2)}}{k_n} \coth(\alpha_n^{(2)} (h-d)) + \overline{\beta}^2 \frac{\hat{k}_n}{\alpha_n^{(2)}} \frac{1-\varepsilon_r}{1-\overline{\beta}^2} \coth(\alpha_n^{(2)} (h-d))$$

$$T_n(\beta_z) = \overline{\beta}_z^{\,2} \left(\frac{k_n}{\alpha_n^{(1)}} \coth(\alpha_n^{(1)} d) + \frac{k_n}{\alpha_n^{(2)}} \coth(\alpha_n^{(2)} (h-d)) \right) \quad (3.33)$$

$$Q_n(\beta) = \frac{k_n}{\alpha_n^{(2)}} \frac{1-\varepsilon_r}{1-\overline{\beta}_z^{\,2}} \coth(\alpha_n^{(2)} (h-d)) \quad (3.34)$$

$$W_n(\beta) = \frac{\varepsilon_r - \overline{\beta}_z^{\,2}}{1-\overline{\beta}_z^{\,2}} \frac{k_n}{\alpha_n^{(1)}} \coth(\alpha_n^{(1)} d) + \frac{k_n}{\alpha_n^{(2)}} \coth(\alpha_n^{(2)} (h-d)) \quad (3.35)$$

Sine the functions $\alpha_n^{(1)} \coth(\alpha_n^{(1)} d)$, $\frac{\coth(\alpha_n^{(1)} d)}{\alpha_n^{(1)}}$ and $\frac{\coth(\alpha_n^{(2)} (h-d))}{\alpha_n^{(2)}}$ are even with respect to $\alpha_n^{(1)}$ and $\alpha_n^{(2)}$ in above expressions, the sign of $\alpha_n^{(1)}$ and $\alpha_n^{(2)}$ in the equations (3.16) and (3.17) never influences the value of the expressions in the equations (3.27 a,b) and (3.28 a,b), so the sign of the square roots in 3.16a and 3.16b doesn't matter to be plus or minus.

3.2.3 Matrix Presentation

By using point matching technique, the above equations can be reduced to a matrix format. Equations (3.27 a,b) and (3.28 a,b) need an orthogonal set to be converted to a matrix format. No entire domain orthogonal set can be found, so we resort to sub-domain orthogonal sets, and delta functions are the simplest kind of sub-domain orthogonal set.

If the ratio of t over L is r, i.e. $r = \frac{t}{L}$, the final matrix resultant is

$$\begin{matrix} rN \text{ points on the strip} \{ \\ (1-r)N \text{ points on the aperture} \{ \\ rN \text{ points on the strip} \{ \\ (1-r)N \text{ points on the aperture} \{ \end{matrix} \begin{bmatrix} \overbrace{[a_{mn}]}^{N} & \overbrace{[0]}^{N} \\ \hline [b_{mn}] & [c_{mn}] \\ \hline [d_{mn}] & [e_{mn}] \\ \hline [f_{mn}] & [g_{mn}] \end{bmatrix} \begin{bmatrix} \vdots \\ \overline{A}_n^{(e)} \\ \vdots \\ \hline \vdots \\ \overline{A}_n^{(h)} \\ \vdots \end{bmatrix} = 0 . \tag{3.36}$$

N is an integer number which truncates the limit of summation in (3.27a,b) and (3.28a,b). N, also, represents the number of matching points throughout the length L, in order to have a square matrix.

3.3 One-Dimensional Periodic Structure

The 1-D strip grating can be analyzed as a boundary-value problem using modal solutions (mode-matching). This structure is confined between two shields. The underneath shield is a ground plane. The right and left boundaries are the periodical boundaries which comply with the Floquet theorem. This shielded configuration is considered as a good model for the open structure provided that the dimensions of h of the structure is equal to or greater than about 5 or 10 times the center conductor strip

width. Moreover, when we enlarge the spatial period, we can reach to the microstrip line structure.

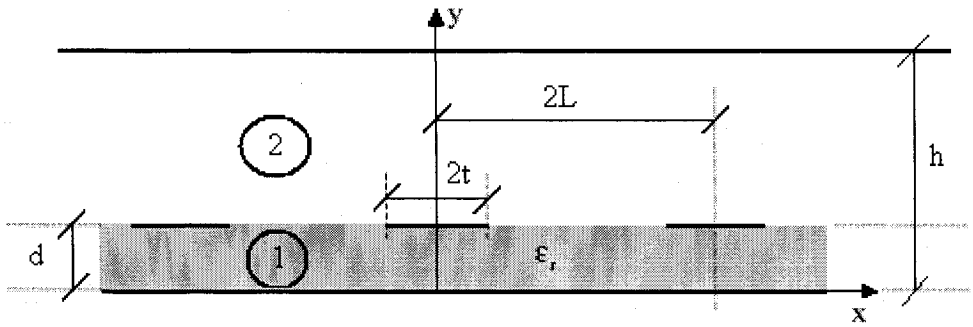

Fig. 3.2: Shielded Grating Strip which consists of periodic microstrip lines.

3.3.1 Electromagnetic Fields in 1-D Printed Periodic Structure

Like a microstrip line, the full wave analysis of this structure is made up a number of steps; however; because of the similarity to the microstrip line some steps have been pointed out very quickly.

According to the Floquet theorem (section 2.3), a typical component of the field in a periodic structure with one periodicity can be written by the summation of its Floquet harmonics. For example the electric field in a media with one periodicity in x direction can be written

$$E(x,y,z) = \sum_{n=-\infty}^{\infty} E_n(y,z)e^{-j\beta_n x} \tag{3.37}$$

where $$\beta_n = \beta_x + \frac{2n\pi}{2L},\ n=...-2,\ -1,\ 0,\ 1,\ 2... \tag{3.38}$$

This field must satisfy the Helmholtz Equation, so

$$\nabla^2 E(x,y,z) + k^2 E(x,y,z) = 0 \Rightarrow \nabla^2 \sum_{n=-\infty}^{\infty} E_n(y,z)e^{-j\beta_n x} + k^2 \sum_{n=-\infty}^{\infty} E_n(y,z)e^{-j\beta_n x} = 0 \Rightarrow$$

$$\sum_{n=-\infty}^{\infty}\left(\nabla^2 E_n(y,z)e^{-j\beta_n x}+k^2 E_n(y,z)e^{-j\beta_n x}\right)=0 \Rightarrow$$

$$\left(\sum_{n=-\infty}^{\infty}\left(\nabla^2 E_n(y,z)+(k^2-\beta_n^2)E_n(y,z)\right)\right)e^{-j\beta_n x}=0$$

Due to the orthogonally for the set of $\left\{e^{-j\beta_n x}\right\}$ in a unit cell, the coefficients should be zero, so the following equation can be obtained:

$$\nabla^2 E_n(y,z)+(k^2-\beta_n^2)E_n(y,z)=0. \tag{3.39}$$

Thus, instead of satisfying the summation, we can satisfy each Floquet wave in the Helmholtz equation.

Now, using the separation of variables technique, we can write the z component of the field in exponential format

$$E_n(y,z)=E_n(y)e^{-j\beta_z z}. \tag{3.40}$$

Then, by satisfying this field into the Helmholtz equation, it reduces to:

$$\nabla^2 E_n(y)+(k^2-\beta_z^2-\beta_n^2)E_n(y)=0. \tag{3.41}$$

The same can be applied for vector potential **A.** According to aforementioned discussion and what we explained in microstrip line, the TM and TE modes can be written

$$TM^z:\ \overline{A}_{n(i)}=\hat{a}_z A_{zn(i)}(x,y,z)=\hat{a}_z\psi_{n(i)}^{(e)}(y)e^{-j\beta_n x}e^{-j\beta_z z} \tag{3.42}$$

$$TE^z:\ \overline{F}_{n(i)}=\hat{a}_z F_{zn(i)}(x,y,z)=\hat{a}_z\psi_{n(i)}^{(h)}(y)e^{-j\beta_n x}e^{-j\beta_z z} \tag{3.43}$$

where $\beta_n=\beta_x+\dfrac{2n\pi}{2L}$ and index i refers to the two media in this way: $i=1$ is for dielectric region and $i=2$ is for air region; moreover, $2L$ is the periodicity along the x axis and β_n is the Floquet wave number in which n is an integer varying from $-\infty$ to $+\infty$.

The scalar function of $\psi(y)$ must satisfy the transverse wave equations which have been obtained by substituting the potential vectors **A** and **F** in Helmholtz equations.

$$TM^z: \frac{\partial^2 \psi_{n(i)}^{(e)}}{\partial y^2} + \left(k_i^2 - \beta_n^2 - \beta_z^2\right)\psi_{n(i)}^{(e)} = 0, \quad i=1, 2 \tag{3.44}$$

$$TE^z: \frac{\partial^2 \psi_{n(i)}^{(h)}}{\partial y^2} + \left(k_i^2 - \beta_n^2 - \beta_z^2\right)\psi_{n(i)}^{(h)} = 0, \quad i=1, 2 \tag{3.45}$$

where $k_1 = \omega\sqrt{\varepsilon_r \varepsilon_0 \mu_0}$ and $k_2 = \omega\sqrt{\varepsilon_0 \mu_0}$ (equations (3.5 a,b))

Like a microstrip line, the scalar function of $\psi(y)$ can be written as follows:

Region 1 (dielectric):

$$\psi_{n(1)}^{(e)} = A_{n(1)}^{(e)} \cos(\beta_{y(1)}^{(e)} y) + B_{n(1)}^{(e)} \sin(\beta_{y(1)}^{(e)} y) \tag{3.46}$$

$$\psi_{n(1)}^{(h)} = A_{n(1)}^{(h)} \cos(\beta_{y(1)}^{(h)} y) + B_{n(1)}^{(h)} \sin(\beta_{y(1)}^{(h)} y) \tag{3.47}$$

Region 2 (air):

$$\psi_{n(2)}^{(e)} = A_{n(2)}^{(e)} \cos(\beta_{y(2)}^{(e)} (h-y)) + B_{n(2)}^{(e)} \sin(\beta_{y(2)}^{(e)} (h-y)) \tag{3.48}$$

$$\psi_{n(2)}^{(h)} = A_{n(2)}^{(h)} \cos(\beta_{y(2)}^{(h)} (h-y)) + B_{n(2)}^{(h)} \sin(\beta_{y(2)}^{(h)} (h-y)) \tag{3.49}$$

The unknown eigenvalues of β_n, $\beta_{y(i)}$ and β_z must satisfy the below constraint equation.

$$\beta_{y(i)}^2 + \beta_n^2 + \beta_z^2 = k_i^2, \text{ i=1, 2} \tag{3.50}$$

The Floquet harmonic fields due to TM^z and TE^z configuration and normalizing by the factor $\frac{-\beta_z}{\omega\mu_0\varepsilon_0}$ can be obtained according to table 3.2 [30]:

TM^z	TE^z
$E_{xn(i)}^{(e)} = \frac{-j\beta_n}{\varepsilon_{r(i)}} \psi_{n(i)}^{(e)} e^{-j\beta_n x} e^{-j\beta_z z}$	$E_{xn(i)}^{(h)} = \frac{\omega\mu_0}{\beta_z \varepsilon_{r(i)}} \frac{\partial \psi_{n(i)}^{(h)}}{\partial y} e^{-j\beta_n x} e^{-j\beta_z z}$
$E_{yn(i)}^{(e)} = \frac{1}{\varepsilon_{r(i)}} \frac{\partial \psi_{n(i)}^{(e)}}{\partial y} e^{-j\beta_n x} e^{-j\beta_z z}$	$E_{yn(i)}^{(h)} = \frac{j\beta_n \omega\mu_0}{\beta_z \varepsilon_{r(i)}} \psi_{n(i)}^{(h)} e^{-j\beta_n x} e^{-j\beta_z z}$
$E_{zn(i)}^{(e)} = \frac{j}{\varepsilon_{r(i)}} \frac{k_i^2 - \beta_z^2}{\beta_z} \psi_{n(i)}^{(e)} e^{-j\beta_n x} e^{-j\beta_z z}$	$E_{zn(i)}^{(h)} = 0$
$H_{xn(i)}^{(e)} = \frac{-\omega\varepsilon_0}{\beta_z} \frac{\partial \psi_{n(i)}^{(e)}}{\partial y} e^{-j\beta_n x} e^{-j\beta_z z}$	$H_{xn(i)}^{(h)} = \frac{-j\beta_n}{\varepsilon_{r(i)}} \psi_{n(i)}^{(h)} e^{-j\beta_n x} e^{-j\beta_z z}$
$H_{yn(i)}^{(e)} = \frac{-j\beta_n \omega\varepsilon_0}{\beta_z} \psi_{n(i)}^{(e)} e^{-j\beta_n x} e^{-j\beta_z z}$	$H_{yn(i)}^{(h)} = \frac{1}{\varepsilon_{r(i)}} \frac{\partial \psi_{n(i)}^{(h)}}{\partial y} e^{-j\beta_n x} e^{-j\beta_z z}$
$H_{zn(i)}^{(e)} = 0$	$H_{zn(i)}^{(h)} = \frac{j}{\varepsilon_{r(i)}} \frac{k_i^2 - \beta_z^2}{\beta_z} \psi_{n(i)}^{(h)} e^{-j\beta_n x} e^{-j\beta_z z}$

Table 3.2: Floquet Harmonic Fields for 1-D periodic Structure.

By expanding the scalar wave function in spatial Fourier components, indeed, the periodical peripheries have been taken into consideration, so there is no need to be worried about that. However, we should enforce the E-filed to comply with metallic boundary conditions on top and the bottom ground plane. Hence, the tangential components of electric fields, i.e. E_x and E_z, for each *TM* and *TE* modes should vanish over metallic walls.

- ***TM* mode in region 1($\psi_{n(1)}^{(e)}$):**

$$E_{x(1)}^{(e)}(y=0)=0 \rightarrow \psi_{n(1)}^{(e)}\Big|_{y=0}=0 \rightarrow A_{n(1)}^{(e)}=0$$

$$E_{z(1)}^{(e)}(y=0)=0 \rightarrow \psi_{n(1)}^{(e)}\Big|_{y=0}=0 \rightarrow \textit{Automatically will be satisfied}$$

- ***TM* mode in region 2 ($\psi_{n(2)}^{(e)}$):**

$$E_{x(2)}^{(e)}(y=h)=0 \rightarrow \psi_{n(2)}^{(e)}\Big|_{y=h}=0 \rightarrow A_{n(2)}^{(e)}=0$$

$$E_{z(2)}^{(e)}(y=h)=0 \rightarrow \psi_{n(2)}^{(e)}\Big|_{y=h}=0 \rightarrow \textit{Automatically will be satisfied}$$

- ***TE* mode in region 1 ($\psi_{n(1)}^{(h)}$):**

$$E_{x(1)}^{(h)}(y=0)=0 \rightarrow \frac{\partial \psi_{n(1)}^{(h)}}{\partial y}\Big|_{y=0}=0 \rightarrow B_{n(1)}^{(h)}=0$$

$$E_{z(1)}^{(h)}(y=0)=0 \rightarrow \textit{Already satisfied}$$

- ***TE* mode in region 2 ($\psi_{n(2)}^{(h)}$):**

$$E_{x(2)}^{(h)}(y=h)=0 \rightarrow \frac{\partial \psi_{n(2)}^{(h)}}{\partial y}\Big|_{y=h}=0 \rightarrow B_{n(2)}^{(h)}=0$$

$$E_{z(2)}^{(h)}(y=h)=0 \rightarrow \textit{Already satisfied}$$

By substitution the above results in ψ formulations, we have

$$\psi_{n(1)}^{(e)} = B_{n(1)}^{(e)} \sin(\beta_{y(1)}^{(e)} y) \tag{3.51}$$

$$\psi_{n(2)}^{(e)} = B_{n(2)}^{(e)} \sin(\beta_{y(2)}^{(e)} (h-y)) \tag{3.52}$$

$$\psi_{n(1)}^{(h)} = A_{n(1)}^{(h)} \cos(\beta_{y(1)}^{(h)} y) \tag{3.53}$$

$$\psi_{n(2)}^{(h)} = A_{n(2)}^{(h)} \cos(\beta_{y(2)}^{(h)} (h-y)) \tag{3.54}$$

Phase constants in x-direction according to the Floquet theorem can be expressed by

$$\beta_n = \beta_x + \frac{2\pi n}{2L}, \quad n=...-2, -1, 0, 1, 2...$$

Similar to the microstrip line, phase constants in y-direction can be found by constraint relation (3.50) as follows:

$$\alpha_n^{(1)} = -j\beta_{y(1)n}^{(e)} = -j\beta_{y(1)n}^{(h)} = \sqrt{(\beta_n^2 + \beta_z^2) - \varepsilon_r k_0^2} \tag{3.55a}$$

$$\alpha_n^{(2)} = -j\beta_{y(2)n}^{(e)} = -j\beta_{y(2)n}^{(h)} = \sqrt{(\beta_n^2 + \beta_z^2) - k_0^2} \tag{3.55b}$$

$$k_0 = \omega\sqrt{\varepsilon_0 \mu_0} \ . \tag{3.56}$$

To satisfy the boundary conditions at the interface between the dielectric and air, the total transverse scalar functions of $\psi_{(i)}(x,y)$ must be written as the summation on $\psi_{n(i)}(y)e^{-j\beta_n x}$, so after some rearrangements, for example the coefficient of A_n is used for the region 1 and B_n is used for the region 2, they can be written as:

$$\psi_1^{(e)} = \sum_{n=-\infty}^{\infty} A_n^{(e)} \sinh(\alpha_n^{(1)} y) e^{-j\beta_n x} \tag{3.57a}$$

$$\psi_2^{(e)} = \sum_{n=-\infty}^{\infty} B_n^{(e)} \sinh(\alpha_n^{(2)} (h-y)) e^{-j\beta_n x} \tag{3.57b}$$

$$\psi_1^{(h)} = \sum_{n=-\infty}^{\infty} A_n^{(h)} \cosh(\alpha_n^{(1)} y) e^{-j\beta_n x} \tag{3.57c}$$

$$\psi_2^{(h)} = \sum_{n=-\infty}^{\infty} B_n^{(h)} \cosh(\alpha_n^{(2)} (h-y)) e^{-j\beta_n x} \tag{3.57d}$$

Now, by introducing new variables $\frac{A_n^{(h)}}{\varepsilon_r} \to A_n^{(h)}$ and $\frac{A_n^{(e)}}{\varepsilon_r} \to A_n^{(e)}$, the TM and TE fields for each region of the dielectric and air are:

- **TM fields**

$$E_{x(1)}^{(e)} = -j\left(\sum_{n=-\infty}^{\infty} A_n^{(e)} \beta_n \sinh(\alpha_n^{(1)} y) e^{-j\beta_n x}\right) e^{-j\beta_z z} \tag{3.58a}$$

$$E_{x(2)}^{(e)} = -j\left(\sum_{n=-\infty}^{\infty} B_n^{(e)} \beta_n \sinh(\alpha_n^{(2)} (h-y)) e^{-j\beta_n x}\right) e^{-j\beta_z z} \tag{3.58b}$$

$$E_{y(1)}^{(e)} = \left(\sum_{n=-\infty}^{\infty} A_n^{(e)} \alpha_n^{(1)} \cosh(\alpha_n^{(1)} y) e^{-j\beta_n x}\right) e^{-j\beta_z z} \tag{3.58c}$$

$$E_{y(2)}^{(e)} = -\left(\sum_{n=-\infty}^{\infty} B_n^{(e)} \alpha_n^{(2)} \cosh(\alpha_n^{(2)} (h-y)) e^{-j\beta_n x}\right) e^{-j\beta_z z} \tag{3.58d}$$

$$E_{z(1)}^{(e)} = j\frac{k_1^2 - \beta_z^2}{\beta_z}\left(\sum_{n=-\infty}^{\infty} A_n^{(e)} \sinh(\alpha_n^{(1)} y) e^{-j\beta_n x}\right) e^{-j\beta_z z} \tag{3.58e}$$

$$E_{z(2)}^{(e)} = j\frac{k_2^2 - \beta_z^2}{\beta_z}\left(\sum_{n=-\infty}^{\infty} B_n^{(e)} \sinh(\alpha_n^{(2)} (h-y)) e^{-j\beta_n x}\right) e^{-j\beta_z z} \tag{3.58f}$$

$$H_{x(1)}^{(e)} = \frac{-\omega\varepsilon_1}{\beta_z}\left(\sum_{n=-\infty}^{\infty} A_n^{(e)} \alpha_n^{(1)} \cosh(\alpha_n^{(1)} y) e^{-j\beta_n x}\right) e^{-j\beta_z z} \tag{3.58g}$$

$$H_{x(2)}^{(e)} = \frac{\omega\varepsilon_0}{\beta_z}\left(\sum_{n=-\infty}^{\infty} B_n^{(e)} \alpha_n^{(2)} \cosh(\alpha_n^{(2)} (h-y)) e^{-j\beta_n x}\right) e^{-j\beta_z z} \tag{3.58h}$$

$$H_{y(1)}^{(e)} = \frac{-j\omega\varepsilon_1}{\beta_z}\left(\sum_{n=-\infty}^{\infty} A_n^{(e)} \beta_n \sinh(\alpha_n^{(1)} y) e^{-j\beta_n x}\right) e^{-j\beta_z z} \tag{3.58i}$$

$$H_{y(2)}^{(e)} = \frac{-j\omega\varepsilon_0}{\beta_z}\left(\sum_{n=-\infty}^{\infty} B_n^{(e)} \beta_n \sinh(\alpha_n^{(2)} (h-y)) e^{-j\beta_n x}\right) e^{-j\beta_z z} \tag{3.58j}$$

$$H_{z(1)}^{(e)} = 0 \tag{3.58k}$$

$$H_{z(2)}^{(e)} = 0 \tag{3.58l}$$

- **TE fields**

$$E_{x(1)}^{(h)} = \frac{\omega\mu_0}{\beta_z}\left(\sum_{n=-\infty}^{\infty} A_n^{(h)}\alpha_n^{(1)}\sinh(\alpha_n^{(1)}y)e^{-j\beta_n x}\right)e^{-j\beta_z z} \tag{3.59a}$$

$$E_{x(2)}^{(h)} = \frac{-\omega\mu_0}{\beta_z}\left(\sum_{n=-\infty}^{\infty} B_n^{(h)}\alpha_n^{(2)}\sinh(\alpha_n^{(2)}(h-y))e^{-j\beta_n x}\right)e^{-j\beta_z z} \tag{3.59b}$$

$$E_{y(1)}^{(h)} = \frac{j\omega\mu_0}{\beta_z}\left(\sum_{n=-\infty}^{\infty} A_n^{(h)}\beta_n\cosh(\alpha_n^{(1)}y)e^{-j\beta_n x}\right)e^{-j\beta_z z} \tag{3.59c}$$

$$E_{y(2)}^{(h)} = \frac{j\omega\mu_0}{\beta_z}\left(\sum_{n=-\infty}^{\infty} B_n^{(h)}\beta_n\cosh(\alpha_n^{(2)}(h-y))e^{-j\beta_n x}\right)e^{-j\beta_z z} \tag{3.59d}$$

$$E_{z(1)}^{(h)} = 0 \tag{3.59e}$$

$$E_{z(2)}^{(h)} = 0 \tag{3.59f}$$

$$H_{x(1)}^{(h)} = -j\left(\sum_{n=-\infty}^{\infty} A_n^{(h)}\beta_n\cosh(\alpha_n^{(1)}y)e^{-j\beta_n x}\right)e^{-j\beta_z z} \tag{3.59g}$$

$$H_{x(2)}^{(h)} = -j\left(\sum_{n=-\infty}^{\infty} B_n^{(h)}\beta_n\cosh(\alpha_n^{(2)}(h-y))e^{-j\beta_n x}\right)e^{-j\beta_z z} \tag{3.59h}$$

$$H_{y(1)}^{(h)} = \left(\sum_{n=-\infty}^{\infty} A_n^{(h)}\alpha_n^{(1)}\sinh(\alpha_n^{(1)}y)e^{-j\beta_n x}\right)e^{-j\beta_z z} \tag{3.59i}$$

$$H_{y(2)}^{(h)} = -\left(\sum_{n=-\infty}^{\infty} B_n^{(h)}\alpha_n^{(2)}\sinh(\alpha_n^{(2)}(h-y))e^{-j\beta_n x}\right)e^{-j\beta_z z} \tag{3.59j}$$

$$H_{z(1)}^{(h)} = j\frac{k_1^2-\beta_z^2}{\beta_z}\left(\sum_{n=-\infty}^{\infty} A_n^{(h)}\cosh(\alpha_n^{(1)}y)e^{-j\beta_n x}\right)e^{-j\beta_z z} \tag{3.59k}$$

$$H_{z(2)}^{(h)} = j\frac{k_2^2-\beta_z^2}{\beta_z}\left(\sum_{n=-\infty}^{\infty} B_n^{(h)}\cosh(\alpha_n^{(2)}(h-y))e^{-j\beta_n x}\right)e^{-j\beta_z z} \tag{3.59l}$$

Final fields are the superposition of TE and TM fields [31]:

$$E_{x(1)} = \left(\sum_{n=-\infty}^{\infty} \left(\frac{\omega\mu_0}{\beta_z} A_n^{(h)} \alpha_n^{(1)} - jA_n^{(e)} \beta_n \right) \sinh(\alpha_n^{(1)} y) e^{-j\beta_n x} \right) e^{-j\beta_z z} \tag{3.60a}$$

$$E_{x(2)} = \left(\sum_{n=-\infty}^{\infty} \left(\frac{-\omega\mu_0}{\beta_z} B_n^{(h)} \alpha_n^{(2)} - jB_n^{(e)} \beta_n \right) \sinh(\alpha_n^{(2)} (h-y)) e^{-j\beta_n x} \right) e^{-j\beta_z z} \tag{3.60b}$$

$$E_{y(1)} = \left(\sum_{n=-\infty}^{\infty} \left(\frac{j\omega\mu_0}{\beta_z} A_n^{(h)} \beta_n + A_n^{(e)} \alpha_n^{(1)} \right) \cosh(\alpha_n^{(1)} y) e^{-j\beta_n x} \right) e^{-j\beta_z z} \tag{3.60c}$$

$$E_{y(2)} = \left(\sum_{n=-\infty}^{\infty} \left(\frac{j\omega\mu_0}{\beta_z} B_n^{(h)} \beta_n - B_n^{(e)} \alpha_n^{(2)} \right) \cosh(\alpha_n^{(2)} (h-y)) e^{-j\beta_n x} \right) e^{-j\beta_z z} \tag{3.60d}$$

$$E_{z(1)} = j \frac{k_1^2 - \beta_z^2}{\beta_z} \left(\sum_{n=-\infty}^{\infty} A_n^{(e)} \sinh(\alpha_n^{(1)} y) e^{-j\beta_n x} \right) e^{-j\beta_z z} \tag{3.60e}$$

$$E_{z(2)} = j \frac{k_2^2 - \beta_z^2}{\beta_z} \left(\sum_{n=-\infty}^{\infty} B_n^{(e)} \sinh(\alpha_n^{(2)} (h-y)) e^{-j\beta_n x} \right) e^{-j\beta_z z} \tag{3.60f}$$

$$H_{x(1)} = \left(\sum_{n=-\infty}^{\infty} \left(-jA_n^{(h)} \beta_n - \frac{\omega\varepsilon_1}{\beta_z} A_n^{(e)} \alpha_n^{(1)} \right) \cosh(\alpha_n^{(1)} y) e^{-j\beta_n x} \right) e^{-j\beta_z z} \tag{3.60g}$$

$$H_{x(2)} = \left(\sum_{n=-\infty}^{\infty} \left(-jB_n^{(h)} \beta_n + \frac{\omega\varepsilon_0}{\beta_z} B_n^{(e)} \alpha_n^{(2)} \right) \cosh(\alpha_n^{(2)} (h-y)) e^{-j\beta_n x} \right) e^{-j\beta_z z} \tag{3.60h}$$

$$H_{y(1)} = \left(\sum_{n=-\infty}^{\infty} \left(A_n^{(h)} \alpha_n^{(1)} - \frac{j\omega\varepsilon_1}{\beta_z} A_n^{(e)} \beta_n \right) \sinh(\alpha_n^{(1)} y) e^{-j\beta_n x} \right) e^{-j\beta_z z} \tag{3.60i}$$

$$H_{y(2)} = \left(\sum_{n=-\infty}^{\infty} \left(-B_n^{(h)} \alpha_n^{(2)} - \frac{j\omega\varepsilon_0}{\beta_z} B_n^{(e)} \beta_n \right) \sinh(\alpha_n^{(2)} (h-y)) e^{-j\beta_n x} \right) e^{-j\beta_z z} \tag{3.60j}$$

$$H_{z(1)} = j \frac{k_1^2 - \beta_z^2}{\beta_z} \left(\sum_{n=-\infty}^{\infty} A_n^{(h)} \cosh(\alpha_n^{(1)} y) e^{-j\beta_n x} \right) e^{-j\beta_z z} \tag{3.60k}$$

$$H_{z(2)} = j \frac{k_2^2 - \beta_z^2}{\beta_z} \left(\sum_{n=-\infty}^{\infty} B_n^{(h)} \cosh(\alpha_n^{(2)} (h-y)) e^{-j\beta_n x} \right) e^{-j\beta_z z} \tag{3.60l}$$

3.3.2 Boundary Conditions for 1-D Printed Periodic Structure

The coefficients $A_n^{(e)}$, $A_n^{(h)}$, $B_n^{(e)}$ and $B_n^{(h)}$ are yet unknowns, and their relations can be found by applying proper boundary conditions along the air-dielectric interface. So, the next step is to apply the appropriate boundary conditions along the air-dielectric interface including the center conductor. It should be stated again that the superposition of the *TE* and *TM* modes must satisfy the boundary along this interface. Considering the symmetry with respect to the y axis, the appropriate boundary conditions along the interface for $x>0$ that must be enforced are following four equations which are mutually independent (the same apply for $x<0$):

$$(1)\ E_{z1} = E_{z2} \qquad (x,z) \in \text{Unit Cell} \qquad 0 < x < L \tag{3.61}$$

$$(2)\ E_{x1} = E_{x2} \qquad (x,z) \in \text{Unit Cell} \qquad 0 < x < L \tag{3.62}$$

$$(3)\ \begin{cases} (a)\ E_{z1} = 0 & (x,z) \in \text{Patch} & 0 < x < t \\ (b)\ H_{x1} = H_{x2} & (x,z) \in \textit{Aperture} & t < x < L \end{cases} \tag{3.63 a,b}$$

$$(4)\ \begin{cases} (a)\ E_{x1} = 0 & (x,z) \in \text{Patch} & 0 < x < t \\ (b)\ H_{z1} = H_{z2} & (x,z) \in \textit{Aperture} & t < x < L \end{cases} \tag{3.64 a,b}$$

Similar to the microstrip line case, the summary of resultant formulations are presented below and the details are given in Appendix II.

$$\begin{cases} \sum_{n=-\infty}^{\infty} \overline{A}_n^{(e)} e^{-j\beta_n x} = 0 & |x| < t \\ \sum_{n=-\infty}^{\infty} \overline{A}_n^{(e)} \beta_n P_n(\beta_z) e^{-j\beta_n x} + \sum_{n=-\infty}^{\infty} \overline{A}_n^{(h)} \beta_n T_n(\beta_z) e^{-j\beta_n x} = 0 & t < |x| < L \end{cases} \tag{3.65a,b}$$

$$\begin{cases} \sum_{n=-\infty}^{\infty} \overline{A}_n^{(e)} \beta_n e^{-j\beta_n x} + \sum_{n=-\infty}^{\infty} \overline{A}_n^{(h)} \beta_n e^{-j\beta_n x} = 0 & |x| < t \\ \sum_{n=-\infty}^{\infty} \overline{A}_n^{(e)} Q_n(\beta_z) e^{-j\beta_n x} + \sum_{n=-\infty}^{\infty} \overline{A}_n^{(h)} W_n(\beta_z) e^{-j\beta_n x} = 0 & t < |x| < L \end{cases} \tag{3.66a,b}$$

$$P_n(\beta_z)=\varepsilon_r\frac{\alpha_n^{(1)}}{\beta_n}\coth(\alpha_n^{(1)}d)+\frac{\alpha_n^{(2)}}{\beta_n}\left(\frac{\varepsilon_r-\overline{\beta}_z^2}{1-\overline{\beta}_z^2}\right)\coth(\alpha_n^{(2)}(h-d))+\overline{\beta}_z^2\frac{\beta_n}{\alpha_n^{(2)}}\left(\frac{1-\varepsilon_r}{1-\overline{\beta}_z^2}\right)\coth(\alpha_n^{(2)}(h-d))$$

$$T_n(\beta_z)=\overline{\beta}_z^2\left(\frac{\beta_n}{\alpha_n^{(1)}}\coth(\alpha_n^{(1)}d)+\frac{\beta_n}{\alpha_n^{(2)}}\coth(\alpha_n^{(2)}(h-d))\right) \tag{3.68}$$

$$Q_n(\beta)=\frac{\beta_n}{\alpha_n^{(2)}}\left(\frac{1-\varepsilon_r}{1-\overline{\beta}_z^2}\right)\coth(\alpha_n^{(2)}(h-d)) \tag{3.69}$$

$$W_n(\beta)=\left(\frac{\varepsilon_r-\overline{\beta}_z^2}{1-\overline{\beta}_z^2}\right)\frac{\beta_n}{\alpha_n^{(1)}}\coth(\alpha_n^{(1)}d)+\frac{\beta_n}{\alpha_n^{(2)}}\coth(\alpha_n^{(2)}(h-d)) \tag{3.70}$$

$$\overline{A}_n^{(h)}=j\frac{\omega\mu_0}{\beta_z}\frac{\alpha_n^{(1)}}{\beta_n}A_n^{(h)}\sinh(\alpha_n^{(1)}d) \tag{3.71}$$

$$\overline{A}_n^{(e)}=A_n^{(e)}\sinh(\alpha_n^{(1)}d) \tag{3.72}$$

$$\overline{\beta}_z=\beta_z/k_0 \tag{3.73}$$

3.3.3 Matrix Presentation of 1-D Printed Periodic Structure

By using delta function as a testing function, the above equations can be reduced to a matrix form. Moreover, the limit of summation should be truncated from $-N$ to N, so there are $2N+1$ coefficients for each $\overline{A}_n^{(e)}$ and $\overline{A}_n^{(h)}$.To have a square matrix, $2N+1$ points should be distributed throughout the unit cell by the ratio of $r=t/L$ for the aperture and strip. The resultant matrix is given by equation (3.75).

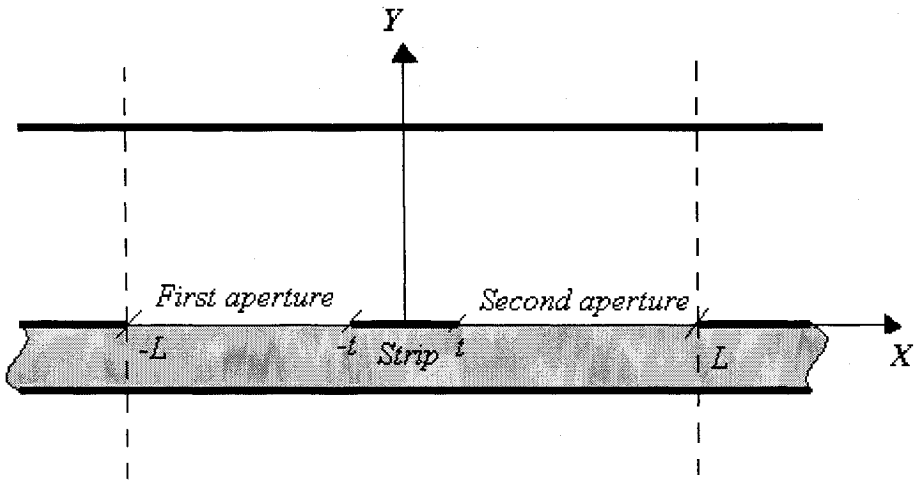

Fig. 3.3: The Unit Cell of the 1-D Periodic Structure.

$$
\begin{array}{r}
(1-r)(2N+1)/2 \text{ points on the first apertute } \{ \\
r(2N+1) \text{points on the strip } \{ \\
(1-r)(2N+1)/2 \text{ points on the first apertute } \{ \\
\text{----------} \\
(1-r)(2N+1)/2 \text{ points on the first apertute } \{ \\
r(2N+1) \text{points on the first apertute } \{ \\
(1-r)(2N+1)/2 \text{ points on the first apertute } \{
\end{array}
\begin{bmatrix}
\overbrace{[a_{mn}]}^{2N+1} & \overbrace{[b_{mn}]}^{2N+1} \\
\text{----} & \text{----} \\
[c_{mn}] & [d_{mn}] \\
\text{----} & \text{----} \\
[e_{mn}] & [f_{mn}] \\
\text{----} & \text{----} \\
[g_{mn}] & [h_{mn}] \\
\text{----} & \text{----} \\
[i_{mn}] & [j_{mn}] \\
\text{----} & \text{----} \\
[k_{mn}] & [l_{mn}]
\end{bmatrix}
\begin{bmatrix}
\vdots \\
\overline{A}_n^{(e)} \\
\vdots \\
\text{----} \\
\vdots \\
\overline{A}_n^{(h)} \\
\vdots
\end{bmatrix}
= 0 \quad (3.74)
$$

In equation (3.74) N is an integer number which truncates the limit of summation in (3.65a,b)- (3.65a,b) in both minus and positive direction. N, also, determines the number of matching points throughout ($-L$, L), in order to have a square matrix, in such a way that there are $2N+1$ points over the unit cell.

Chapter 4

Numerical Results

The validity of the approach presented in chapter 3 to find the dispersion curve is demonstrated in this chapter. Results including dispersion curves for both dominant mode and high order modes are given in this chapter. It is demonstrated that the results for shielded microstrip line are matched with those of SIE method. Some results are devoted to show the good convergence of MM technique. Also the effect of changing the height and distance of the side walls are illustrated. For one-dimensional periodic structures, the dispersion curve for dominant mode is in good agreement with those from MoM in spectral domain.

4.1 Microstrip Line

For the structure shown in Fig.3.1, the geometrical parameters are: L= 6.35mm, h= 12.7mm, d=1.27mm and t=0.635mm. With ε_r =2.65 or ε_r =20. Since the ratio of strip's width to aperture's width is 0.1, the ratio of the points on strip to those on the aperture is taken as 0.1.

The homogenous $2N$-by-$2N$ matrix equation (3.36) has the form of $\mathbf{A}(\beta,f)\mathbf{X}=\mathbf{0}$, so $|\det(\mathbf{A}(\beta,f))|=0$ to have a nontrivial solution. The dispersion curve is a graph of this equation such that for certain frequency the value of β is sought. To find the solution for

singularity, we can set the determinant, the smallest eigenvalue or the smallest singular value to zero. In Fig.4.2 it is demonstrated that they are equivalent. In this work, the smallest singular value is preferred, because it is more stable. The dominant mode is the solution that has the biggest β_z in addition to the lowest cut-off frequency as shown in the Fig.4.1. It should be also noted that dominant mode appears just before the spurious dispersion characteristic of dielectric.

As mentioned in section 2.1.3 the convergence is a big concern when MM technique is used. However, Fig.4.3 shows that for this structure there is a good convergence for the dominant mode even for N=10, but for the higher order modes, more terms should be included, i.e. N=40, to meet the convergence condition. Hence, the MM-PM technique is very efficient to generate the dispersion curve for the dominant mode.

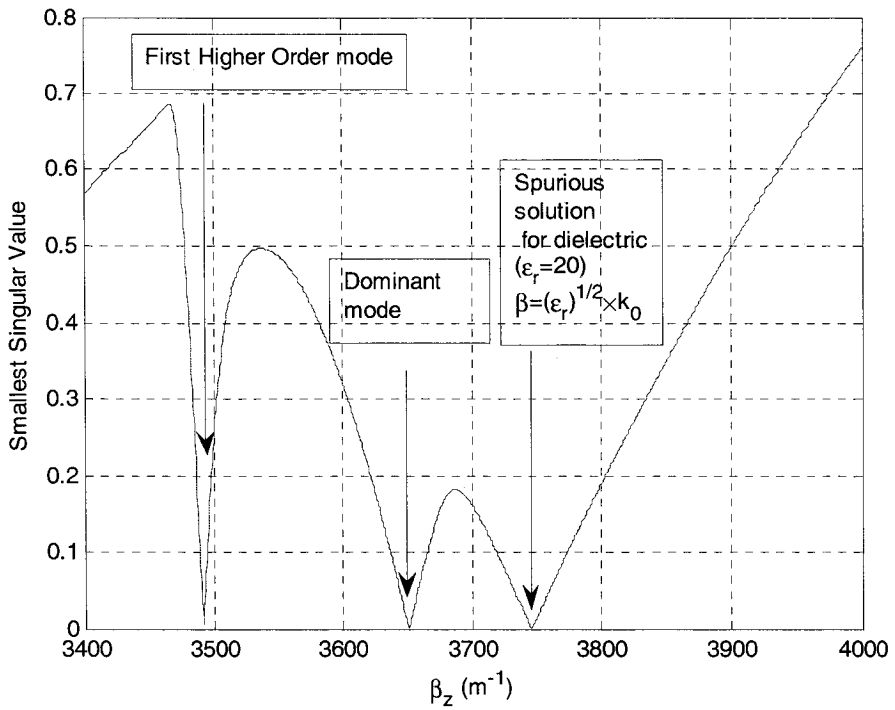

Fig. 4.1 Dominant and first higher order mode at the frequency 40GHz, $\varepsilon_r = 20$.

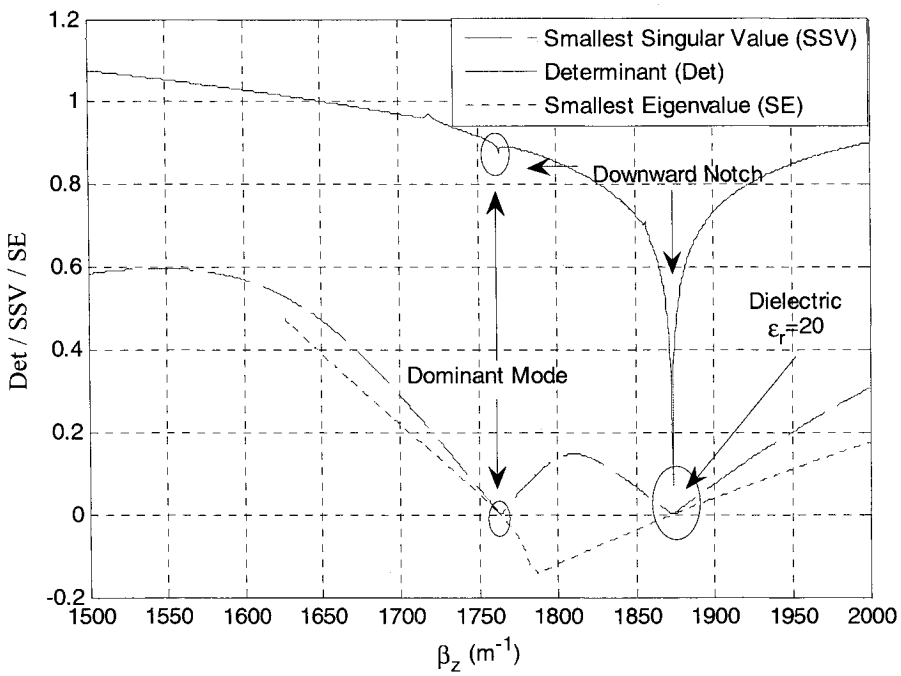

Fig. 4.2: Values of β, based on three techniques for the singularity of the matrix equation, f=20GHz, ε_r=20.

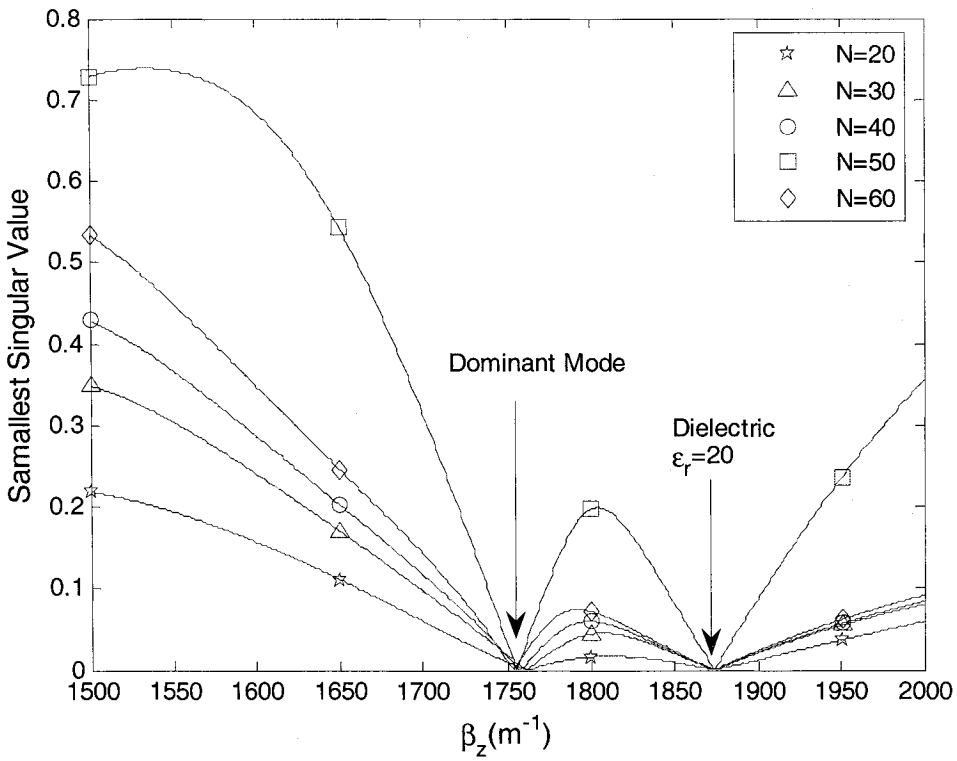

Fig. 4.3: The effect of truncation on the convergence of MM-PM method, f=20GHz.

In Fig.4.4, we changed the height of the shield from h=20t to h=5t and h=100t, but all results (solid lines) are the same, so Fig.4.4 demonstrates that the height of the shield has a minor influence on the structure, as long as the distance between PEC side-walls is constant. However, by changing the distance between side walls from L=10t to L=5t, L=20t and L=30t, the results differ (dashed lines). Therefore, this shielded configuration is considered as a good model for the open microstrip lines, when the distance between side walls has been fixed. Explaining the reason, by increasing the length L the ratio of t/L has decreased and we have to increase N (number of points on the interface and terms inside the sigma) such that the number of points on aperture and strip become reasonable.

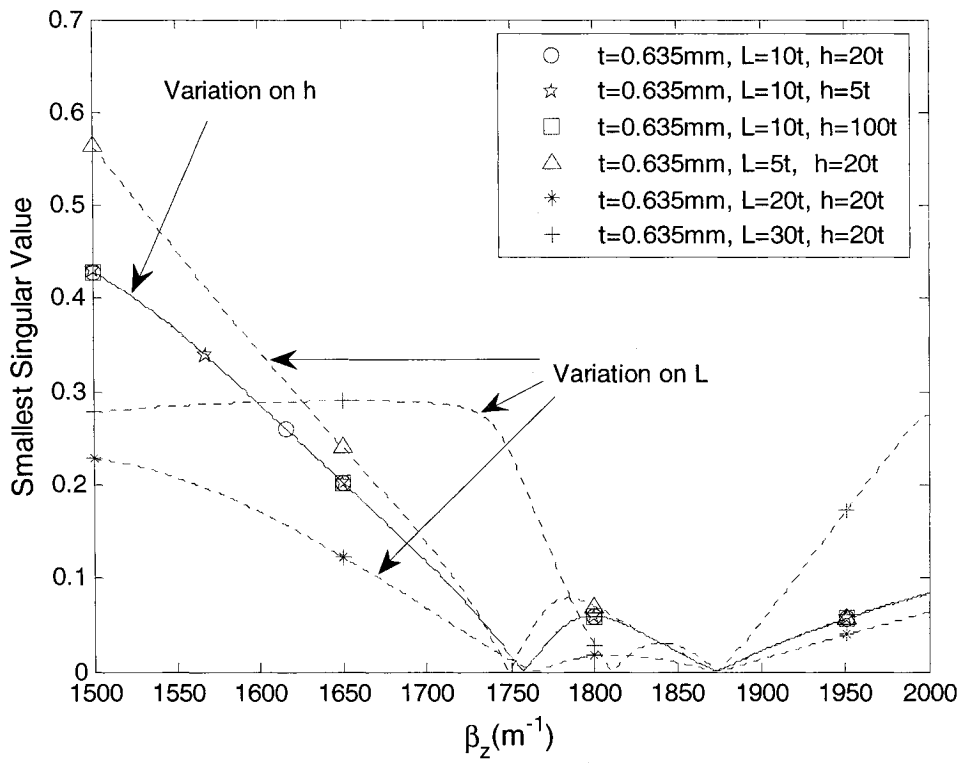

Fig. 4.4: The effect of changing different geometrical parameters on β, f=20GHz.

As pointed out, the MM-PM works well even for the structures solved by conventional classic MM techniques such as ordinary waveguides. The result for a typical air-filled

waveguide is given in Fig.4.5. In this case, the width of the strip is set to zero and ε_r of the dielectric to 1. Consequently, the matching points are laid all on the aperture.

It is evident that β in air-field rectangular waveguide satisfy the following equation [24]

$$\beta_{mn} = \sqrt{k^2 - (\frac{m\pi}{a})^2 - (\frac{n\pi}{b})^2} \quad . \tag{4.1}$$

Substituting geometrical parameters a=b=12.7mm at the frequency of f=30GHz, the propagation constant for TE_{12} mode is β=297.3645 rad/m. Fig.5.4 gives the result from MM-PM analysis for the waveguide which is completely matched with the equation (4.1).

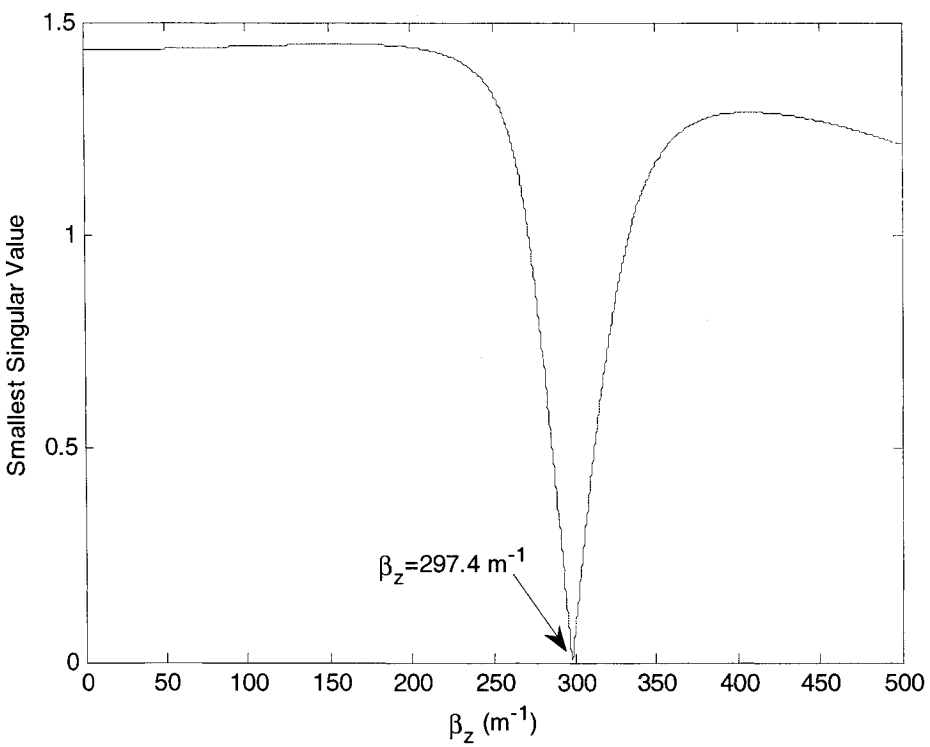

Fig. 4.5: The β for TE_{mn} mode in an air-filled rectangular waveguide at f=30GHz and with parameters a=b=12.7mm, m=1, n=2.

The dispersion curves of a shielded microstrip line in Fig.4.6, Fig.4.7 and Fig.4.8 are provided by scanning the frequency over a proper interval. Fig.4.5 and Fig.4.6 reveals

that the dispersion curve for the dominant mode is in quite good agreement with the results from the singular integral equation (SIE) method [33]. The complete dispersion graph containing higher order modes is depicted in Fig. 4.6 and Fig .4.8 for $\varepsilon_r = 20$, and $\varepsilon_r = 2.65$ respectively.

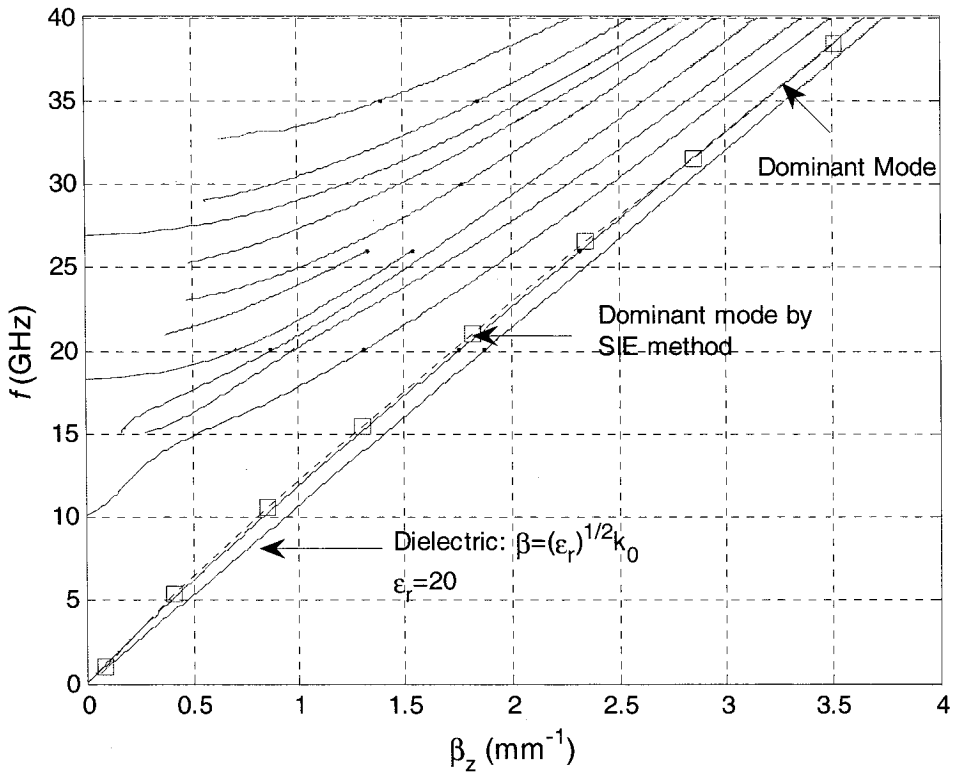

Fig. 4.6: Dispersion curve for dominant and higher order mode, ε_r=20 and comparison with the result in [33].

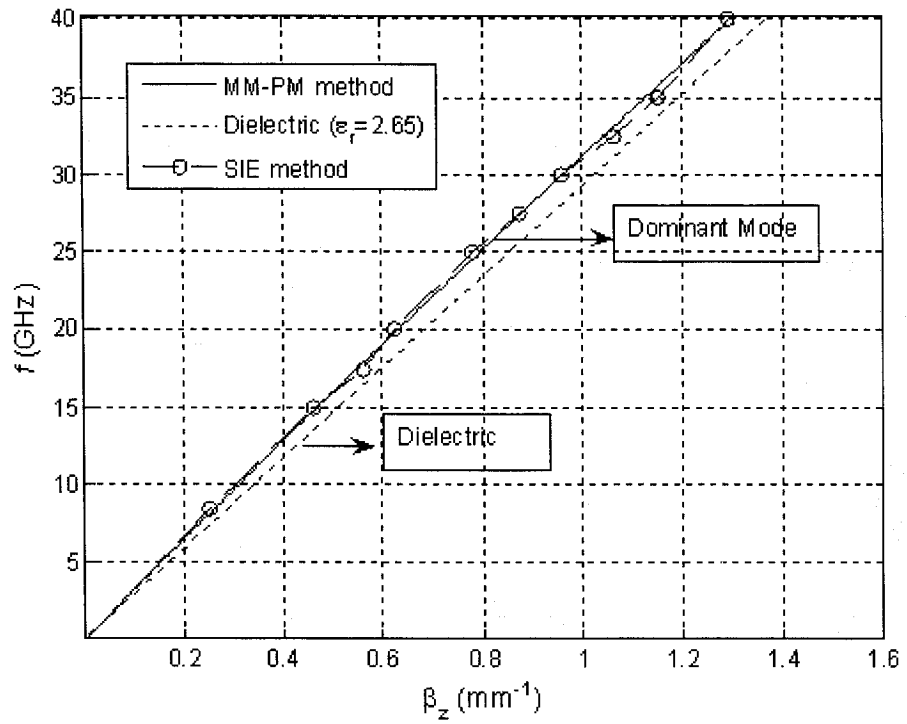

Fig. 4.7: Dispersion curve for dominant mode, ε_r=2.65 and comparison with the result in [33].

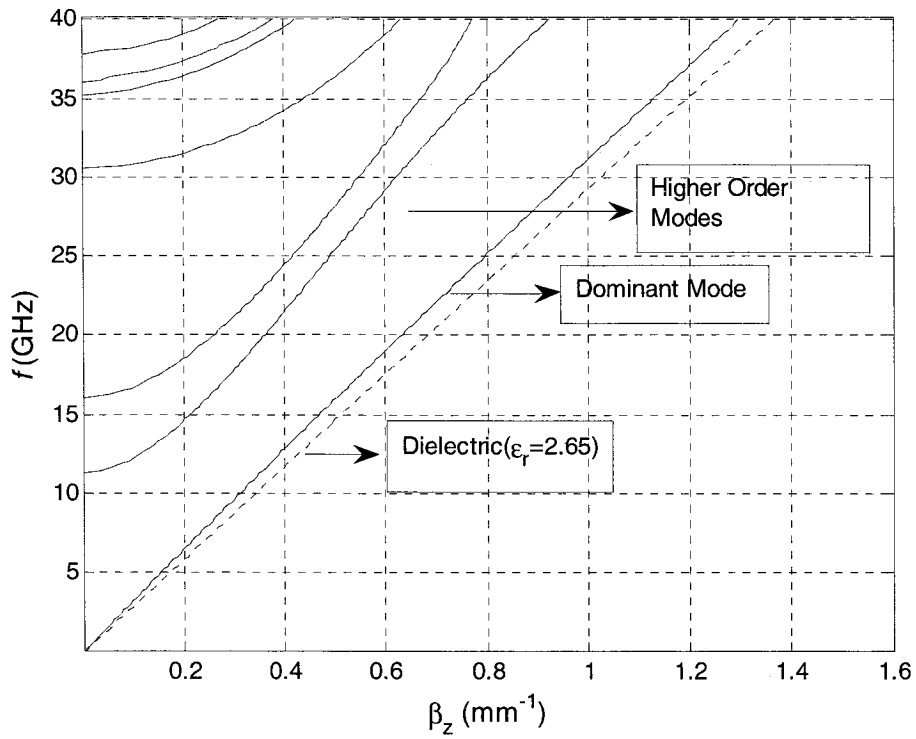

Fig.4.8: Dispersion curve for dominant and higher order modes, ε_r=2.65.

4.2 One-Dimensional Periodic Structure

For the structure shown in Fig.3.2, the geometrical parameters are: d=1.27mm, t=0.5d=0.635mm, L=5d= 6.35mm, h=20t=12.7mm. With ε_r =8.875. These parameters are chosen from [14]. Since the ratio of strip's width to aperture's width is r=0.1, the ratio of points on strip to those on the aperture is taken as 0.1.

In this research, it is assumed that β_x=0, as the dispersion curve along the z-axis (or Γ-X portion in Brillion zone) is of interest, since the variation on β_x has a slight effect on the dispersion curve, according to the Fig.4.11.

Thus, the homogenous (2N+1)-by-(2N+1) matrix equation (4.3) has the from of $\mathbf{A}(\beta_z, f)\mathbf{X}=\mathbf{0}$, so the matrix **A** must be singular to have a nontrivial solution. To find the solution at singularity, we set the smallest singular value to zero because of its good stability. The issue of the convergence is shown in Fig.4.9. This figure demonstrates that if N is chosen more than 30, e.g. N=40, the result converges well.

The effect of the height of the PEC shield is given in Fig.4.10. This graph reveals the fact that by increasing the height of the shield, it doesn't influence the root of singularity at all, so this shield doesn't cause any concern.

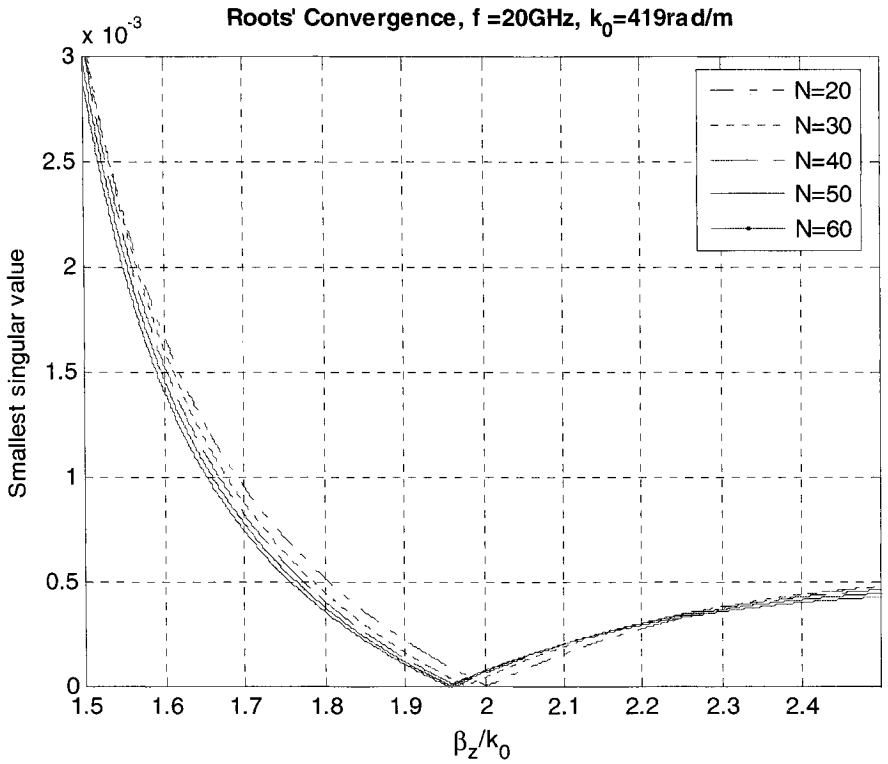

Fig. 4.9: Investigation on the convergence for MM-PM technique at f=20GHz.

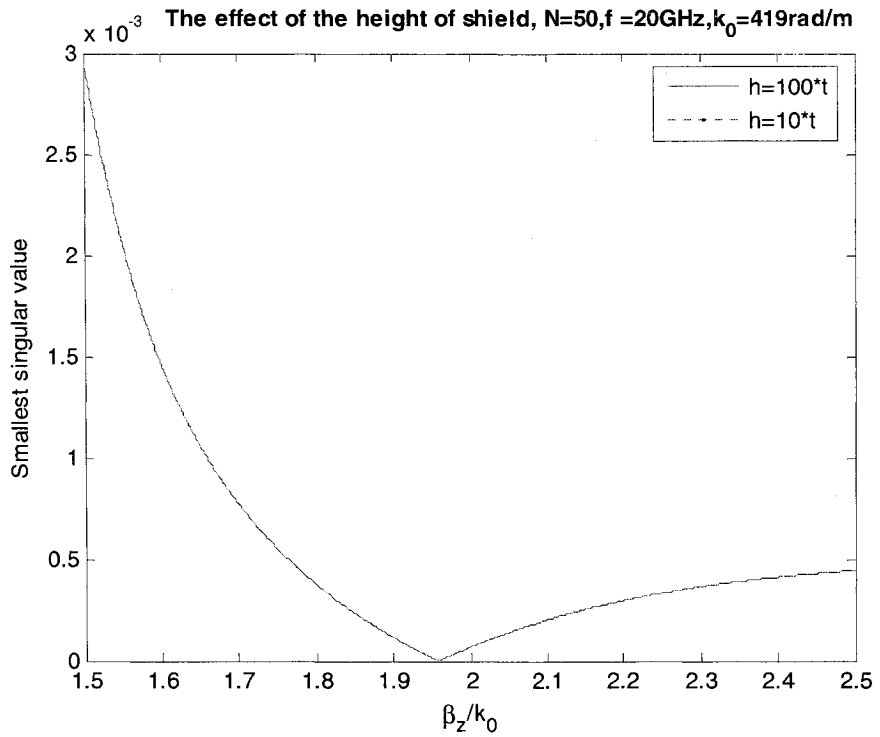

Fig. 4.10: The affect of changing the height of the PEC shield on β_z at f=20GHz, N=50

As pointed out before, by changing β_x up to $\beta_x=30k_0$, no deviation will be observed on the root of singularity. Fig.4.11 shows this fact, and it is quiet matched with the graphs reported in [14].

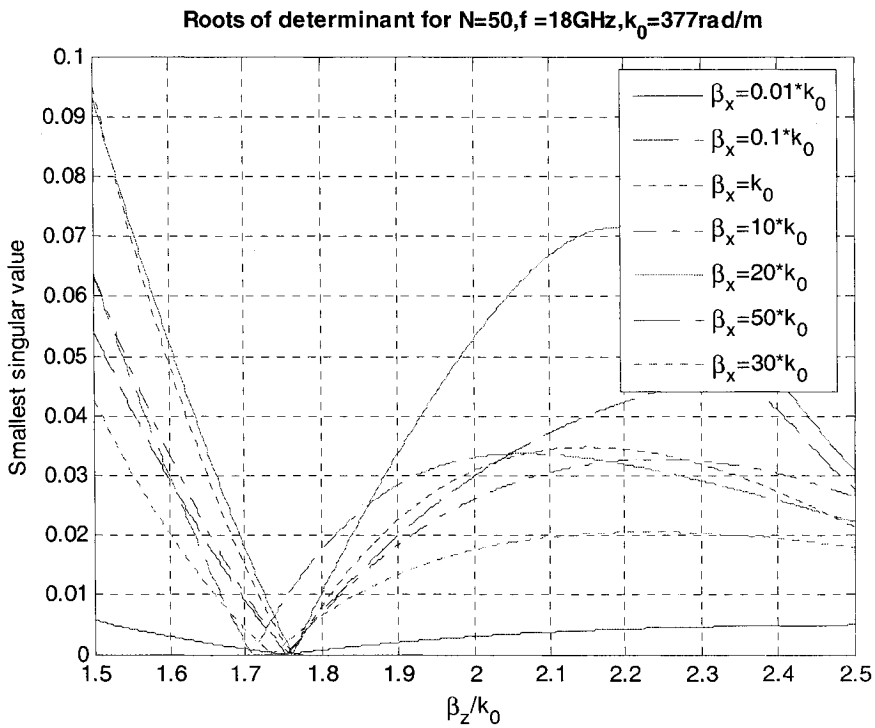

Fig. 4.11: The effect of β_x on β_z.

The dispersion curve of the dominant mode for the traveling wave in the z-direction with $\beta_x=0$ is sketched in Fig.4.12 for the normalized β_z with respect to the frequency. In this figure the result from MM-PM technique which was developed in this paper is compared with the MoM technique in spectral domain which is reported in [14], and they are in a prefect agreement. The complete dispersion curve for even higher order modes are plotted in Fig.4.13.

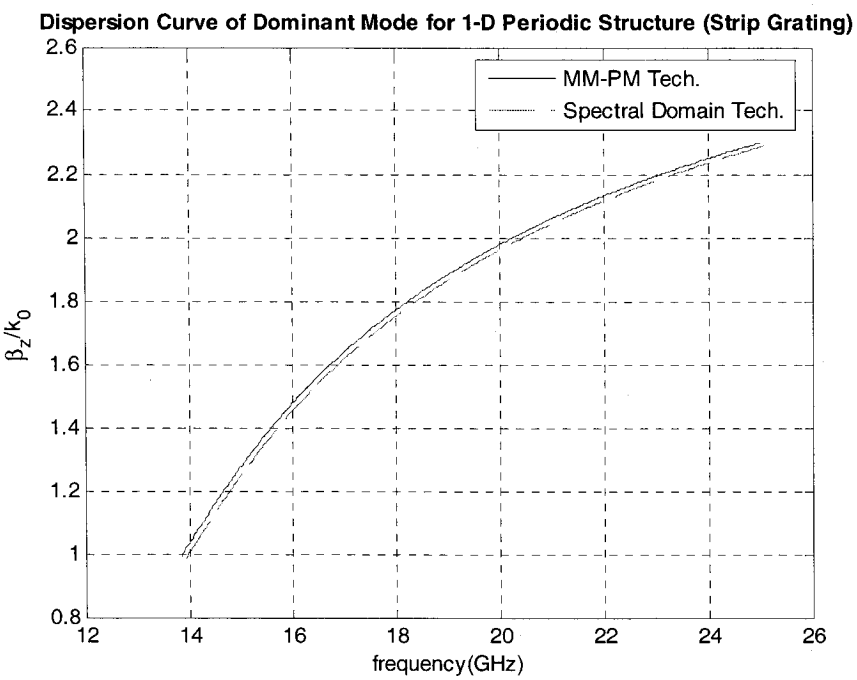

Fig. 4.12: Dispersion curve for the dominant traveling wave in 1-D periodic structure. The results from MM-PM was compared with the results of MoM technique in Spectral Domain [14].

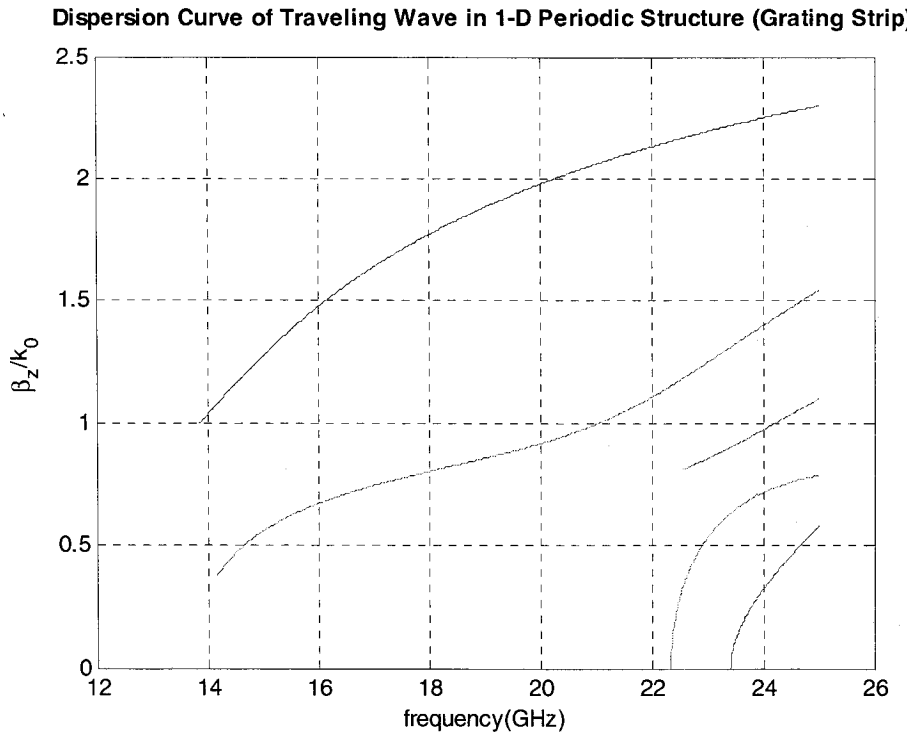

Fig. 4.13: Dispersion curve obtained by MM-PM technique including dominant and higher order modes.

Chapter 5

Conclusion

5.1 Conclusion

In this thesis, the rigorous Mode Matching (MM) technique is invoked to find the dispersion curve of the traveling electromagnetic wave in one-dimensional periodic structure. The structure consists of a homogenous dielectric substrate backed by a ground plane and infinite number of perfect strip conductors on the top. These strips are repeated periodically. Moreover, the thickness of the strips is infinitely small. To avoid radiation condition's issue, a perfect metallic shield is placed above the structure at reasonable height. It is demonstrated in this thesis that if this shield is put quite far away from the substrate, this kind of bounded structure is a good model of the open structure.

In a 1-D periodic structure, the Floquet theorem is used to write the fields in two media: the substrate and air. Next, using the boundary conditions on the interface, a set of algebraic equations is found. Then, these equations are converted into a proper matrix form. This matrix has all information about the dispersion curve. Finally, a MATLAB code is written to obtain the graphical representation of the complete dispersion curve for the structure.

Unlike the regular MM, a simple sub-domain orthogonal set is required in order to convert the algebraic equations obtained from boundary conditions into a matrix form. A set of delta functions is applied for this purpose, so this method of implementation is similar to the Point Matching (PM) technique. Therefore, this technique can be called as a hybrid "MM-PM". The result for the dominant mode is compared well with published results based on the MoM in spectral domain. To further examine the validity of this method, first, a simple shielded microstrip line is investigated by MM technique. The results for microstrip line are matched well with those from the Singular Integral Equation method. Then, MM technique is applied to the aforementioned strip grating structure.

Furthermore, as the matrix is badly ill-conditional, the Singular Value Decomposition (SVD) technique is used to guarantee stable and reliable results. A major concern in dealing with MM is its relative convergence. Fortunately; it is demonstrated in this work that for both structures of microstrip line and strip grating MM-PM has a good convergence. The results of this method are also compared with published results based on the MoM in spectral domain and excellent agreement is obtained.

5.2 Future work

Key components of MM-PM have already been developed in this thesis. This opens up a number of possibilities for future study.

- For one-dimensional periodic structure (strip grating) whose propagating wave is investigated in this thesis, its leaky-wave behavior can be also explored [14]. We assumed that the propagation constant β is real. However; the propagation

constant can be complex in the form $\gamma = \alpha + j\beta$. By doing this, we can predict which band gap (if any) is better, since we already have the information about the attenuation constant α. The other advantage of this extension is to obtain some information from the incident wave when the structure is considered as a Frequency Selective Surface (FSS). There is a correlation between reflection constant and dispersion curve for a traveling wave: the reflection coefficient will be minimum, when we trace the dispersion curve.

- The other future work is generalization to two-dimensional periodic structure. A 2-D structure consists of infinite number of periodic patches on the substrate. However, its matrix conditional number should be addressed. If this method works well for the simple shape of patches, the novel design of the shape of the patches can also be investigated [9], [10]-[13].
- Spectral Domain is another approach developed well for both microstrip lines and FSS structures. Both MoM [23] and FDTD [21] in spectral domain have been used. The calculation of the dispersion curve for periodic structures using one of these methods is another potential future work.
- The efficient Singular Integral Equations (SIE) in [33] can also be applied to periodic structures, but it needs lots of math preparations.

Appendix I

Microstrip Line's Equations

In this appendix, the details of deriving algebraic microstrip line's equations (3.27) - (3.35) from boundary conditions (3.23) - (3.26) are described.

Conditions (3.23) and (3.24) are used to express $B_n^{(e)}$ and $B_n^{(h)}$ in terms of $A_n^{(e)}$ and $A_n^{(h)}$:

$$E_{z1} = E_{z2} \rightarrow \frac{k_1^2 - \beta_z^2}{k_2^2 - \beta_z^2} \sum_{n=1}^{\infty} A_n^{(e)} \cos(k_n x) \sinh(\alpha_n^{(1)} y) = \sum_{n=1}^{\infty} B_n^{(e)} \cos(k_n x) \sinh(\alpha_n^{(2)} (h - y))$$

$$\rightarrow \sum_{n=1}^{\infty} \left[\frac{k_1^2 - \beta_z^2}{k_2^2 - \beta_z^2} A_n^{(e)} \sinh(\alpha_n^{(1)} d) - B_n^{(e)} \sinh(\alpha_n^{(2)} (h - d)) \right] \cos(k_n x) = 0$$

Since the set of $\{\cos(k_n x)\}$ with $k_n = (n - \frac{1}{2})\frac{\pi}{L}$ are a complete orthogonal set over the interval of $0 < x < L$, so the expression inside the bracket should be zero.

$$B_n^{(e)} = A_n^{(e)} \frac{k_1^2 - \beta_z^2}{k_2^2 - \beta_z^2} \frac{\sinh(\alpha_n^{(1)} d)}{\sinh(\alpha_n^{(2)} (h - d))} \qquad \text{(A1.1)}$$

$$E_{x1} = E_{x2} \rightarrow \sum_{n=1}^{\infty} \left(- A_n^{(e)} k_n + \frac{\omega \mu_0}{\beta_z} A_n^{(h)} \alpha_n^{(1)} \right) \sin(k_n x) \sinh(\alpha_n^{(1)} y) =$$

$$\sum_{n=1}^{\infty} \left(- B_n^{(e)} k_n - \frac{\omega \mu_0}{\beta_z} B_n^{(h)} \alpha_n^{(2)} \right) \sin(k_n x) \sinh(\alpha_n^{(2)} (h - y)) \rightarrow$$

$$\sum_{n=1}^{\infty} \left[\left(- A_n^{(e)} k_n + \frac{\omega \mu_0}{\beta_z} A_n^{(h)} \alpha_n^{(1)} \right) \frac{\sinh(\alpha_n^{(1)} d)}{\sinh(\alpha_n^{(2)} (h - d))} + \left(B_n^{(e)} k_n + \frac{\omega \mu_0}{\beta_z} B_n^{(h)} \alpha_n^{(2)} \right) \right] \sin(k_n x) = 0$$

Since the set of $\{\sin(k_n x)\}$ with $k_n = (n-\frac{1}{2})\frac{\pi}{L}$ are a complete orthogonal set over the interval of $0 < x < L$, so the expression inside the bracket should be zero, and by substituting $B_n^{(e)}$ in this equation, it reduces as follows:

$$B_n^{(h)} = \left[A_n^{(e)} \frac{k_n \beta_z}{\omega \mu \alpha_n^{(2)}} \left(1 - \frac{k_1^2 - \beta_z^2}{k_2^2 - \beta_z^2} \right) - A_n^{(h)} \frac{\alpha_n^{(1)}}{\alpha_n^{(2)}} \right] \frac{\sinh(\alpha_n^{(1)} d)}{\sinh(\alpha_n^{(2)}(h-d))} \tag{A1.2}$$

Applying (3.25a) leads to:

$$E_{z1} = 0 \rightarrow E_{z(1)} = j \frac{k_1^2 - \beta_z^2}{\beta_z} \left(\sum_{n=1}^{\infty} A_n^{(e)} \cos(k_n x) \sinh(\alpha_n^{(1)} d) \right) e^{-j\beta_z z} = 0 \rightarrow$$

$$\sum_{n=1}^{\infty} A_n^{(e)} \cos(k_n x) \sinh(\alpha_n^{(1)} d) = 0 \rightarrow$$

$$\sum_{n=1}^{\infty} \overline{A}_n^{(e)} \cos(k_n x) = 0 \tag{A1.3}$$

where

$$\overline{A}_n^{(e)} = A_n^{(e)} \sinh(\alpha_n^{(1)} d) . \tag{A1.4}$$

Applying (3.25b) leads to:

$$H_{x1} = H_{x2} \rightarrow$$

$$\sum_{n=1}^{\infty} \left(\frac{-\omega \varepsilon_1}{\beta_z} A_n^{(e)} \alpha_n^{(1)} + A_n^{(h)} k_n \right) \cosh(\alpha_n^{(1)} d) \cos(k_n x) =$$

$$\sum_{n=1}^{\infty} \left(\frac{\omega \varepsilon_0}{\beta_z} B_n^{(e)} \alpha_n^{(2)} + B_n^{(h)} k_n \right) \cosh(\alpha_n^{(2)}(h-d)) \cos(k_n x)$$

By letting $B_n^{(e)}$ and $B_n^{(h)}$ in terms of $A_n^{(e)}$ and $A_n^{(h)}$ from equations (A1.1) and (A1.2), we can simplify the operand of the sigma in above relations as follows:

$$\left(\frac{-\omega \varepsilon_1}{\beta_z} A_n^{(e)} \alpha_n^{(1)} + A_n^{(h)} k_n \right) \cosh(\alpha_n^{(1)} d) - \left(\frac{\omega \varepsilon_0}{\beta_z} B_n^{(e)} \alpha_n^{(2)} + B_n^{(h)} k_n \right) \cosh(\alpha_n^{(2)}(h-d)) =$$

$$\left(\frac{-\omega\varepsilon_1}{\beta_z}A_n^{(e)}\alpha_n^{(1)}+A_n^{(h)}k_n\right)\cosh(\alpha_n^{(1)}d)-$$
$$\left(\frac{\omega\varepsilon_0}{\beta_z}A_n^{(e)}\frac{k_1^2-\beta_z^2}{k_2^2-\beta_z^2}\alpha_n^{(2)}+k_n\left[A_n^{(e)}\frac{k_n\beta_z}{\omega\mu\alpha_n^{(2)}}\left(1-\frac{k_1^2-\beta_z^2}{k_2^2-\beta_z^2}\right)-A_n^{(h)}\frac{\alpha_n^{(1)}}{\alpha_n^{(2)}}\right]\right)\sinh(\alpha_n^{(1)}d)\coth(\alpha_n^{(2)}(h-d))=$$

$$\left(\frac{-\omega\varepsilon_1}{\beta_z}A_n^{(e)}\alpha_n^{(1)}+A_n^{(h)}k_n\right)\sinh(\alpha_n^{(1)}d)\coth(\alpha_n^{(1)}d)-$$
$$\left(\frac{\omega\varepsilon_0}{\beta_z}A_n^{(e)}\frac{k_1^2-\beta_z^2}{k_2^2-\beta_z^2}\alpha_n^{(2)}+k_n\left[A_n^{(e)}\frac{k_n\beta_z}{\omega\mu\alpha_n^{(2)}}\left(1-\frac{k_1^2-\beta_z^2}{k_2^2-\beta_z^2}\right)-A_n^{(h)}\frac{\alpha_n^{(1)}}{\alpha_n^{(2)}}\right]\right)\sinh(\alpha_n^{(1)}d)\coth(\alpha_n^{(2)}(h-d))=$$

$$A_n^{(e)}\sinh(\alpha_n^{(1)}d)\times$$
$$\left[\frac{-\omega\varepsilon_1\alpha_n^{(1)}}{\beta_z}\coth(\alpha_n^{(1)}d)-\frac{\omega\varepsilon_0\alpha_n^{(2)}}{\beta_z}\frac{\varepsilon_r-\overline{\beta}_z^2}{1-\overline{\beta}_z^2}\coth(\alpha_n^{(2)}(h-d))-k_n\frac{k_n\beta_z}{\omega\mu\alpha_n^{(2)}}\left(\frac{1-\varepsilon_r}{1-\overline{\beta}_z^2}\right)\coth(\alpha_n^{(2)}(h-d))\right]$$
$$+A_n^{(h)}\sinh(\alpha_n^{(1)}d)\left[k_n\coth(\alpha_n^{(1)}d)+\frac{k_n\alpha_n^{(1)}}{\alpha_n^{(2)}}\coth(\alpha_n^{(2)}(h-d))\right]=$$

$$\overline{A}_n^{(e)}k_n\left[\frac{-\omega\varepsilon_1\alpha_n^{(1)}}{\beta_z k_n}\coth(\alpha_n^{(1)}d)-\frac{\omega\varepsilon_0\alpha_n^{(2)}}{\beta_z k_n}\frac{\varepsilon_r-\overline{\beta}_z^2}{1-\overline{\beta}_z^2}\coth(\alpha_n^{(2)}(h-d))-\frac{k_n\beta_z}{\omega\mu\alpha_n^{(2)}}\left(\frac{1-\varepsilon_r}{1-\overline{\beta}_z^2}\right)\coth(\alpha_n^{(2)}(h-d))\right]$$
$$+\frac{k_n\beta_z}{\alpha_n^{(1)}\omega\mu_0}\overline{A}_n^{(h)}k_n\left[\coth(\alpha_n^{(1)}d)+\frac{\alpha_n^{(1)}}{\alpha_n^{(2)}}\coth(\alpha_n^{(2)}(h-d))\right]=$$

$$\overline{A}_n^{(e)}k_n\frac{\omega\varepsilon_0}{\beta_z}\left[\frac{-\varepsilon_r\alpha_n^{(1)}}{k_n}\coth(\alpha_n^{(1)}d)-\frac{\alpha_n^{(2)}}{k_n}\frac{\varepsilon_r-\overline{\beta}_z^2}{1-\overline{\beta}_z^2}\coth(\alpha_n^{(2)}(h-d))-\frac{k_n\beta_z^2}{\omega^2\mu\varepsilon_0\alpha_n^{(2)}}\left(\frac{1-\varepsilon_r}{1-\overline{\beta}_z^2}\right)\coth(\alpha_n^{(2)}(h-d))\right]$$
$$+\frac{\omega\varepsilon_0}{\beta_z}\frac{k_n\beta_z^2}{\alpha_n^{(1)}\omega^2\varepsilon_0\mu_0}\overline{A}_n^{(h)}k_n\left[\coth(\alpha_n^{(1)}d)+\frac{\alpha_n^{(1)}}{\alpha_n^{(2)}}\coth(\alpha_n^{(2)}(h-d))\right]=$$

$$\frac{-\omega\varepsilon_0}{\beta_z}\left\{\overline{A}_n^{(e)}k_n\left[\frac{\varepsilon_r\alpha_n^{(1)}}{k_n}\coth(\alpha_n^{(1)}d)+\frac{\alpha_n^{(2)}}{k_n}\frac{\varepsilon_r-\overline{\beta}_z^2}{1-\overline{\beta}_z^2}\coth(\alpha_n^{(2)}(h-d))+\frac{k_n\overline{\beta}_z^2}{\alpha_n^{(2)}}\left(\frac{1-\varepsilon_r}{1-\overline{\beta}_z^2}\right)\coth(\alpha_n^{(2)}(h-d))\right]\right\}$$
$$-\frac{\omega\varepsilon_0}{\beta_z}\left\{\frac{k_n\overline{\beta}_z^2}{\alpha_n^{(1)}}\overline{A}_n^{(h)}k_n\left[\coth(\alpha_n^{(1)}d)+\frac{\alpha_n^{(1)}}{\alpha_n^{(2)}}\coth(\alpha_n^{(2)}(h-d))\right]\right\}=$$

$$\frac{-\omega\varepsilon_0}{\beta_z}\left\{\overline{A}_n^{(e)}k_n\left[\frac{\varepsilon_r\alpha_n^{(1)}}{k_n}\coth(\alpha_n^{(1)}d)+\frac{\alpha_n^{(2)}}{k_n}\frac{\varepsilon_r-\overline{\beta}_z^2}{1-\overline{\beta}_z^2}\coth(\alpha_n^{(2)}(h-d))+\frac{k_n\overline{\beta}_z^2}{\alpha_n^{(2)}}\left(\frac{1-\varepsilon_r}{1-\overline{\beta}_z^2}\right)\coth(\alpha_n^{(2)}(h-d))\right]\right\}$$
$$-\frac{\omega\varepsilon_0}{\beta_z}\left\{\overline{A}_n^{(h)}k_n\overline{\beta}_z^2\left[\frac{k_n}{\alpha_n^{(1)}}\coth(\alpha_n^{(1)}d)+\frac{k_n}{\alpha_n^{(2)}}\coth(\alpha_n^{(2)}(h-d))\right]\right\}=\frac{-\omega\varepsilon_0}{\beta_z}\overline{A}_n^{(e)}k_nP_n-\frac{\omega\varepsilon_0}{\beta_z}\overline{A}_n^{(h)}k_nT_n$$

Therefore,

$$\sum_{n=1}^{\infty} \overline{A}_n^{(e)} k_n P_n(\beta_z)\cos(k_n x) - \sum_{n=1}^{\infty} \overline{A}_n^{(h)} k_n T_n(\beta_z)\cos(k_n x) = 0 \qquad \text{(A1.5)}$$

where $$\overline{A}_n^{(h)} = \frac{\omega\mu_0}{\beta_z}\frac{\alpha_n^{(1)}}{k_n} A_n^{(h)} \sinh(\alpha_n^{(1)} d)\ , \qquad \text{(A1.6)}$$

$$P_n(\beta_z) = \varepsilon_r \frac{\alpha_n^{(1)}}{k_n}\coth(\alpha_n^{(1)} d) + \frac{\varepsilon_r - \overline{\beta}^2}{1-\overline{\beta}^2}\frac{\alpha_n^{(2)}}{k_n}\coth(\alpha_n^{(2)}(h-d)) + \overline{\beta}^2 \frac{\hat{k}_n}{\alpha_n^{(2)}}\frac{1-\varepsilon_r}{1-\overline{\beta}^2}\coth(\alpha_n^{(2)}(h-d))$$

$$T_n(\beta_z) = \overline{\beta}_z^{\,2}\left(\frac{k_n}{\alpha_n^{(1)}}\coth(\alpha_n^{(1)} d) + \frac{k_n}{\alpha_n^{(2)}}\coth(\alpha_n^{(2)}(h-d))\right) \qquad \text{(A1.8)}$$

and $\overline{\beta}_z = \beta_z / k_0$ which is the normalized propagation constant.

Applying (3.26a) leads to:

$$E_{x1} = 0 \rightarrow \left(\sum_{n=1}^{\infty}\left(-A_n^{(e)} k_n + \frac{\omega\mu_0}{\beta_z} A_n^{(h)} \alpha_n^{(1)}\right)\sin(k_n x)\sinh(\alpha_n^{(1)} d)\right) e^{-j\beta_z z} = 0 \rightarrow$$

$$\sum_{n=1}^{\infty}\left(-A_n^{(e)} k_n + \frac{\omega\mu_0}{\beta_z} A_n^{(h)} \alpha_n^{(1)}\right)\sin(k_n x)\sinh(\alpha_n^{(1)} d) = 0 \rightarrow$$

$$\sum_{n=1}^{\infty} \overline{A}_n^{(e)} k_n \sin(k_n x) - \sum_{n=1}^{\infty} \overline{A}_n^{(h)} k_n \sin(k_n x) = 0\,. \qquad \text{(A1.9)}$$

Applying (3.26b) leads to:

$$H_{z1} = H_{z2} \rightarrow j\frac{k_1^2 - \beta_z^2}{\beta_z}\left(\sum_{n=1}^{\infty} A_n^{(h)} \sin(k_n x)\cosh(\alpha_n^{(1)} d)\right) e^{-j\beta_z z} =$$

$$j\frac{k_2^2 - \beta_z^2}{\beta_z}\left(\sum_{n=1}^{\infty} B_n^{(h)} \sin(k_n x)\cosh(\alpha_n^{(2)}(h-d))\right) e^{-j\beta_z z} \rightarrow$$

$$\left(k_1^2 - \beta_z^2\right)\left(\sum_{n=1}^{\infty} A_n^{(h)} \sin(k_n x)\cosh(\alpha_n^{(1)} d)\right) = \left(k_2^2 - \beta_z^2\right)\left(\sum_{n=1}^{\infty} B_n^{(h)} \sin(k_n x)\cosh(\alpha_n^{(2)}(h-d))\right)$$

$$\rightarrow \left(k_1^2-\beta_z^2\right)\left(\sum_{n=1}^{\infty} A_n^{(h)} \sin(k_n x)\cosh(\alpha_n^{(1)} d)\right)=$$

$$\left(\sum_{n=1}^{\infty}\left[A_n^{(e)} \frac{k_n \beta_z}{\omega\mu\alpha_n^{(2)}}\left(1-\frac{k_1^2-\beta_z^2}{k_2^2-\beta_z^2}\right)-A_n^{(h)} \frac{\alpha_n^{(1)}}{\alpha_n^{(2)}}\right]\frac{\sinh(\alpha_n^{(1)} d)}{\sinh(\alpha_n^{(2)}(h-d))}\sin(k_n x)\cosh(\alpha_n^{(2)}(h-d))\right)$$

$$\rightarrow \left(k_1^2-\beta_z^2\right)\left(\sum_{n=1}^{\infty} A_n^{(h)} \sin(k_n x)\cosh(\alpha_n^{(1)} d)\right)=\left(k_2^2-\beta_z^2\right)\times$$

$$\left(k_2^2-\beta_z^2\right)\left(\sum_{n=1}^{\infty}\left[A_n^{(e)} \frac{k_n \beta_z}{\omega\mu\alpha_n^{(2)}}\left(\frac{k_2^2-k_1^2}{k_2^2-\beta_z^2}\right)-A_n^{(h)} \frac{\alpha_n^{(1)}}{\alpha_n^{(2)}}\right]\sinh(\alpha_n^{(1)} d)\sin(k_n x)\coth(\alpha_n^{(2)}(h-d))\right)$$

$\rightarrow$

$$\sum_{n=1}^{\infty} A_n^{(h)}\left[\left(k_1^2-\beta_z^2\right)\cosh(\alpha_n^{(1)} d)+\left(k_2^2-\beta_z^2\right)\frac{\alpha_n^{(1)}}{\alpha_n^{(2)}}\sinh(\alpha_n^{(1)} d)\coth(\alpha_n^{(2)}(h-d))\right]\sin(k_n x)=$$

$\rightarrow$

$$\sum_{n=1}^{\infty}\left[A_n^{(e)} \frac{k_n \beta_z}{\omega\mu\alpha_n^{(2)}}\left(k_2^2-k_1^2\right)\right]\sinh(\alpha_n^{(1)} d)\sin(k_n x)\coth(\alpha_n^{(2)}(h-d))$$

$$\sum_{n=1}^{\infty} \overline{A}_n^{(h)}\left[\frac{k_n}{\alpha_n^{(1)}}\left(k_1^2-\beta_z^2\right)\coth(\alpha_n^{(1)} d)+\frac{k_n}{\alpha_n^{(2)}}\left(k_2^2-\beta_z^2\right)\coth(\alpha_n^{(2)}(h-d))\right]\sin(k_n x)=$$

$\rightarrow$

$$\sum_{n=1}^{\infty}\left[\overline{A}_n^{(e)} \frac{k_n}{\alpha_n^{(2)}}\left(k_2^2-k_1^2\right)\right]\sin(k_n x)\coth(\alpha_n^{(2)}(h-d))$$

$$\sum_{n=1}^{\infty} \overline{A}_n^{(h)}\left[\frac{k_n}{\alpha_n^{(1)}}\left(\varepsilon_r-\overline{\beta}_z^2\right)\coth(\alpha_n^{(1)} d)+\frac{k_n}{\alpha_n^{(2)}}\left(1-\overline{\beta}_z^2\right)\coth(\alpha_n^{(2)}(h-d))\right]\sin(k_n x)=$$

$\rightarrow$

$$\sum_{n=1}^{\infty}\left[\overline{A}_n^{(e)} \frac{k_n}{\alpha_n^{(2)}}\left(1-\varepsilon_r\right)\right]\sin(k_n x)\coth(\alpha_n^{(2)}(h-d))$$

$$\sum_{n=1}^{\infty} \overline{A}_n^{(h)}\left[\frac{k_n}{\alpha_n^{(1)}}\left(\frac{\varepsilon_r-\overline{\beta}_z^2}{1-\overline{\beta}_z^2}\right)\coth(\alpha_n^{(1)} d)+\frac{k_n}{\alpha_n^{(2)}}\coth(\alpha_n^{(2)}(h-d))\right]\sin(k_n x)=$$

$\rightarrow$

$$\sum_{n=1}^{\infty} \overline{A}_n^{(e)}\left[\frac{k_n}{\alpha_n^{(2)}}\left(\frac{1-\varepsilon_r}{1-\overline{\beta}_z^2}\right)\coth(\alpha_n^{(2)}(h-d))\right]\sin(k_n x)$$

$$\sum_{n=1}^{\infty} \overline{A}_n^{(e)} Q_n(\beta_z)\sin(k_n x)-\sum_{n=1}^{\infty} \overline{A}_n^{(h)} W_n(\beta_z)\sin(k_n x)=0 \qquad \text{(A1.10)}$$

where

$$Q_n(\beta) = \frac{k_n}{\alpha_n^{(2)}} \frac{1-\varepsilon_r}{1-\overline{\beta}_z^{\,2}} \coth(\alpha_n^{(2)}(h-d)), \tag{A1.11}$$

$$W_n(\beta) = \frac{\varepsilon_r - \overline{\beta}_z^{\,2}}{1-\overline{\beta}_z^{\,2}} \frac{k_n}{\alpha_n^{(1)}} \coth(\alpha_n^{(1)} d) + \frac{k_n}{\alpha_n^{(2)}} \coth(\alpha_n^{(2)}(h-d)). \tag{A1.12}$$

Appendix II

Strip Grating's Equations

In this appendix, the details of deriving algebraic strip grating's equations (3.65) - (3.73) from boundary conditions (3.61) - (3.64) are described. The procedure is similar to microstrip line in appendix I.

Conditions (3.61) and (3.62) are used to express $B_n^{(e)}$ and $B_n^{(h)}$ in terms of $A_n^{(e)}$ and $A_n^{(h)}$:

$$E_{z1} = E_{z2} \rightarrow \frac{k_1^2 - \beta_z^2}{k_2^2 - \beta_z^2}\left(\sum_{n=-\infty}^{\infty} A_n^{(e)} \sinh(\alpha_n^{(1)} d) e^{-j\beta_n x}\right) = \left(\sum_{n=-\infty}^{\infty} B_n^{(e)} \sinh(\alpha_n^{(2)}(h-d)) e^{-j\beta_n x}\right)$$

$$\rightarrow \sum_{n=-\infty}^{\infty}\left[\frac{k_1^2 - \beta_z^2}{k_2^2 - \beta_z^2} A_n^{(e)} \sinh(\alpha_n^{(1)} d) - B_n^{(e)} \sinh(\alpha_n^{(2)}(h-d))\right] e^{-j\beta_n x} = 0$$

Since the set of $\{e^{-j\beta_n x}\}$ with $\beta_n = \beta_x + \frac{2\pi m}{2L}$ are a complete orthogonal set over the interval of $-L < x < L$, so the expression inside the bracket should be zero.

$$B_n^{(e)} = A_n^{(e)} \frac{k_1^2 - \beta_z^2}{k_2^2 - \beta_z^2} \frac{\sinh(\alpha_n^{(1)} d)}{\sinh(\alpha_n^{(2)}(h-d))} \qquad \text{(A2.1)}$$

$$E_{x1} = E_{x2} \rightarrow \sum_{n=-\infty}^{\infty}\left(\frac{\omega\mu_0}{\beta_z} A_n^{(h)} \alpha_n^{(1)} - jA_n^{(e)} \beta_n\right) \sinh(\alpha_n^{(1)} d) e^{-j\beta_n x} =$$

$$\sum_{n=-\infty}^{\infty}\left(\frac{-\omega\mu_0}{\beta_z} B_n^{(h)} \alpha_n^{(2)} - jB_n^{(e)} \beta_n\right) \sinh(\alpha_n^{(2)}(h-d)) e^{-j\beta_n x} \rightarrow$$

$$\sum_{n=-\infty}^{\infty}\left[\left(\frac{\omega\mu_0}{\beta_z}A_n^{(h)}\alpha_n^{(1)}-jA_n^{(e)}\beta_n\right)\sinh(\alpha_n^{(1)}d)+\left(\frac{\omega\mu_0}{\beta_z}B_n^{(h)}\alpha_n^{(2)}+jB_n^{(e)}\beta_n\right)\sinh(\alpha_n^{(2)}(h-d))\right]e^{-j\beta_n x}=0$$

Since the set of $\{e^{-j\beta_n x}\}$ with $\beta_n=\beta_x+\frac{\pi n}{L}$ are a complete orthogonal set over the interval of $-L<x<L$, so the expression inside the bracket should be zero, and by substituting $B_n^{(e)}$ in this equation, it reduces as follows:

$$\left(\frac{\omega\mu_0}{\beta_z}A_n^{(h)}\alpha_n^{(1)}-jA_n^{(e)}\beta_n\right)\sinh(\alpha_n^{(1)}d)+\left(\frac{\omega\mu_0}{\beta_z}B_n^{(h)}\alpha_n^{(2)}+jB_n^{(e)}\beta_n\right)\sinh(\alpha_n^{(2)}(h-d))=0$$

$\rightarrow$

$$\left(\frac{\omega\mu_0}{\beta_z}A_n^{(h)}\alpha_n^{(1)}-jA_n^{(e)}\beta_n\right)\frac{\sinh(\alpha_n^{(1)}d)}{\sinh(\alpha_n^{(2)}(h-d))}=\frac{-\omega\mu_0}{\beta_z}B_n^{(h)}\alpha_n^{(2)}-jB_n^{(e)}\beta_n\rightarrow$$

$$\left(\frac{\omega\mu_0}{\beta_z}A_n^{(h)}\alpha_n^{(1)}-jA_n^{(e)}\beta_n\right)\frac{\sinh(\alpha_n^{(1)}d)}{\sinh(\alpha_n^{(2)}(h-d))}=$$

$$\frac{-\omega\mu_0}{\beta_z}B_n^{(h)}\alpha_n^{(2)}-jA_n^{(e)}\frac{k_1^2-\beta_z^2}{k_2^2-\beta_z^2}\frac{\sinh(\alpha_n^{(1)}d)}{\sinh(\alpha_n^{(2)}(h-d))}\beta_n\rightarrow$$

$$\left(\frac{\omega\mu_0}{\beta_z}A_n^{(h)}\alpha_n^{(1)}-jA_n^{(e)}\beta_n+jA_n^{(e)}\beta_n\frac{k_1^2-\beta_z^2}{k_2^2-\beta_z^2}\right)\frac{\sinh(\alpha_n^{(1)}d)}{\sinh(\alpha_n^{(2)}(h-d))}=\frac{-\omega\mu_0}{\beta_z}B_n^{(h)}\alpha_n^{(2)}\rightarrow$$

$$\left(\frac{\omega\mu_0}{\beta_z}A_n^{(h)}\alpha_n^{(1)}-jA_n^{(e)}\beta_n\left(\frac{k_2^2-k_1^2}{k_2^2-\beta_z^2}\right)\right)\frac{\sinh(\alpha_n^{(1)}d)}{\sinh(\alpha_n^{(2)}(h-d))}=\frac{-\omega\mu_0}{\beta_z}B_n^{(h)}\alpha_n^{(2)}\rightarrow$$

$$B_n^{(h)}=\left(\frac{j\beta_n\beta_z}{\omega\mu_0\alpha_n^{(2)}}\left(\frac{k_2^2-k_1^2}{k_2^2-\beta_z^2}\right)A_n^{(e)}-\frac{\alpha_n^{(1)}}{\alpha_n^{(2)}}A_n^{(h)}\right)\frac{\sinh(\alpha_n^{(1)}d)}{\sinh(\alpha_n^{(2)}(h-d))}\qquad\text{(A2.2)}$$

Applying (3.63a) simply leads to

$$\sum_{n=-\infty}^{\infty}\overline{A}_n^{(e)}e^{-j\beta_n x}=0\qquad -t<x<t\qquad\text{(A2.3)}$$

where

$$\overline{A}_n^{(e)}=A_n^{(e)}\sinh(\alpha_n^{(1)}d)\,.\qquad\text{(A2.4)}$$

Applying (3.63b) leads to:

$$H_{x1} = H_{x2} \rightarrow \sum_{n=-\infty}^{\infty}\left(-jA_n^{(h)}\beta_n - \frac{\omega\varepsilon_1}{\beta_z}A_n^{(e)}\alpha_n^{(1)}\right)\cosh(\alpha_n^{(1)}d)e^{-j\beta_n x} =$$

$$\sum_{n=-\infty}^{\infty}\left(-jB_n^{(h)}\beta_n + \frac{\omega\varepsilon_0}{\beta_z}B_n^{(e)}\alpha_n^{(2)}\right)\cosh(\alpha_n^{(2)}(h-d))e^{-j\beta_n x} \rightarrow$$

$$\sum_{n=-\infty}^{\infty}\left(-jA_n^{(h)}\beta_n - \frac{\omega\varepsilon_1}{\beta_z}A_n^{(e)}\alpha_n^{(1)}\right)\cosh(\alpha_n^{(1)}d)e^{-j\beta_n x} =$$

$$\sum_{n=-\infty}^{\infty}\left[\left(-j\left(\frac{j\beta_n\beta_z}{\omega\mu_0\alpha_n^{(2)}}\left(\frac{k_2^2-k_1^2}{k_2^2-\beta_z^2}\right)A_n^{(e)} - \frac{\alpha_n^{(1)}}{\alpha_n^{(2)}}A_n^{(h)}\right)\beta_n + \frac{\omega\varepsilon_0}{\beta_z}A_n^{(e)}\frac{k_1^2-\beta_z^2}{k_2^2-\beta_z^2}\alpha_n^{(2)}\right)\times\right.$$

$$\left.\frac{\sinh(\alpha_n^{(1)}d)}{\sinh(\alpha_n^{(2)}(h-d))}\cosh(\alpha_n^{(2)}(h-d))e^{-j\beta_n x}\right] \rightarrow$$

$$\sum_{n=-\infty}^{\infty}\left(-jA_n^{(h)}\beta_n - \frac{\omega\varepsilon_1}{\beta_z}A_n^{(e)}\alpha_n^{(1)}\right)\cosh(\alpha_n^{(1)}d)e^{-j\beta_n x} =$$

$$\sum_{n=-\infty}^{\infty}\left[\left(\frac{\beta_n^2\beta_z}{\omega\mu_0\alpha_n^{(2)}}\left(\frac{k_2^2-k_1^2}{k_2^2-\beta_z^2}\right)A_n^{(e)} + \frac{\omega\varepsilon_0\alpha_n^{(2)}}{\beta_z}\frac{k_1^2-\beta_z^2}{k_2^2-\beta_z^2}A_n^{(e)} + j\frac{\beta_n\alpha_n^{(1)}}{\alpha_n^{(2)}}A_n^{(h)}\right)\times\right.$$

$$\left.\sinh(\alpha_n^{(1)}d)\coth(\alpha_n^{(2)}(h-d))e^{-j\beta_n x}\right] \rightarrow$$

$$\sum_{n=-\infty}^{\infty}\left(-jA_n^{(h)}\beta_n - \frac{\omega\varepsilon_1}{\beta_z}A_n^{(e)}\alpha_n^{(1)}\right)\sinh(\alpha_n^{(1)}d)\coth(\alpha_n^{(1)}d)e^{-j\beta_n x} =$$

$$\sum_{n=-\infty}^{\infty}\left[\left(\frac{\beta_n^2\beta_z}{\omega\mu_0\alpha_n^{(2)}}\left(\frac{k_2^2-k_1^2}{k_2^2-\beta_z^2}\right)A_n^{(e)} + \frac{\omega\varepsilon_0\alpha_n^{(2)}}{\beta_z}\frac{k_1^2-\beta_z^2}{k_2^2-\beta_z^2}A_n^{(e)} + j\frac{\beta_n\alpha_n^{(1)}}{\alpha_n^{(2)}}A_n^{(h)}\right)\times\right.$$

$$\left.\sinh(\alpha_n^{(1)}d)\coth(\alpha_n^{(2)}(h-d))e^{-j\beta_n x}\right] \rightarrow$$

$$\sum_{n=-\infty}^{\infty}\left(-jA_n^{(h)}\sinh(\alpha_n^{(1)}d)\beta_n-\frac{\omega\varepsilon_1}{\beta_z}A_n^{(e)}\sinh(\alpha_n^{(1)}d)\alpha_n^{(1)}\right)\coth(\alpha_n^{(1)}d)e^{-j\beta_n x}=$$

$$\sum_{n=-\infty}^{\infty}\left[\left(\frac{\beta_n^2\beta_z}{\omega\mu_0\alpha_n^{(2)}}\left(\frac{1-\varepsilon_r}{1-\overline{\beta}_z^2}\right)A_n^{(e)}\sinh(\alpha_n^{(1)}d)+\frac{\omega\varepsilon_0\alpha_n^{(2)}}{\beta_z}\frac{\varepsilon_r-\overline{\beta}_z^2}{1-\overline{\beta}_z^2}A_n^{(e)}\sinh(\alpha_n^{(1)}d)+j\frac{\beta_n\alpha_n^{(1)}}{\alpha_n^{(2)}}A_n^{(h)}\sinh(\alpha_n^{(1)}d)\right)\times\right.$$

$$\left.\coth(\alpha_n^{(2)}(h-d))e^{-j\beta_n x}\right]\rightarrow$$

$$\sum_{n=-\infty}^{\infty}\left(-j\frac{\beta_z}{\omega\mu_0}\frac{\beta_n}{\alpha_n^{(1)}}\overline{A}_n^{(h)}\beta_n-\frac{\omega\varepsilon_1}{\beta_z}\overline{A}_n^{(e)}\alpha_n^{(1)}\right)\coth(\alpha_n^{(1)}d)e^{-j\beta_n x}=$$

$$\rightarrow$$

$$\sum_{n=-\infty}^{\infty}\left(\frac{\beta_n^2\beta_z}{\omega\mu_0\alpha_n^{(2)}}\left(\frac{1-\varepsilon_r}{1-\overline{\beta}_z^2}\right)\overline{A}_n^{(e)}+\frac{\omega\varepsilon_0\alpha_n^{(2)}}{\beta_z}\frac{\varepsilon_r-\overline{\beta}_z^2}{1-\overline{\beta}_z^2}\overline{A}_n^{(e)}+j\frac{\beta_n\alpha_n^{(1)}}{\alpha_n^{(2)}}\frac{\beta_z}{\omega\mu_0}\frac{\beta_n}{\alpha_n^{(1)}}\overline{A}_n^{(h)}\right)\coth(\alpha_n^{(2)}(h-d))e^{-j\beta_n x}$$

$$\sum_{n=-\infty}^{\infty}\left(-j\frac{\beta_z}{\omega\mu_0}\frac{\beta_n}{\alpha_n^{(1)}}\overline{A}_n^{(h)}\beta_n\coth(\alpha_n^{(1)}d)-j\frac{\beta_z\beta_n^2\alpha_n^{(1)}}{\omega\mu_0\alpha_n^{(1)}\alpha_n^{(2)}}\overline{A}_n^{(h)}\coth(\alpha_n^{(2)}(h-d))\right)e^{-j\beta_n x}=$$

$$\sum_{n=-\infty}^{\infty}\left(\left(\frac{\beta_n^2\beta_z}{\omega\mu_0\alpha_n^{(2)}}\left(\frac{1-\varepsilon_r}{1-\overline{\beta}_z^2}\right)+\frac{\omega\varepsilon_0\alpha_n^{(2)}}{\beta_z}\left(\frac{\varepsilon_r-\overline{\beta}_z^2}{1-\overline{\beta}_z^2}\right)\right)\overline{A}_n^{(e)}\coth(\alpha_n^{(2)}(h-d))+\frac{\omega\varepsilon_1}{\beta_z}\overline{A}_n^{(e)}\alpha_n^{(1)}\coth(\alpha_n^{(1)}d)\right)e^{-j\beta_n x}$$

$$\rightarrow$$

$$\sum_{n=-\infty}^{\infty}\left(j\frac{\beta_z\beta_n}{\omega\mu_0\alpha_n^{(1)}}\coth(\alpha_n^{(1)}d)+j\frac{\beta_z\beta_n}{\omega\mu_0\alpha_n^{(2)}}\coth(\alpha_n^{(2)}(h-d))\right)\overline{A}_n^{(h)}\beta_n e^{-j\beta_n x}+$$

$$\sum_{n=-\infty}^{\infty}\left(\left(\frac{\beta_z\beta_n}{\omega\mu_0\alpha_n^{(2)}}\left(\frac{1-\varepsilon_r}{1-\overline{\beta}_z^2}\right)+\frac{\omega\varepsilon_0\alpha_n^{(2)}}{\beta_z\beta_n}\left(\frac{\varepsilon_r-\overline{\beta}_z^2}{1-\overline{\beta}_z^2}\right)\right)\coth(\alpha_n^{(2)}(h-d))+\frac{\omega\varepsilon_1}{\beta_z\beta_n}\alpha_n^{(1)}\coth(\alpha_n^{(1)}d)\right)\overline{A}_n^{(e)}\beta_n e^{-j\beta_n x}=0$$

$$\rightarrow$$

$$\sum_{n=-\infty}^{\infty}\left(j\frac{\beta_n}{\alpha_n^{(1)}}\coth(\alpha_n^{(1)}d)+j\frac{\beta_n}{\alpha_n^{(2)}}\coth(\alpha_n^{(2)}(h-d))\right)\overline{A}_n^{(h)}\beta_n e^{-j\beta_n x}+$$

$$\sum_{n=-\infty}^{\infty}\left(\left(\frac{\beta_n}{\alpha_n^{(2)}}\left(\frac{1-\varepsilon_r}{1-\overline{\beta}_z^2}\right)+\frac{\omega^2\mu_0\varepsilon_0\alpha_n^{(2)}}{\beta_z^2\beta_n}\left(\frac{\varepsilon_r-\overline{\beta}_z^2}{1-\overline{\beta}_z^2}\right)\right)\coth(\alpha_n^{(2)}(h-d))+\frac{\omega^2\mu_0\varepsilon_0\varepsilon_r}{\beta_z^2\beta_n}\alpha_n^{(1)}\coth(\alpha_n^{(1)}d)\right)\overline{A}_n^{(e)}\beta_n e^{-j\beta_n x}=0$$

$$\rightarrow$$

$$j\sum_{n=-\infty}^{\infty}\left(\frac{\beta_n}{\alpha_n^{(1)}}\coth(\alpha_n^{(1)}d)+\frac{\beta_n}{\alpha_n^{(2)}}\coth(\alpha_n^{(2)}(h-d))\right)\overline{A}_n^{(h)}\beta_n e^{-j\beta_n x}+$$

$$\sum_{n=-\infty}^{\infty}\left(\left(\frac{\beta_n}{\alpha_n^{(2)}}\left(\frac{1-\varepsilon_r}{1-\overline{\beta}_z^2}\right)+\frac{\alpha_n^{(2)}}{\overline{\beta}_z^2\beta_n}\left(\frac{\varepsilon_r-\overline{\beta}_z^2}{1-\overline{\beta}_z^2}\right)\right)\coth(\alpha_n^{(2)}(h-d))+\frac{\varepsilon_r\alpha_n^{(1)}}{\overline{\beta}_z^2\beta_n}\coth(\alpha_n^{(1)}d)\right)\overline{A}_n^{(e)}\beta_n e^{-j\beta_n x}=0$$

$$\rightarrow$$

$$\sum_{n=-\infty}^{\infty}\left(\frac{\varepsilon_r\alpha_n^{(1)}}{\beta_n}\coth(\alpha_n^{(1)}d)+\frac{\alpha_n^{(2)}}{\beta_n}\left(\frac{\varepsilon_r-\overline{\beta}_z^2}{1-\overline{\beta}_z^2}\right)\coth(\alpha_n^{(2)}(h-d))+\frac{\overline{\beta}_z^2\beta_n}{\alpha_n^{(2)}}\left(\frac{1-\varepsilon_r}{1-\overline{\beta}_z^2}\right)\coth(\alpha_n^{(2)}(h-d))\right)\overline{A}_n^{(e)}\beta_n e^{-j\beta_n x}+$$

$$j\sum_{n=-\infty}^{\infty}\overline{\beta}_z^2\left(\frac{\beta_n}{\alpha_n^{(1)}}\coth(\alpha_n^{(1)}d)+\frac{\beta_n}{\alpha_n^{(2)}}\coth(\alpha_n^{(2)}(h-d))\right)\overline{A}_n^{(h)}\beta_n e^{-j\beta_n x}=0$$

Therefore,

$$\sum_{n=-\infty}^{\infty}\overline{A}_n^{(e)}\beta_n P_n(\beta_z)e^{-j\beta_n x}+j\sum_{n=-\infty}^{\infty}\overline{A}_n^{(h)}\beta_n T_n(\beta_z)e^{-j\beta_n x}=0 \quad -L<x<-t \ \ or \ \ t<x<L \qquad \text{(A2.5)}$$

where

$$\overline{A}_n^{(h)}=\frac{\omega\mu_0}{\beta_z}\frac{\alpha_n^{(1)}}{\beta_n}A_n^{(h)}\sinh(\alpha_n^{(1)}d), \qquad \text{(A2.6)}$$

$$P_n(\beta_z)=\frac{\varepsilon_r\alpha_n^{(1)}}{\beta_n}\coth(\alpha_n^{(1)}d)+\frac{\alpha_n^{(2)}}{\beta_n}\left(\frac{\varepsilon_r-\overline{\beta}_z^2}{1-\overline{\beta}_z^2}\right)\coth(\alpha_n^{(2)}(h-d))+\frac{\overline{\beta}_z^2\beta_n}{\alpha_n^{(2)}}\left(\frac{1-\varepsilon_r}{1-\overline{\beta}_z^2}\right)\coth(\alpha_n^{(2)}(h-d))$$

$$T_n(\beta_z)=\overline{\beta}_z^2\left(\frac{\beta_n}{\alpha_n^{(1)}}\coth(\alpha_n^{(1)}d)+\frac{\beta_n}{\alpha_n^{(2)}}\coth(\alpha_n^{(2)}(h-d))\right) \qquad \text{(A2.8)}$$

and $\overline{\beta}_z=\beta_z/k_0$ which is the normalized propagation constant.

Applying (3.64a) leads to

$$E_{x1}=0\rightarrow\sum_{n=-\infty}^{\infty}\left(\frac{\omega\mu_0}{\beta_z}A_n^{(h)}\alpha_n^{(1)}-jA_n^{(e)}\beta_n\right)\sinh(\alpha_n^{(1)}d)e^{-j\beta_n x}=0\rightarrow$$

$$\sum_{n=-\infty}^{\infty}\left(\frac{\omega\mu_0}{\beta_z}\frac{\alpha_n^{(1)}}{\beta_n}A_n^{(h)}\beta_n-jA_n^{(e)}\beta_n\right)\sinh(\alpha_n^{(1)}d)e^{-j\beta_n x}=0\rightarrow$$

$$\sum_{n=-\infty}^{\infty}\frac{\omega\mu_0}{\beta_z}\frac{\alpha_n^{(1)}}{\beta_n}A_n^{(h)}\beta_n\sinh(\alpha_n^{(1)}d)e^{-j\beta_n x}-j\sum_{n=-\infty}^{\infty}A_n^{(e)}\beta_n\sinh(\alpha_n^{(1)}d)e^{-j\beta_n x}=0\rightarrow$$

$$\sum_{n=-\infty}^{\infty}\overline{A}_n^{(e)}\beta_n e^{-j\beta_n x}+j\sum_{n=-\infty}^{\infty}\overline{A}_n^{(h)}\beta_n e^{-j\beta_n x}=0 \qquad -t<x<t \qquad \text{(A2.9)}$$

Applying (3.64b) leads to:

$$H_{z1}=H_{z2}\rightarrow\frac{\varepsilon_r-\overline{\beta}_z^2}{1-\overline{\beta}_z^2}\left(\sum_{n=-\infty}^{\infty}A_n^{(h)}\cosh(\alpha_n^{(1)}d)e^{-j\beta_n x}\right)=\left(\sum_{n=-\infty}^{\infty}B_n^{(h)}\cosh(\alpha_n^{(2)}(h-d))e^{-j\beta_n x}\right)$$

$$\rightarrow\frac{\varepsilon_r-\overline{\beta}_z^2}{1-\overline{\beta}_z^2}\left(\sum_{n=-\infty}^{\infty}A_n^{(h)}\cosh(\alpha_n^{(1)}d)e^{-j\beta_n x}\right)=\left(\sum_{n=-\infty}^{\infty}B_n^{(h)}\cosh(\alpha_n^{(2)}(h-d))e^{-j\beta_n x}\right)\rightarrow$$

$$\frac{\varepsilon_r-\overline{\beta}_z^2}{1-\overline{\beta}_z^2}\left(\sum_{n=-\infty}^{\infty}\frac{\beta_z\beta_n}{\omega\mu_0\alpha_n^{(1)}}\overline{A}_n^{(h)}\coth(\alpha_n^{(1)}d)e^{-j\beta_n x}\right)=$$

$$\sum_{n=-\infty}^{\infty}\left(\frac{j\beta_n\beta_z}{\omega\mu_0\alpha_n^{(2)}}\left(\frac{1-\varepsilon_r}{1-\overline{\beta}_z^2}\right)\overline{A}_n^{(e)}-\frac{\beta_z\beta_n}{\omega\mu_0\alpha_n^{(2)}}\overline{A}_n^{(h)}\right)\coth(\alpha_n^{(2)}(h-d))e^{-j\beta_n x}$$

$\rightarrow$

$$\sum_{n=-\infty}^{\infty}\left(\left(\frac{\varepsilon_r-\overline{\beta}_z^2}{1-\overline{\beta}_z^2}\right)\frac{\beta_z\beta_n}{\omega\mu_0\alpha_n^{(1)}}\coth(\alpha_n^{(1)}d)+\frac{\beta_z\beta_n}{\omega\mu_0\alpha_n^{(2)}}\coth(\alpha_n^{(2)}(h-d))\right)\overline{A}_n^{(h)}e^{-j\beta_n x}=$$

$\rightarrow$

$$j\sum_{n=-\infty}^{\infty}\frac{\beta_n\beta_z}{\omega\mu_0\alpha_n^{(2)}}\left(\frac{1-\varepsilon_r}{1-\overline{\beta}_z^2}\right)\overline{A}_n^{(e)}\coth(\alpha_n^{(2)}(h-d))e^{-j\beta_n x}$$

$$\sum_{n=-\infty}^{\infty}\frac{\beta_n}{\alpha_n^{(2)}}\left(\frac{1-\varepsilon_r}{1-\overline{\beta}_z^2}\right)\overline{A}_n^{(e)}\coth(\alpha_n^{(2)}(h-d))e^{-j\beta_n x}+$$

$$j\sum_{n=-\infty}^{\infty}\left(\left(\frac{\varepsilon_r-\overline{\beta}_z^2}{1-\overline{\beta}_z^2}\right)\frac{\beta_n}{\alpha_n^{(1)}}\coth(\alpha_n^{(1)}d)+\frac{\beta_n}{\alpha_n^{(2)}}\coth(\alpha_n^{(2)}(h-d))\right)\overline{A}_n^{(h)}e^{-j\beta_n x}=0$$

$$\sum_{n=-\infty}^{\infty}\overline{A}_n^{(e)}Q_n(\beta_z)e^{-j\beta_n x}+j\sum_{n=-\infty}^{\infty}\overline{A}_n^{(h)}W_n(\beta_z)e^{-j\beta_n x}=0\qquad -L<x<-t\ \ or\ \ t<x<L \tag{A2.10}$$

where

$$Q_n(\beta)=\frac{\beta_n}{\alpha_n^{(2)}}\left(\frac{1-\varepsilon_r}{1-\overline{\beta}_z^2}\right)\coth(\alpha_n^{(2)}(h-d)) \tag{A2.11}$$

$$W_n(\beta)=\left(\frac{\varepsilon_r-\overline{\beta}_z^2}{1-\overline{\beta}_z^2}\right)\frac{\beta_n}{\alpha_n^{(1)}}\coth(\alpha_n^{(1)}d)+\frac{\beta_n}{\alpha_n^{(2)}}\coth(\alpha_n^{(2)}(h-d)) \tag{A2.12}$$

References

[1] E. R. Brown, C. D. Parker, and E.Yablonovitch, "Radiation Properties of a planar antenna on a photonic-crystal substrate," *J. Opt. Soc. Am. B10, 404-407, 1993.*

[2] D. Sievenpiper, L. Zhang, J. Broas, N. Alexopolous and E. Yablonovitch. "High-Impedance Electromagnetic Surfaces with a Forbidden Frequency Band," *IEEE Transactions on Microwave Theory and Techniques, 47, 11, pp. 2059-2074, Nov. 1999.*

[3] C. Kittel, "*Introduction to Solid State Physics*," John Wiley & Sons, Inc., 1986.

[4] J. D. Joannopoulos, "*Photonic Crystals: Molding the Flow of Light*," Princeton: Princeton University Press,1995.

[5] B. A. Munk, "*Frequency Selective Surfaces Theory and Design,*" John Wiley & Sons, Inc., 2000.

[6] A. F. Peterson, S. L. Ray and R. Mittra, "*Computational Methods for Electromagnetics*," IEEE Press, 1998.

[7] C. Berginc, C. Bourrely, C. Ordenovic and B. Torresani, "A Numerical Study of Absorption by Multilayered Biperiodic Structures," *PIER 19, pp. 199-222, 1998.*

[8] F. Terracher and G. Berginc, "A Numerical Study of TM-Type Surface Waves on a Grounded Dielectric Slab Covered by a Doubly Periodic Array of Metallic Patches," *PIER 43, pp. 75-100, 2003.*

[9] M. Bozzi, S. Germani, L. Minelli, L. Perregrini and P. Maagt, " Efficient Calculation of the Dispersion Diagram of Planar Electromagnetic Band-Gap

Structures by the MoM/BI-RME Method," *IEEE Transactions on Antennas and Propagation, vol. 53, no. 1, pp. 29-35, Jan. 2005.*

[10] M. Bozzi, S. Germani, L. Minelli, L. Perregrini and P. Maagt, "On the Solution of Eigenvalue Problems Deriving from the MoM Analysis of EBG structures," *34th European Microwave Conference, pp. 869-872, Amesterdam 2004.*

[11] F. Yang, K. Ma, Y. Qian and T. Itoh, "A Uniplanar Compact Photonic-Bandgap (UC-PBG) Structure and its Applications for Microwave Circuit," *IEEE Trans. Microwave Theory Tech. vol. 47, no. 8, pp.1509 – 1514, Aug. 1999.*

[12] C. C. Chang, Y. Qian and T. Itoh, "Analysis and Applications of Uniplanar Compact Photonic Bandgap Structure," *PIER 41, pp. 211-235, 2003.*

[13] M.Quin, "Photonic Band Structures for Surface Waves on Structured Metal Surfaces," *Optics Express, vol. 13, no. 13, pp.7583-7588, Sept. 2005.*

[14] P. Baccarelli, P. Burghignoli, C. Di Nallo, F. Frezza, A. Galli, P. Lampariello and G. Ruggieri, " Full-Wave Analysis of Printed Leaky-Wave Phased Arrays," *Int. J. RF and Microwave CAE vol.12, Iss. 3, pp.: 272-287, May 2002.*

[15] K. Sakoda, "*Optical Properties of Photonic Crystals*," 2001.

[16] R. E. Collin and F. J. Zucker, "*Antenna Theory*," vol. 1 & 2 , McGraw-Hill Book Company, 1969.

[17] G. Guida, A. de Lustrac, A. Priou "An introduction to photonic band gap (PBG) materials," *PIER 41, pp. 1–20, 2003.*

[18] S. Clavijo, R. E. Diaz, and W. E. McKinzie, "Design methodology for Sievenpiper High-Impedance Surfaces: An Artificial Magnetic Conductor for

Positive Gain Electrically Small Antennas", *IEEE Transactions on Antennas and Propagation, vol. 51, no. 10, pp.2678-2690, October 2003.*

[19] T. Itoh, "*Planar Transmission Line Structures*," IEEE Press, 1987.

[20] L. Young and H. Sobol, "*Advances in Microwaves*," vol. 8, Academic Press, 1966.

[21] A. Aminian, F. Yang and Y. Rahmat Samii, " Bandwidth Determination for Soft and Hard Ground Planes by Spectral FDTD: A Unified Approach in Visible and Surface Wave Regions," *IEEE Transactions on Antennas and Propagation, vol. 53, no. 1, pp. 18-28, Jan. 2005.*

[22] Manuals for Ansoft HFSS and Ansoft Designer, version 9, www.ansoft.com, 2005.

[23] T. Itoh, "*Numerical Techniques for Microwave and Millimeter-Wave Passive Structure*," John Wiley & Sons, Inc., 1989.

[24] D. M. Pozar, "*Microwave Engineering*," Addison-Welsey Publishing Company, 1990.

[25] R. Mittra, "*Analytical techniques in the theory of guided waves,*" Mcmillan, New York, 1971.

[26] G. Kowalski and R. Pregla, "Dispersion Characteristics of Shielded Microstrip with Finite Thickness," *Archiv fur Elektronik Ubertragungstechnik, vol. 25, pp. 193-196, 1971.*

[27] Z. Ma and E. Yamashita, "Space Wave Leakage From Higher Order Modes On Various Planar Transmission Line Structures," *IEEE Microwave Theory Tech., S Digest, pp. 1033-1036, 1994.*

[28] R. Mittra, " Relative Convergence of the Solution of a Doubly Infinite Set of Equations," *Journal of Research of the National Bureau of Standards-D Radio Propagation, vol. 67D, no. 2, pp. 245–254, March-April 1963.*

[29] D. G. Zill and M. R. Cullin, "*Advanced Engineering Mathematics*," Jones and Bartlett Publishers, Inc., 2000.

[30] C. A. Balanis, "*Advanced Engineering Electromagnetics*," John Wiley & Sons, Inc., 1989.

[31] R. F. Harington, "*Time-Harmonic Electromagnetic Fields*," McGraw-Hill Book Co., 1961.

[32] R. E. Collin, "*Foundations for Microwave Engineering*," McGraw-Hill Book Company, 1992.

[33] R. Mittra and T. Itoh, "A New Technique for the Analysis of the Dispersion Characteristic of Microstrip Lines," *IEEE Trans. Microwave Theory Tech. vol. MTT-19, no.1, Jan. 1971.*

[34] S. D. Cheng, R. Biswas, E. Ozbay, S. McClamont, G. Tuttle, and K. M. Ho, "Optimized dipole antennas on photonic band gap crystals," *Appl. Phys. Lett. 67, pp. 3399-3401, 2003.*

[35] V.A. Labay and J. Bornemann, "Marrix Singular Value Decomposition for Pole-Free Solutions of Homogenous Matrix Equations as Applied to Numerical Modeling Methods," *IEEE Microwave and Guided Wave Letters, vol. 2, no. 2, pp. 49-51, Feb. 1992.*

[36] R. A. Horn and C. R. Johnson, "*Matrix Analysis,*" Cambridge University Press, 1985.